UNIVERSITY OF CALIFORNIA,
IRVINE

Thrombosis and hemodynamic changes in the CNS during *Toxoplasma gondii* infection

DISSERTATION

submitted in partial satisfaction of the requirements
for the degree of

DOCTOR OF PHILOSOPHY

in Molecular Biology and Biochemistry

by

Evelyn Maria Hoover

Dissertation Committee:
Associate Professor Melissa Lodoen, Chair
Associate Professor Naomi Morrissette
Associate Professor Robert Edwards

2021

DEDICATION

To

My teachers and mentors, who helped me catch the research bug.

"You must do the thing you think you cannot do."
Eleanor Roosevelt, *You Learn by Living*

"I believe I have a personal responsibility to make a positive impact on society. I've tried to accomplish this goal by choosing a life of public service."
Anthony Fauci, *A Goal of Service to Humankind*

TABLE OF CONTENTS

LIST OF FIGURES

ACKNOWLEDGEMENTS

Many people made the work presented here possible.

First, I wish to thank my committee members. Dr. Melissa Lodoen, my committee chair and research advisor, has been my scientific role model and supportive mentor for the last several years. Melissa always made me feel more optimistic after our weekly meetings to discuss data, even when experiments went in unexpected directions. Dr. Naomi Morrissette and Dr. Robert Edwards have provided me with great input while developing my dissertation research and ensured that my project was rationale and feasible.

Additionally, my research could not have been as impactful without my collaborators both in and out of the Lodoen lab, including Dr. Bernard Choi, Dr. Sunil Gandhi, Dr. Dritan Agalliu, Christine Schneider, Christian Crouzet, Dario Figueroa Velez, and Cuong Joseph Tran. They all helped me master new techniques and provided guidance in research direction.

I would also like to thank the Medical Scientist Training Program for providing me the opportunity to pursue a PhD at UC Irvine. Thank you especially to Dr. Alan Goldin, who accepted me into the program many years ago, to Dr. Edwin Monuki, who provided career guidance, and to Joanne Wu, who makes my life much easier by being an excellent administrative director. Additionally, the MSTP family provided me with many colleagues, who I often turned to for advice, including Suzi Klaus, Bassem M. Shoucri, Sung Goan Ji, Tobias Dong, and many others.

Thank you also to my funding sources, including the American Heart Association, which provided me with a predoctoral fellowship, UCI's Institute of Immunology, which provided me

with funding as a Kirschstein-NRSA T32 Trainee, and the MSTP, which provided me with funding as a Kirschstein-NRSA T32 Trainee.

To those who helped me decide to pursue science and develop a love for microbiology, thank you. Especially important to my journey were Dr. Michael Polymenis and Scott Hoose, for being my first research mentors. Dr. Manuela Raffatellu and Dr. Judith Behnsen helped me develop important research skills. Sharat Gadde, my high school biology teacher, started my fascination with parasites through a book report.

I also wish to acknowledge the rest of the Lodoen lab, who worked with me during my dissertation and were not previously mentioned. They include Tatiane Lima, William Pandori, Armond Franklin Murray, Sharmila Mallya, Stephanie Orchanian, Stephanie Matsuno, Olivia Yanes, Tiffany Haojane Kao, and Joshua Thao. You all made it a pleasure to come to work every day, and helped the lab run smoothly.

Finally thank you to my friends and family, who have supported me throughout this process. Thank you especially to Ziwei Zhong for being my research sounding board at home. Also, thank you to Michelle Heare, Kenneth Loonam, Shay Fort, Laura Caflisch, Adrian Castellanos, Aneesh Rai, and many others for being great friends.

VITA

Evelyn Maria Hoover

Education

2021 Ph.D. in Molecular Biology and Biochemistry

University of California, Irvine

Advisor: Dr. Melissa B. Lodoen

2013 B.S. in Microbiology,

Texas A&M University, College Station

Research

2016-2021 Doctoral student

Department of Molecular Biology and Biochemistry

University of California, Irvine

Advisor: Dr. Melissa Lodoen

- Investigated thrombosis and hemodynamic changes in the brain during *T. gondii* infection.
- Developed a method to achieve chronic optical access, allowing longitudinal monitoring of cerebral blood flow with laser speckle imaging for >100 days.

2015-2016 Graduate student researcher

Department of Microbiology and Molecular Genetics

University of California, Irvine

Advisor: Dr. Manuela Raffatellu

- Studied the interactions between the probiotic bacteria *Escherichia coli* Nissle 1917, the pathogenic bacteria *Salmonella enterica* serovar Typhimurium, and the host in the intestines.

2011-2013 Undergraduate student researcher

Department of Biochemistry

Texas A&M University, College Station

Advisor: Dr. Michael Polymenis

- Studied cell cycle regulation using *Saccharomyces cerevisiae*, screening for novel cell cycle regulatory genes using flow cytometry and the commercially available *S. cerevisiae* deletion library.
- Studied whether currently FDA approved drugs have previously unidentified suppressive cell cycle effects, by screening a large panel of approved therapeutics using *S. cerevisiae* growth curve analyses.

2012 DAAD RISE Research scholar

Department of Molecular Microbiology and Bee Diseases

Humboldt-Universität zu Berlin, Germany

Advisor: Dr. Elke Genersch

- Examined host-pathogen interactions between honeybees and the pathogen *Paenibacillus larvae* to establish the kinetics of the immune response of bee larvae to the two main genotypes of *P. larvae*, ERIC-I and ERIC-II, using RT-qPCR.

Awards and Honors

2018-2020 American Heart Association Predoctoral Fellowship 19PRE34380476

2019 Loh Down on Science Fellowship program

2016-2017 Kirschstein-NRSA T32 Trainee, NIAID, Grant Number AI60573

2013-2014 Kirschstein-NRSA T32 Trainee, NIH, Grant Number GM008620

2013 Magna Cum Laude, Texas A&M University

2013 University and Foundation Honors, Texas A&M University

2012-2013 Undergraduate Research Fellow, Texas A&M University

2012 DAAD RISE Scholarship, German Research Council

2009-2013 Academic Achievement Scholarship, Texas A&M University

2009-2013 National Hispanic Merit Scholarship, Texas A&M University

Publications

Hoover, E.M., Crouzet, C., Bordas, J.M., Figueroa Velez, D.X., Gandhi, S.P., Choi, B., Lodoen, M.B., 2021. Transcranial chronic optical access to longitudinally measure cerebral blood flow. J. Neurosci. Methods 350, 109044. https://doi.org/10.1016/j.jneumeth.2020.109044

Zhi, H., Behnsen, J., Aron, A., Subramanian, V., Liu, J., Gerner, R., Petras, D., Green, K., Price, S., Camacho, J., Hillman, H., Tjokrosurjo, J., Montaldo, N., **Hoover, E.**, Treacy-Abarca, S., Gilston, B., Skaar, E., Chazin, W., Garneau-Tsodikova, S., Lawrenz, M., Perry, R., Nuccio, S.-P., Dorrestein, P., Raffatellu, M., 2020. Siderophore-mediated zinc acquisition enhances enterobacterial colonization of the inflamed gut. bioRxiv 2020.07.20.212498. https://doi.org/10.1101/2020.07.20.212498

Schneider, C.A., Figueroa Velez, D.X., Azevedo, R., **Hoover, E.M.**, Tran, C.J., Lo, C., Vadpey, O., Gandhi, S.P., Lodoen, M.B., 2019. Imaging the dynamic recruitment of monocytes to the blood–brain barrier and specific brain regions during Toxoplasma gondii infection. Proc. Natl. Acad. Sci. U. S. A. 116, 24796–24807. https://doi.org/10.1073/pnas.1915778116

Shukla, A.K., McIntyre, L.L., Marsh, S.E., Schneider, C.A., **Hoover, E.M.**, Walsh, C.M., Lodoen, M.B., Blurton-Jones, M., Inlay, M.A., 2018. CD11a expression distinguishes infiltrating myeloid cells from plaque-associated microglia in Alzheimer's disease. Glia. https://doi.org/10.1002/glia.23575

Hoose, S.A., Duran, C., Malik, I., Eslamfam, S., Shasserre, S.C., Downing, S.S., **Hoover, E.M.**, Dowd, K.E., Smith, R., Polymenis, M., 2012. Systematic analysis of cell cycle effects of common drugs leads to the discovery of a suppressive interaction between gemfibrozil and fluoxetine. PLoS One 7, e36503. https://doi.org/10.1371/journal.pone.0036503

Hoose, S.A., Rawlings, J.A., Kelly, M.M., Leitch, M.C., Ababneh, Q.O., Robles, J.P., Taylor, D., **Hoover, E.M.**, Hailu, B., McEnery, K.A., Downing, S.S., Kaushal, D., Chen, Y., Rife, A., Brahmbhatt, K.A., Smith, R. 3rd, Polymenis, M., 2012. A systematic analysis of cell cycle regulators in yeast reveals that most factors act independently of cell size to control initiation of division. PLoS Genet. 8, e1002590. https://doi.org/10.1371/journal.pgen.1002590

Oral Presentations

"*Toxoplasma gondii* Induces Coagulation in the Microvasculature and Decreased Cerebral Perfusion During Acute Infection." Evelyn M. Hoover, Christine A. Schneider, Christian Crouzet, Dario X. Figueroa Velez, Cuong Joseph Tran, Julianna M. Bordas, Bernard Choi, Sunil P. Gandhi, Melissa B. Lodoen. *XVII Annual UC Irvine Immunology Fair*. Irvine, CA. December 5, 2019.

"*Toxoplasma gondii* induces coagulation in the microvasculature and decreased cerebral perfusion during acute infection." Evelyn M. Hoover, Christine A. Schneider, Christian Crouzet, Dario X. Figueroa Velez, Cuong Joseph Tran, Julianna M. Bordas, Bernard Choi, Sunil P. Gandhi, Melissa B. Lodoen. *9th Annual Southern California Eukaryotic Pathogen Symposium*. Riverside, CA. October 30, 2019.

"*Toxoplasma gondii* induces endothelial cell activation and coagulation at the blood-brain barrier." Evelyn M. Hoover, Christine A. Schneider, Dario X. Figueroa Velez, Cuong J. Tran, Sunil P. Gandhi, Melissa B. Lodoen. *UC Irvine Medical Scientist Training Program Retreat*. Lake Arrowhead, CA. October 5, 2019.

"Toxoplasma gondii induces endothelial cell activation and coagulation at the blood-brain barrier." Evelyn M. Hoover, Christine A. Schneider, Dario X. Figueroa Velez, Cuong J. Tran, Sunil P. Gandhi, Melissa B. Lodoen. *The Woods Hole Immunoparasitology Meeting*. Woods Hole, MA. April 15, 2019.

"Organ-specific Regulation of Endothelial Cell Activation and Thrombosis in Response to *Toxoplasma gondii*." Evelyn M. Hoover, Tatiane Soares de Lima, Christine Schneider, and Melissa B. Lodoen. *Keystone Symposia on Uncomplicating Diabetes / Vascular Biology and Human Diseases*. Santa Fe, NM. February 26, 2018.

"The vascular immune response to infection differs in the brain and the periphery." Evelyn M. Hoover, Christine A. Schneider, Melissa B. Lodoen. *UC Irvine Medical Scientist Training Retreat*. Lake Arrowhead, CA. October 28, 2017.

Poster Presentations

"Hemodynamic consequences of Toxoplasma gondii infection." Evelyn M. Hoover, Christine Schneider, Christian Crouzet, Dario X. Figueroa Velez, Cuong Joseph Tran, Julianna Maria Bordas, Bernard Choi, Sunil Gandhi, Melissa B. Lodoen. *10th Annual Southern California Eukaryotic Pathogen Symposium*. Riverside, CA. October 21, 2020.

"Organ-specific Regulation of Endothelial Cell Activation and Thrombosis in Response to *Toxoplasma gondii*." Evelyn M. Hoover, Tatiane Soares de Lima, Christine Schneider, and Melissa B. Lodoen. *Keystone Symposia on Uncomplicating Diabetes / Vascular Biology and Human Diseases*. Santa Fe, NM. February 26, 2018.

"*Salmonella* Typhimurium and Fungi Interactions through Siderophores in the Gut." Evelyn Hoover, Judith Behnsen, Joshua Tjokrosurjo, and Manuela Raffatellu. *UC Irvine Medical Scientist Training Program Retreat*. Lake Arrowhead, CA. November 1, 2014.

"Insertion Site Factors of the Retrotransposon TY3." Evelyn Hoover, Kurt Patterson, James Yu, Suzanne Sandmeyer. *UC Irvine Medical Scientist Training Program Retreat*. Lake Arrowhead, CA. October 23, 2013.

ABSTRACT OF THE DISSERTATION

Thrombosis and hemodynamic changes in the CNS during *Toxoplasma gondii* infection

by

Evelyn Maria Hoover

Doctor of Philosophy in Social Ecology

University of California, Irvine, 2021

Associate Professor Melissa Lodoen, Chair

Mammalian circulation relies on a closed high-pressure system to deliver oxygen to tissues via red blood cells within blood vessels lined by endothelial cells. However, this high-pressure system makes us vulnerable to hemorrhage if a blood vessel is damaged. Therefore, we have a mechanism to rapidly seal a damaged vessel with a platelet-fibrin clot in a physiological process called hemostasis. However, clots can form in an intact blood vessel and obstruct blood flow, in a pathological process called thrombosis. Such clots can be life threatening if they interfere with blood flow in critical organs, such as the brain (i.e., ischemic stroke). However, recent research has revealed that thrombosis can be involved in augmenting and supporting the innate immune response to control infection through immunothrombosis.

As recent work has demonstrated that *Toxoplasma gondii* infects and lyses central nervous system endothelial cells that form the blood-brain barrier (BBB), *T. gondii*-infection is a good model to study the interplay between coagulation, immunity, and infection. However, little is known about the effect of *T. gondii* infection on the BBB and the functional consequences of infection on cerebral blood flow (CBF) during the different stages of infection. To study CBF changes during *T. gondii* infection longitudinally we developed a surgical method to achieve

chronic optical access for >100 days. Then, using an *in vivo* infection model in mice, we demonstrated that brain endothelial upregulate the adhesion molecules ICAM-1 and VCAM-1 and become morphologically more tortuous during *T. gondii* infection. Longitudinal two-photon imaging of cerebral blood vessels during infection revealed vascular occlusion in the brain, prompting an analysis of the coagulation cascade. We detected platelet-fibrin clots within the cerebral vasculature during acute infection. Longitudinal analysis of CBF using laser-speckle imaging during *T. gondii* infection demonstrated that CBF decreased during acute infection, recovered during stable chronic infection, and decreased again during reactivation of the infection. Finally, we demonstrate that treatment of mice with an anticoagulant, during infection partially rescued CBF in *T. gondii*-infected mice. These data provide insight into the host-pathogen interactions of a CNS pathogen within the brain vasculature and suggest that thrombosis and changes in cerebral hemodynamics may be an unappreciated aspect of infection with *T. gondii*.

Chapter 1

Introduction to Immunothrombosis During Infection

Hemostasis

Mammalian circulation relies on a closed high-pressure system to deliver oxygen to tissues via red blood cells (RBCs) within blood vessels lined by endothelial cells. When there is a break in a blood vessel, for instance due to a laceration, a rapid response is needed to seal the break and prevent gross hemorrhage. This response is called hemostasis, which is the physiological response to blood vessel damage, in which platelets and the coagulation cascade are activated (Mackman et al., 2007). Platelets are small (~1-3 μm) enucleated cells derived from megakaryocytes in the bone marrow, which circulate in the blood (Yeaman, 2010). The coagulation cascade culminates in the formation of a fibrin, an insoluble protein that forms a matrix with itself. Together, fibrin and activated platelets form a fibrin-platelet clot to seal the injured vessel.

There are two major mechanisms by which the clotting cascade can be initiated, the "intrinsic" and "extrinsic" pathways (Fig. 1.1). The intrinsic pathway was named because researchers noted that blood removed from the body coagulated on its own, needing no additional factors. This pathway relies on the activation of factors (F)XII, FXI, and FIX (canonically in that order), and is activated when FXII comes in contact with negatively charged molecules (e.g., silica, DNA, RNA, or the plasma membrane of activated platelets) (Grover and Mackman, 2019). The extrinsic pathway requires an additional stimulus from outside the blood, tissue factor (TF or FIII), which activates FVII (Mackman et al., 2007). The pathways converge on the common pathway, made up of FX, prothrombin (FII), and fibrinogen (FI) (Fig. 1.1). Notably components of the extrinsic and common pathways can also activate the intrinsic pathway, which is important for the sustained activity of the coagulation cascade (Grover and Mackman, 2019; Mackman et al., 2007).

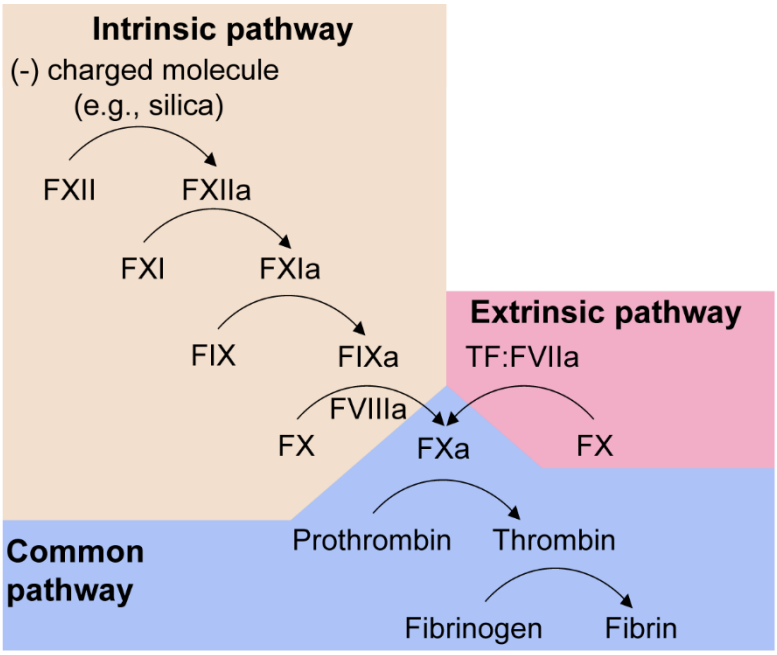

Figure 1.1 Coagulation Cascade. A schematic of the intrinsic, extrinsic, and common pathways of the coagulation cascade.

In vivo, the extrinsic pathway is the primary activator of coagulation, with the intrinsic pathway amplifying the coagulation cascade, contributing to the propagation of a thrombus and the recruitment of platelets (Mackman et al., 2007). TF is constitutively expressed in subendothelial cells (e.g., fibroblasts, vascular smooth muscle cells, and astrocytes in the brain) and is physically separated from the other factors, which are found in plasma (Fig. 1.2) (Drake et al., 1989; Eddleston et al., 1993; Fleck et al., 1990; Mackman et al., 2007). However, there are some conditions in which TF can be found in the blood compartment, which will be discussed in detail later. All the factors, except TF, are zymogens, requiring cleavage to become active. In contrast, TF is active on the surface of cells and is typically an integral membrane protein (Mackman et al., 2007). TF also has tissue-specificity and is expressed at higher levels in some

organs, including the brain, heart, lungs, kidney, placenta, and testis (Mackman, 2005; Mackman et al., 1993). This distribution of TF is thought to reflect the physiological intolerance of these organs to hemorrhage (Mackman, 2005). In the event of vessel injury, TF rapidly binds to FVII, and initiates a series of proteolytic cleavages, culminating in the cleavage of fibrinogen (FI) to fibrin (FIa) (Fig. 1.2) (Mackman et al., 2007). FXIIIa (fibrin stabilizing factor) stabilizes the clot by crosslinking fibrin (Dorgalaleh and Rashidpanah, 2016). Cross-linked fibrin together with activated platelets forms the hemostatic plug, preventing hemorrhage (Fig. 1.2) (Mackman et al., 2007).

Additionally, platelets collaborate with the coagulation cascade to amplify the clotting response (Semple et al., 2011). In response to vessel damage, platelets rapidly adhere to the lesion, undergo activation, and aggregate. Activated platelets support coagulation by exposing phospholipids on their surface, such as phosphatidylserine, which activate FXII (Semple et al., 2011). Conversely, thrombin contributes to the activation of platelets through cleavage of proteinase-activated receptor 1 and 4 (PAR1 and PAR4) on platelets (Engelmann and Massberg, 2012).

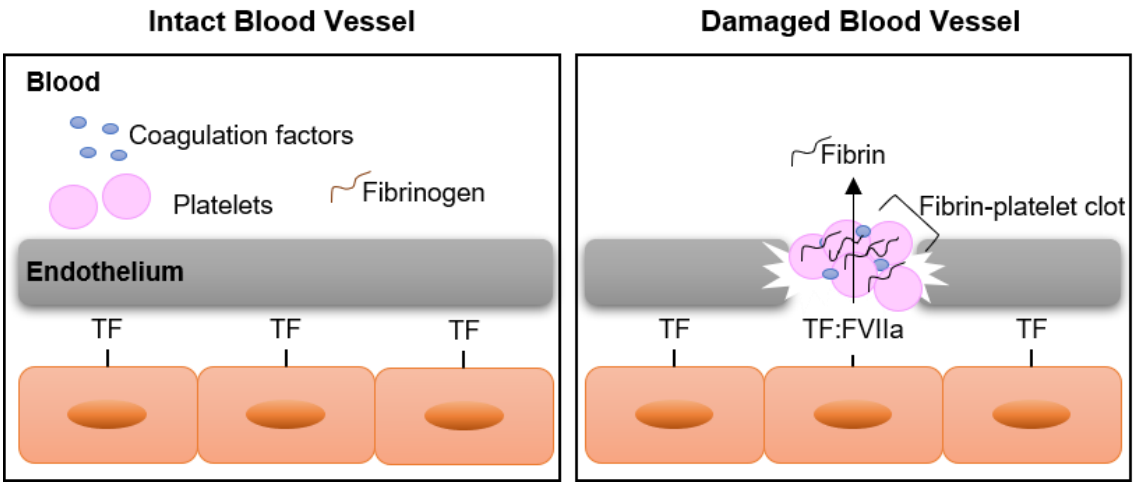

Figure 1.2. Formation of a clot at a site of injury. In the intact blood vessel, coagulation factors in the blood (blue circles) are separated from TF on the surface of subendothelial cells. However, in the event of injury (right), TF activates FVIIa, and the coagulation cascade ultimately produces insoluble fibrin, which forms a fibrin-platelet clot to seal the injured vessel and prevent hemorrhage.

Thrombosis

Thrombosis is generally considered to be a pathological variation of hemostasis and occurs when a thrombus (clot) forms intravascularly and obstructs blood flow. Such clots can be life threatening if they interfere with blood flow in critical organs, such as the brain (i.e., ischemic stroke), heart (i.e., myocardial infarction), or lungs (i.e., pulmonary embolism) (Mackman, 2008). The mechanisms leading to thrombosis vary depending on where in the vascular system they occur. Thrombi in the high-pressure arterial system are often caused by the rupture of an atherosclerotic plaque, and the subsequent clot formation occurs very similarly to physiological hemostasis (discussed earlier) (Mackman, 2008). In contrast, venous thrombosis tends to involve blood stasis and endothelial activation, which can occur during long periods of immobility (a risk factor for deep vein thrombosis) or during sepsis (i.e. disseminated intravascular coagulation) (Mackman, 2008).

One of the major differences between thrombosis and physiological hemostasis is the involvement of innate immune cells (i.e., monocytes, neutrophils, and dendritic cells) in the former (Engelmann and Massberg, 2012). The coagulation cascade and platelets activate the innate immune system. Conversely, the innate immune system can also activate the coagulation cascade and platelets. For example, thrombin and activated factor Xa activate PAR1 on dendritic cells (Niessen et al., 2008). Activation of PAR1 activates sphingosine 1-phosphate 3 (S1P3), which leads to an inflammatory phenotype in dendritic cells (i.e., the release of cytokines, activation of the inflammasome, and increased mobility) (Niessen et al., 2008). Furthermore, mice lacking PAR1 or S1P3 had attenuated coagulation in a LPS model of disseminated intravascular coagulation (Niessen et al., 2008). Activated platelets can also recruit immune cells through the release of inflammatory chemokines (e.g., CXCL1, CXCL4, CXCL5), which help to recruit leukocytes to nascent clots (Semple et al., 2011). Activated platelets also express selectins, which help cells such as neutrophils adhere to thrombi (Semple et al., 2011). During inflammation, monocytes and neutrophils have been shown to express TF, and monocytes can also release TF in microparticles, which can be involved in the formation and amplification of clots (Brühl et al., 2012; Maugeri et al., 2006; Todoroki et al., 2000). Additionally, neutrophil extracellular traps (NETs) released by activated neutrophils can contribute to coagulation through a variety of mechanisms (Engelmann and Massberg, 2012; Fuchs et al., 2010; Massberg et al., 2010). During NETosis neutrophils release neutrophil elastase, which inactivates two anticoagulant molecules, tissue factor pathway inhibitor (TFPI) and thrombomodulin (Glaser et al., 1992; Massberg et al., 2010). NETs also activate platelets, and act as a scaffold for platelets to adhere to, thereby contributing to the localized growth of a thrombus (Fuchs et al., 2010).

Histones released in NETs can also activate platelets through Toll-like receptor 2 (TLR2) and TLR4 signaling (Semeraro et al., 2011; Xu et al., 2011).

Immunothrombosis

Although, thrombosis is usually thought of as a pathological condition, research has revealed that the connection between the innate immune system and coagulation in mammals can be beneficial in protecting against pathogens. This processes was termed 'immunothrombosis' in 2012 by Engelmann and Massberg (Engelmann and Massberg, 2012). This link between the innate immune systems and thrombosis makes is intuitive because a break in the endothelium (i.e., in the skin), can be an entry point for pathogens (T G Loof et al., 2011). This connection was first made clear within arthropods (i.e., horseshoe crabs) because they lack an adaptive immune system, and innate pathways of immunity play a larger role in their defense against pathogens (Krem and Cera, 2002; Torsten G Loof et al., 2011). The horseshoe crab has only one blood cell called an amoebocyte. In the event of injury, amoebocytes rapidly migrate to the injured site and release factors that initiate coagulation. This is functionally analogous to the thrombotic process in the mammalian system and cumulates in the cleavage of the zymogen coagulogen to coagulin (analogous to fibrinogen to fibrin conversion) to form a coagulin-amoebocyte clot. This clot allows the amoebocytes to efficiently phagocytose invading pathogens while sealing the injury and preventing further invasion by pathogens (Torsten G Loof et al., 2011).

In the mammalian system, immunothrombosis has been shown to help defend against several pathogens. This is thought to occur through a variety of concordant mechanisms. First,

microthrombi have been shown to entrap pathogens (i.e., *E. coli, Yersinia enterocolitica*). This entrapment limits pathogen dissemination through the vasculature and migration of pathogens into tissues. Second, microthrombi create a compartment in which antimicrobial peptides can accumulate. Third, thrombi create an environment near the invading pathogen to which additional immune cells can quickly aggregate. Finally, activated platelets can directly participate in the innate immune response by releasing inflammatory cytokines (e.g., CXCL1, CXCL4, CXCL5) (Semple et al., 2011).

Unfortunately, some pathogens have evolved systems to evade or exploit coagulation. *Streptococcus pyogenes* can enhance clot dissolution through the expression of streptokinase and DNase. Streptokinase activates the host's plasminogen, which helps to resolve clots by breaking down fibrin (Bergmann and Hammerschmidt, 2007; Sun et al., 2004). *Streptococcus pneumonia* has also been shown to express EndA, a DNase that breaks down the DNA matrix in prothrombotic NETs (Beiter et al., 2006). Using different mechanisms, *Staphylococcus aureus* can exploit thrombotic responses by facilitating platelet aggregation and then adhering to platelets, thus preventing clearance by the immune system (Yeaman, 2010).

Additionally, thrombosis in response to pathogens can be detrimental to the host, especially if it is very widespread (as in disseminated intravascular coagulation) or in critical tissues (i.e., brain, heart, lungs), where it can interfere with blood flow as occurs in ischemic stroke (Siegel et al., 2015). Examples of this pathological response include patients with COVID-19 and sepsis, who suffer from reduced cerebral blood flow (CBF) in conjunction with cerebral thrombi (Helms et al., 2020; Semmler et al., 2008; Soldatelli et al., 2020). Additionally, clotting during cerebral malaria, caused by the Apicomplexa parasite *Plasmodium falciparum,* has been associated with worse outcomes in pediatric cases (Hemmer et al., 1991; Moxon et al.,

2015, 2013; Vogetseder et al., 2004). *Plasmodium* induces infected erythrocytes to adhere to blood vessels through the formation of 'knobs' on the infected RBC surface. Knobs are nano-scale structures made up of knob-associated histidine rich protein (KAHRP) and *P. falciparum* erythrocyte membrane protein 1 (PfEMP1) (Aikawa et al., 1990; Crabb et al., 1997; Roberts et al., 1985), and can adhere to CD36, ICAM-1, and chondroitin sulfate A on the endothelium (Lubiana et al., 2020; Rowe et al., 2009; Turner et al., 2013).

Interestingly, another Apicomplexa parasite, *Toxoplasma gondii* has been shown to cause clotting in the liver (Johnson et al., 2003a). *T. gondii* is a highly successful eukaryotic parasite, which chronically infects 1/3 of humans worldwide (Pappas et al., 2009). The most common route of infection is oral, and the parasite initially disseminates throughout the periphery during acute infection, before being cleared by the host's immune response (Dupont et al., 2012; Hill and Dubey, 2002). However, *T. gondii* persists within tissue cysts in brain and muscle tissue. Often the acute infection stage is mild within immunocompetent individuals, but the parasite can cause major pathology in immunocompromised individuals, discussed in further detail below. Unlike *P. falciparum*, which replicates inside hepatocytes and red blood cells, *T. gondii* can replicate and eventually lyse any nucleated cell, including endothelial cells at the blood-brain barrier (Konradt et al., 2016a; Kumar and Tolia, 2019), which could expose subendothelial TF in the brain. Furthermore, recent work showed that cerebral blood flow is disrupted during *T. gondii* infection in a mouse model (Estato et al., 2018). However, these previous studies have not examined whether thrombosis occurred in the brains of mice infected with *T. gondii*.

Toxoplasma gondii life cycle

Toxoplasma gondii is an obligate intracellular eukaryotic parasite in the Apicomplexa phylum (Dubey and Frenkel, 1972; Hill and Dubey, 2002). It can infect any warm-blooded animal, including humans. *T. gondii* has three different infectious stages: sporozoites in oocysts, the rapidly growing tachyzoite stage found during acute infection, and the slowly growing bradyzoite form found in tissue cysts (Hill and Dubey, 2002).

Oocysts are a critical stage for the spread of *T. gondii* because they can survive within the environment for months (Tenter et al., 2000). Furthermore, they are resistant to disinfectants, due to their relative impermeability (Tenter et al., 2000). Oocysts are formed after *T. gondii* undergoes sexual reproduction within the intestines of a feline (the definitive host). Cats are the only host that can naturally excrete oocysts (Frenkel et al., 1970). For decades, the reason that *T. gondii* only undergoes sexual reproduction in felids remained a mystery. However, it was recently discovered that the enzyme delta-6-desaturase, which metabolizes linoleic acid, was responsible for this species specificity (Martorelli Di Genova et al., 2019). Felines are the only mammals that lack delta-6-desaturase activity in their small intestine, and therefore, they do not metabolize linoleic acid, which results in increased levels of linoleic acid in the gut. Linoleic acid is cytotoxic to the asexual tachyzoite stage (Martorelli Di Genova et al., 2019; Shamseddin et al., 2015; Sinclair et al., 1979) and induces sexual reproduction in another eukaryotic organism (i.e., fungi) (Horowitz Brown et al., 2008; Martorelli Di Genova et al., 2019). Interestingly, researchers were able to reverse the species specificity of the sexual reproduction of *T. gondii* by blocking delta-6-desaturase activity or supplementing linoleic acid in mice, which resulted in *T. gondii*-infected mice secreting oocysts (Martorelli Di Genova et al., 2019). Once the oocyst is

excreted from the infected feline in feces it can enter the food or water supply (e.g., by contaminating livestock or vegetables) (Tenter et al., 2000).

Intermediate hosts, including non-felid warm-blooded animals such as humans, can become infected if they consume water or food contaminated with oocysts or tissue cysts containing bradyzoites. Within the small intestines the parasites excyst and convert into the rapidly growing tachyzoite form and begin to infect nearby host cells (i.e., enterocytes) (Dubey, 1998). The tachyzoite form of *T. gondii* destroyed by acid in the stomach, so are not typically infectious orally (Dubey, 1998).

T. gondii can infect any nucleated cell within its host, where it will grow and replicate inside a parasitophorous vacuole (Fig. 1.3). *T. gondii* invasion into a cell has three major parts: loose attachment, tight attachment, and finally, entry. Loose attachment is mediated by proteins which coat the surface of *T. gondii* tachyzoites, including glycosylphosphatidylinositol (GPI)-anchored surface antigens (SAGs), particularly SAG1-2 (Blader and Saeij, 2009; Lekutis et al., 2001). Neutralization of SAG1 and SAG2 with monoclonal antibodies causes diminished adhesion of *T. gondii* to host cells (Lekutis et al., 2001). After the initial loose attachment, *T. gondii* establishes a tighter connection to the host cell, which is mediated by secreted microneme proteins (e.g. MIC2) and the formation of the moving junction. MIC2 is a transmembrane adhesin, which is rapidly moved to the apical surface upon contact with a host cell. MIC2 binds to host molecules, such as intracellular adhesion molecule-1 (ICAM-1), heparin, and chondroitin sulfate A and C (Barragan et al., 2005; Brossier and Sibley, 2005; Harker et al., 2014; Huynh and Carruthers, 2006). The moving junction is established by the cooperation of several *T. gondii* proteins, including the apical membrane antigen 1 (AMA1) and rhoptry neck proteins (RON proteins). In the moving junction, AMA1 anchored to the plasma membrane of *T. gondii* binds to

the RON complex injected in the host cell's plasma membrane (Blader et al., 2015). Once the moving junction is established, *T. gondii* enters the host cell through invagination, creating the parasitophorous vacuole membrane out of the host's own plasma membrane (Fig. 1.3)(Mordue et al., 1999). The moving junction also acts as a sieve to prevent the host's transmembrane proteins from transferring over to the surface of the parasitophorous vacuole, thus creating a nonfusogenic compartment, avoiding the host cells endocytic and exocytic machinery (Mordue et al., 1999).

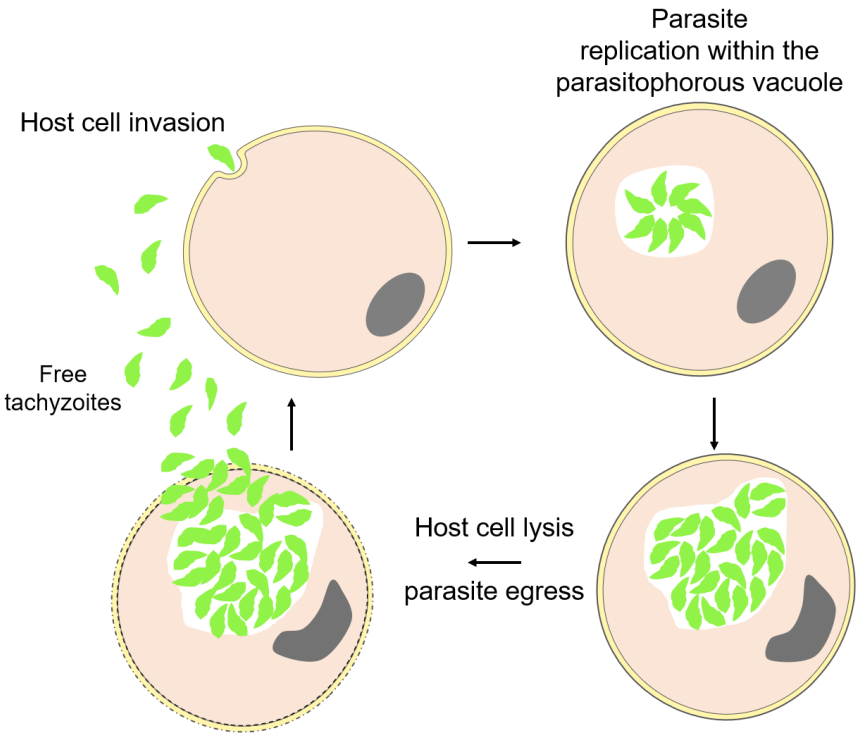

Figure 1.3. Lytic lifecycle of *T. gondii*. A model of the *T. gondii* invasion, replication, and lysis cycle.

After replication, *T. gondii* will egress from the host cell, lysing the cell in the process (Fig. 1.3)(Blader et al., 2015). After approximately 1-2 days in mouse models, parasitemia (tachyzoites within the blood) can be detected after oral infection (Dubey, 1998). During acute

infection, the parasites can be found in many organs throughout the body. But eventually, *T. gondii* is cleared from most tissues, persisting in the bradyzoite form within tissue cysts in long-lived tissues, such as the muscle and brain (Dubey, 1998). This chronic infection lasts for the lifetime of the host. It is hypothesized that tissue cysts occasionally rupture, releasing parasites, but that the excysted parasites are rapidly killed in an immunocompetent host (Dubey, 1998). Failure to control the excysted parasites can result in reactivation of widespread infection of the host and serious CNS pathology, which will be discussed later.

T. gondii epidemiology

Approximately, 1/3 of the global population is chronically infected with *T. gondii*, with geographical variation in prevalence (Pappas et al., 2009). In the United States approximately 10% of the population carries *T. gondii* (Maldonado et al., 2017; Pappas et al., 2009). Risk factors include eating undercooked meat contaminated with tissue cysts, having greater than three cats (though limiting their hunting by keeping them indoors minimizes risk), handling raw meat, and consuming raw shellfish (Hill and Dubey, 2002; Maldonado et al., 2017). Additionally, outbreaks have been linked to contamination of vegetables and water supplies by infected cat feces containing oocysts (Hill and Dubey, 2002; Maldonado et al., 2017).

Genotyping studies have found that there are three major clonal lineages (Type I, II, and III) of *T. gondii* in North America and Europe. These types are very similar to each other, with greater than 98% sequence identity at the nucleotide level, and the Type I and III lineage may have evolved from a Type II ancestor (Boyle et al., 2006; Su et al., 2006). Additionally, a recent lineage has been found in North American wildlife (Type XII) (Khan et al., 2011). In contrast to

the conserved lineages observed in North America and Europe, *T. gondii* in South America are highly diverse, and have been termed 'atypical' (Khan et al., 2007; Su et al., 2012). This genetic diversity has been hypothesized to suggest that *T. gondii* primarily propagates asexually in North America and Europe, while sexual propagation, resulting in genetic recombination, is more common in South America than in other regions (Su et al., 2012). Atypical strains have also been found in Australia and Africa. These 'atypical' strains have been associated with more serious disease than infection with the Type I-III lineages in immunocompetent individuals, such as eye pathology and multi-organ involvement (Dardé et al., 1998; Demar et al., 2007; Grigg et al., 2001).

T. gondii clinical disease

The most common route of *T. gondii* infection is oral, through the consumption of tissue cysts in undercooked meat or oocysts from contaminated vegetables or water (Hill and Dubey, 2002). However, *T. gondii* can also be acquired through tissue transplant with an infected tissue, or congenitally if a pregnant woman becomes infected for the first time during a pregnancy and lacks preexisting maternal antibodies to control the infection (Hill and Dubey, 2002; Maldonado et al., 2017). The consequences of infection vary greatly in severity based on the immunocompetency of the host or the development of the immune system and will be discussed in the following groups: immunocompetent individuals, immunocompromised individuals, and fetuses.

In immunocompetent individuals, the initial acute infection is typically asymptomatic, though patients may experience flu-like symptoms (Hill and Dubey, 2002). The infected

individual is often not aware they have been infected (Maldonado et al., 2017). However, as mentioned previously, immunocompetent hosts can develop more serious ocular disease when infected with 'atypical' strains. Since the parasite persists within tissue cysts in the brain, if an individual becomes immunocompromised later in life (e.g., due to untreated HIV infection, chemotherapy for cancer, or by taking immunosuppressive drugs for organ transplantation), they can develop much more serious pathology, as discussed below.

In immunocompromised individuals, severe toxoplasmosis is often the result of reactivation of a latent infection (Luft and Remington, 1992; Roth et al., 1992). One of the most common and serious presentations is toxoplasmic encephalitis with one or more brain abscesses (Montoya and Liesenfeld, 2004). Toxoplasmic encephalitis can present acutely or as a more progressive condition over weeks with neurological issues, such as mental status changes (including confusion), seizures, motor defects (such as hemiparesis), speech abnormalities, cerebellar symptoms, and sensory abnormalities (Montoya and Liesenfeld, 2004). Patients can be diagnosed with neuroimaging (i.e., magnetic resonance imaging) and PCR. With imaging, 'ring-enhancing' lesions can often be found, however, to rule out lymphomas or other pathogens, PCR of the cerebrospinal fluid for *T. gondii* DNA can be used as a highly specific follow-up exam (Marra, 2018). Toxoplasmosis in immunocompromised patients can also present as chorioretinitis, pneumonia, or with multi-organ involvement. Treatment occurs in two stages, a primary treatment to control the infection, followed by longer-term suppressive treatment until immune recovery occurs. Common therapeutics to treat *T. gondii* infection include pyrimethamine, sulfadiazine, and combination trimethoprim/sulfamethoxazole (Marra, 2018). Notably, these therapeutics do not cure *T. gondii* infection, as they have limited efficacy on the bradyzoite form of the parasite.

Congenital infection (vertical transmission) occurs when *T. gondii* transverses the placenta in a pregnant woman. This can occur during several scenarios, most commonly when a naïve pregnant woman (not previously exposed to *T. gondii*) becomes acutely infected, if an infected woman becomes immunosuppressed while pregnant and the parasites reactivate, or more rarely, if a previously infected woman is infected by a more virulent atypical *T. gondii* strain (Maldonado et al., 2017). The likelihood of congenital infection increases with gestational age; however, the severity of symptoms decreases with gestational age (Dunn et al., 1999; Sterkers et al., 2012). The most severe consequence of congenital infection is spontaneous abortion. But children born with congenital toxoplasmosis can suffer ocular (e.g., chorioretinitis, cataracts, macular degeneration, visual impairment), CNS (e.g., seizures, brain masses, developmental delays), and many other more systemic and peripheral issues (e.g., pre-term birth, anemia, myocarditis) (Maldonado et al., 2017). Universal prenatal screening for maternal *T. gondii* seroconversion during pregnancy is common in countries such as France, Austria, and Slovenia but rare in the US (however, Massachusetts and New Hampshire carryout neonatal screening), and was recently found to be more cost-effective than postnatal screening efforts (Binquet et al., 2019).

Immunity to T. gondii

Control of *T. gondii* infection requires the activation of both innate and adaptive immune cells. Initially, dendritic cells release IL-12 in response to *T. gondii* infection, which stimulates $CD4^+$ T cells and NK cells to produce IFN-γ (Scharton-Kersten et al., 1998; Yarovinsky, 2014). Additionally, neutrophils release IFN-γ through a IL-12-independent pathway, which is instead regulated by TNF and IL-1β (Sturge et al., 2013). IFN-γ is involved in host-defense against *T.*

gondii through several different mechanisms. First, IFN-γ upregulates indoleamine 2-3-dioxygenase (IDO), which converts tryptophan to N-formylkynurenine (Pfefferkorn et al., 1986). This conversion decreases the availability of tryptophan, thus starving *T. gondii* of one of its essential amino acids (Pfefferkorn, 1984). Second, IFN-γ induces the production of nitrogen oxide (NO), which involves the production of nonpolar uncharged intermediates. These NO intermediates can modify proteins (for example at reactive thiols, heme groups, and iron-sulfur clusters) and can cross cell membranes to interact directly with *T. gondii*, interfering with metabolic enzymes (Fang, 2004; Yarovinsky, 2014). Furthermore, NO synthesis depletes arginine, which is also an essential amino acid for *T. gondii* (Adams et al., 1990; Fox et al., 2004). Finally, IFN-γ activates immunity-related GTPases (IRGs), which cause vesiculation of the parasitophorous vacuole membrane, leading to disruption of the parasitophorous vacuole and killing of the parasite through lysosome-mediated degradation (Ling et al., 2006; Martens et al., 2005). Interestingly, these host-defense mechanisms are species specific, as humans only have one IRG, compared to 21 in mice, and its role in *T. gondii* defense is controversial (Bekpen et al., 2005; Yarovinsky, 2014).

Monocytes also have an essential role in host defense against *T. gondii,* and are present in the CNS during acute and chronic *T. gondii* infection (Biswas et al., 2015; Dunay et al., 2010, 2008; Robben et al., 2005; Schneider et al., 2019). During *T. gondii* infection inflammatory ($Ly6C^{high}CCR2^{+}$) monocytes contribute to *T. gondii* control through the production of cytokines, including IL-1α, IL-1β, TNF-α, and IL-6 (Biswas et al., 2015). Monocytes also release anti-parasitic effector molecules during *T. gondii* infection (e.g., reactive oxygen species and NO) (Biswas et al., 2015). However, monocytes may also play a role in *T. gondii* dissemination across the blood-brain barrier, discussed below.

Ultimately, a strong T cell response is necessary to establish long-term protection against *T. gondii*. This is demonstrated by the inability of patients with acquired immunodeficiency syndrome (AIDS) to control latent *T. gondii* infection after their $CD4^+$ T cells are depleted (Luft and Remington, 1992). Additionally, severe combined immunodeficient (SCID) mice, which lack T and B cells, die during *T. gondii*-infection and can be rescued with adoptive transfer of lymphocytes from immunocompetent mice (Hunter et al., 1993; Johnson, 1992). $CD4^+$ and $CD8^+$ cells contribute to host defense against *T. gondii* mainly through the production of protective cytokines, including IFN-γ and TNF-α (Yap and Sher, 1999). T cells also mediate perforin-dependent cytotoxicity, which is involved in the immune response against *T. gondii*, but may have a smaller role in the brain, where many infected cells are MHC class I^- neurons (Schlüter and Barragan, 2019).

T. gondii dissemination across the blood-brain barrier

The blood-brain barrier is a specialized barrier within the host, acting to limit the dissemination of many molecules and cells from the blood into the brain parenchyma. This is largely due to the unique nature of endothelial cells that make up the blood-brain barrier, as they have low rates of endocytosis, express tight junction proteins (e.g., Claudin-5 and Occludin), and have selective transporters for specific molecules [e.g., glucose transporter 1 (GLUT1)]. These properties of endothelial cells at the blood-brain barrier are induced, and maintained by the surrounding cells in the brain (i.e., pericytes, astrocytes, microglia, and neurons)(Abbott et al., 2006). Functionally, the restrictive nature of the blood-brain barrier to cells and molecules makes it a formidable barrier to cross, which protects the CNS against invasion by most pathogens (Coureuil et al., 2017).

However, *T. gondii* can breach the blood-brain barrier. Currently, there is evidence for several different mechanisms by which *T. gondii* crosses the blood-brain barrier (BBB). One mechanism is the intracellular "Trojan horse" mechanism, which involves parasites entering the brain parenchyma within infected leukocytes (e.g., monocytes), which extravasate across the blood-brain barrier during *T. gondii* infection (Fig. 1.4)(Courret et al., 2006; Lachenmaier et al., 2011). Eventually, the parasites lyse the infected leukocyte, and can infect surrounding cells (e.g., neurons). Interestingly, *in vitro* work demonstrated that *T. gondii*-infected monocytes move more quickly and further distances than non-infected monocytes (Ueno et al., 2014). Recent work has also suggested that another approach *T. gondii* may use to breach the BBB is direct infection and lysis of vascular endothelial cells in the brain (Konradt et al., 2016a).

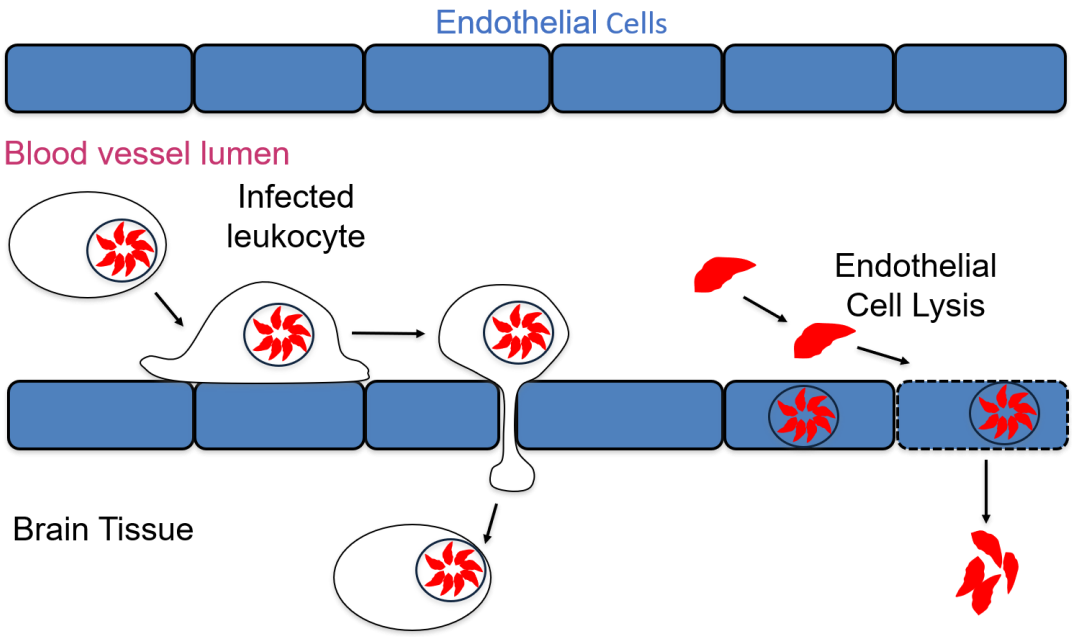

Figure 1.4. Mechanisms of *T. gondii* dissemination across the BBB. The left side shows the Trojan horse model of *T. gondii* dissemination, by which *T. gondii* crosses the BBB in an infected leukocyte. The right side shows endothelial cell lysis, another possible mechanism by which *T. gondii* can disseminate across the BBB.

The evidence of endothelial cell lysis and the presence of monocytes in the brain during *T. gondii* infection may support the formation of thrombi in the CNS. Indeed, previous research has shown that mice deficient in clotting, or treated with warfarin [a commonly used anti-coagulative therapeutic, which lowers the bioavailability of Vitamin K a cofactor needed for activation of FII, FVII, FIX, FX (Holbrook et al., 2005)], do not survive acute *T. gondii* infection, unlike their control counterparts (Johnson et al., 2003a; Mullarky et al., 2006). Furthermore these mice were found to have gross hemorrhage in their livers upon necropsy (Johnson et al., 2003a). However, whether *T. gondii* infection induced thrombosis in the brain was not examined. Therefore, this work sought to investigate whether thrombosis was occurring in the brains of mice infected with *T. gondii* and whether cerebral blood flow was affected in these mice. In order to do this, we first developed a technique to longitudinally measure cerebral blood flow in mice relatively non-invasively over the course of 100+ days (Hoover et al., 2021). We then examined *T. gondii*-infected animals for evidence of clotting and disrupted cerebral blood flow. Ultimately, these findings could contribute to a better understanding of cerebral pathology and thrombotic responses during infection.

Chapter 2

Transcranial chronic optical access method to longitudinally measure cerebral blood flow

Introduction

Cerebral blood flow (CBF) regulation is essential for normal brain functioning, and many physiological and pathological conditions may cause disruption in CBF. Stroke (Siegel et al., 2015), Alzheimer's disease (Kogure et al., 2000; Ruitenberg et al., 2005), and aging (Martin et al., 1991) can have long-lasting negative effects on CBF, whereas acute infection, such as with SARS-CoV2, can cause short-term effects on CBF in Covid-19 patients (Helms et al., 2020; Soldatelli et al., 2020). There are currently few techniques to study long-term CBF changes or the efficacy of therapeutic modulation of CBF in animal models.

The ability to measure CBF in the same animals longitudinally over time has several advantages. First, it reduces the number of experimental animals needed to examine the kinetics of CBF changes, as researchers can investigate CBF dynamics in the same set of mice, rather than euthanizing separate cohorts of mice for each time-point. Second, the ability to determine a baseline measurement of CBF before a pathology manifests or prior to induced changes in blood flow controls for inter-animal variation in CBF, as each animal can serve as its own internal control. Current approaches for measuring CBF in animal models include methods based on magnetic resonance imaging (Calamante et al., 1999), positron emission tomography (Heiss et al., 1994), microscopy, such as two-photon excitation fluorescence microscopy (Drew et al., 2010; Kleinfeld et al., 1998; Schaffer et al., 2006; Shih et al., 2015; Zhang and Murphy, 2007), and wide-field optical techniques like laser speckle imaging (LSI) (Boas and Dunn, 2010; Dunn et al., 2001; Fercher and Briers, 1981). Among these techniques, only two-photon microscopy and LSI provide the spatial resolution necessary to image individual blood vessels (Dunn et al., 2001; Shih et al., 2012).

LSI has been used to measure CBF dynamics in a wide-range of neurologically relevant conditions, such as cardiac arrest (Crouzet et al., 2016), cortical spreading depression (Dunn et al., 2001), and stroke (Schrandt et al., 2015; Sunil et al., 2020). Unlike two-photon microscopy, which enables absolute measurements of cerebral blood flow, LSI detects relative blood flow in biological tissues (Boas and Dunn, 2010; Dunn et al., 2001; Fercher and Briers, 1981). However, LSI involves a simpler imaging platform and does not require the use of exogenous dyes or transgenic animals with fluorescently labeled vasculature (e.g., Tie2-GFP mice) to visualize the dynamics of flow in cerebral vessels (Drew et al., 2010; Kleinfeld et al., 1998; Schaffer et al., 2006; Shih et al., 2015; Zhang and Murphy, 2007).

An important consideration in imaging cerebral blood flow is balancing clear optical access with the potential for damage inflicted by a surgical procedure. Craniotomy and skull-thinning surgeries can provide optimal access for two-photon microscopy and LSI. However, these approaches require highly precise surgical skill to avoid inducing permeability of the blood-brain barrier (BBB) due to heat from drilling (Luan et al., 2017; Shoffstall et al., 2018). Removing a portion of the skull may also cause a temporary inflammatory response or induce bone re-growth, resulting in diminished optical access (Xu et al., 2007). LSI does not require a craniotomy or skull-thinning surgery, since this technique can be done through the intact hydrated skull of mice once the scalp is resected (Ayata et al., 2004b). Resecting the scalp is a simpler surgical procedure than craniotomy or skull thinning. The shorter time-frame for surgery may increase the number of animals a researcher can reasonably include in a study (since a craniotomy can require four or more hours to perform (Goldey et al., 2014)), while also reducing the length of time that each animal is under anesthesia. However, to our knowledge, there have

been no reports of maintaining long-term optical access to measure CBF with LSI through an intact skull.

Here we describe a surgical method in mice that we have named cyanoacrylate skull (CAS), which enables continuous chronic optical access through an intact skull. The CAS approach enables bi-hemispheric imaging of cerebral blood vessels using LSI or other wide-field optical imaging techniques. Using CAS, we were able to stably measure functional CBF for more than 100 days post-surgery and detect acute changes in CBF due to hypercapnia (elevated CO_2). This procedure can take a skilled researcher less than one hour to complete, which is significantly less time than performing a craniotomy. The CAS technique may prove useful for researchers investigating relative cerebral blood flow, as it will enable studies on changes in long-term CBF in human-relevant disease models (e.g., Alzheimer's disease, stroke, infection), as well as the ability to evaluate therapy-induced CBF changes over time.

Materials and Methods

Animals

All procedures and protocols were approved by the Institutional Animal Care and Use Committee at the University of California, Irvine. Procedures were performed on 2-5 month-old male and female C57BL/6J mice purchased from Jackson Laboratories.

Surgical Preparation

A schematic of the surgery is shown in Fig. 2.1A, and accompanying images of each step of the surgery are shown in Fig. 2.1B-E. Mice were anesthetized with O_2 vaporized isoflurane

(2% for induction, 1-1.5% for maintenance, Patterson Veterinary, Devens, MA). Body temperature was maintained at 37˚C with a feedback heating pad (Harvard Apparatus, Holliston, MA). Sterile eye ointment (Rugby, Livonia, MI) was applied to prevent corneal drying. Carprofen (10 mg/kg, s.c., Zoetis) and topical 2% lidocaine hydrochloride jelly (Akorn, Lake Forest, IL) were administered to provide systemic and local analgesia, respectively. Mice were given Ringer's lactate solution (0.2 mL/20 g/hr, s.c.) to replace fluids. All surgical tools were sterilized using a glass bead sterilizer (Germinator 500). Following shaving and sterilization with Povidone-iodine for five minutes, the scalp was resected to expose bregma and lambda. 2% lidocaine hydrochloride jelly was reapplied to the exposed fascia (Fig. 2.1B), which was subsequently removed. Afterwards, the skull was dried with ethanol (70% in DI water) (Fig. 2.1C). Three thin layers of cyanoacrylate (Vetbond, 3M) were applied using a double-ended micro spatula (Fine Science Tools). Each layer was composed of a single drop of cyanoacrylate (~15 µL) and allowed to dry between applications to ensure smoothness (Fig. 2.1D). Multiple layers of cyanoacrylate prevented potential skull exposure from the mice, as they occasionally scratch at the surface. After the cyanoacrylate layers were dry, a ~2 mm deep well was then made using acrylic resin Ortho-Jet BCA (Lang Dental, Wheeling, IL) around the edges of the surgical prep, and a final thin layer of cyanoacrylate was applied over the previous cyanoacrylate layers (Fig. 2.1E, Supplemental Video 1). A second dose of Carprofen (10 mg/kg, s.c., Zoetis) was administered one day post-operation (dpo). Mice were not returned to their home cages until their skulls were uniformly covered with cyanoacrylate to prevent infection. After the procedure, mice can be co-housed and handled as normal (i.e., being held by the scruff for injections). No signs of distress (i.e., low activity, hunched poster, or piloerection) were noted. Animals were allowed to recover from the surgery for 3-5 days before longitudinal imaging was performed.

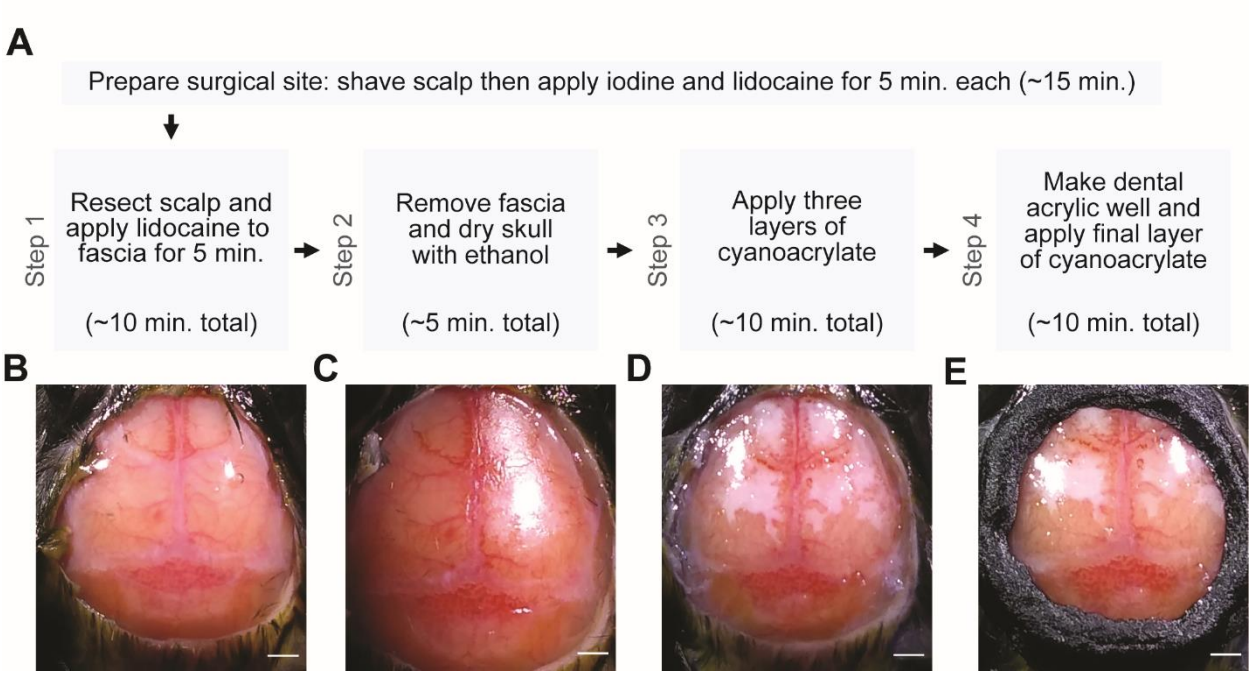

Figure 2.1. Surgical procedure for chronic optical access. A) Flowchart showing steps for the surgical procedure, as well as the approximate time that it takes to complete each step. B-E) Representative image of surgical site after each step of the surgical procedure. Scale bars: 1 mm.

Imaging Instrumentation

To obtain cerebral blood flow (CBF) data, we used laser speckle imaging (LSI) (Crouzet et al., 2016; Dunn et al., 2001). A schematic of the setup is shown in Fig. 2.2A. A long-coherence 785 nm laser (Ondax, Monrovia, CA) was used as the excitation source. Laser light was transmitted through beam expansion optics, which included an aspheric lens (ThorLabs, Newton, NJ) and ground glass diffuser (ThorLabs, Newton, NJ), to achieve near-uniform illumination of the cortex. Raw speckle images (10 ms exposure time) were acquired using a 4x Achrovid objective with a 37 mm working distance (Edmund Optics, Barrington, NJ) and monochrome CMOS camera (FLIR, Wilsonville, OR). Cross-polarization optics between the source and detector were used to remove specular reflection.

Imaging, Data Acquisition, and Data Processing

For imaging, mice were anesthetized with O_2 vaporized isoflurane (2% for induction and 1.5% for maintenance, Patterson Veterinary, Devens, MA). Sterile eye ointment (Rugby, Livonia, MI) was applied to prevent corneal drying. Body temperature was maintained at 37˚ C with a feedback heating pad (Harvard Apparatus, Holliston, MA), as described above. Saline was then applied to the cyanoacrylate and a glass coverslip (Fisherbrand, 12CIR-2) was placed on top for 10 min prior to image acquisition to allow the relative blood flow to stabilize. Total imaging time takes approximately 14 minutes per mouse. Each mouse was imaged 11 to 14 times over 105 days.

Raw speckle images were acquired at 60 Hz using a LabVIEW (National Instruments, Austin, TX) program. First, all raw speckle images were converted to CBF maps using the spatial speckle contrast algorithm to detect periods of motion artifact. A 5 x 5 sliding window was used to convert each raw speckle image to a corresponding speckle contrast (K) image using the equation $K = \sigma / < I >$, where σ is the standard deviation of the intensity and <I> is the average intensity within each sliding window position. Each speckle contrast image was then converted to a CBF map using a simplified speckle imaging equation $CBF = \frac{1}{2TK^2}$ (Ramirez-San-Juan et al., 2008). Next, sharp spikes due to breathing were manually defined in the CBF time course as periods of motion artifact. These time points were removed from the calculation of the temporal speckle contrast.

MATLAB (MathWorks, Natick, MA) code was written to convert raw speckle images to CBF maps using the temporal speckle contrast algorithm (Cheng et al., 2003). The temporal algorithm was chosen, as it is less susceptible to static scatterers, such as the skull, than the spatial algorithm (Li et al., 2006; Ramirez-San-Juan et al., 2014). Speckle contrast (K) was

calculated as the ratio between the standard deviation and the mean intensity at each pixel over 60 raw speckle images without motion artifact caused by breathing. A 3x3 spatial averaging filter was then applied to the temporal speckle contrast image to reduce noise. Each speckle contrast image was then converted to a CBF map using a simplified speckle imaging equation $\mathrm{CBF} = \frac{1}{2TK^2}$, where T is the exposure time (Ramirez-San-Juan et al., 2014).

Hypercapnia Experiments

Mice were imaged continuously for 15 minutes. For the first 5 minutes, they breathed room air to establish baseline readings. Then they were challenged for 5 min with 5% CO_2 with balanced room air to induce hypercapnia, and for the last 5 minutes they breathed room air (Fig. 2.3A).

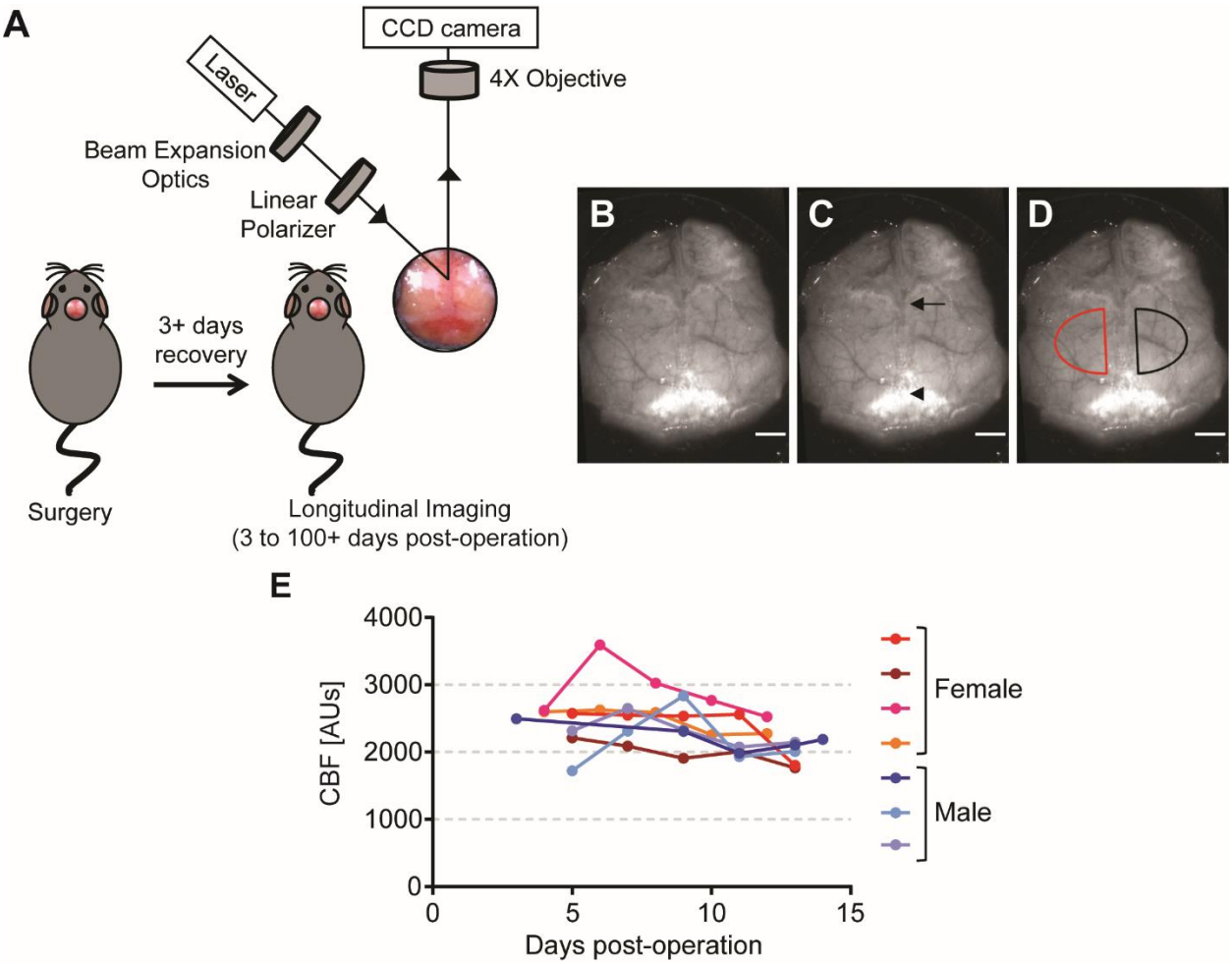

Figure 2.2. Laser speckle imaging of mice. A) Schematic of laser speckle imaging set-up. B) Example of green light image of the brain. C) Green light imaging showing bregma (arrow) and lambda (arrowhead). D) Green light image showing ROIs (half circles) over left and right side of the skull. Scale bars: 1 mm. E) Cerebral blood flow (CBF) of all animals during first two weeks.

Data Quantification

To assess longitudinal CBF changes using the CAS preparation, speckle contrast images at each time point were aligned using MATLAB code (Lertsakdadet et al., 2018). Using the aligned data, a point at bregma and lambda were selected. Two semi-elliptical regions of interest (ROIs) offset by +/- 0.5 mm from the midline with radii of 1.05 mm along the short axis and 1.63 mm along the long axis. were used to obtain longitudinal CBF data. The same ROI per animal was

used for every time point. A representative example of ROI selection is shown in Fig. 2.2B-D. The median CBF from each ROI was calculated, and the median CBF values for the right and left hemispheres were averaged and used for further statistical analyses. In the case of one mouse (Fig 2E, light blue), only the CBF from the right hemisphere was included, as the other ROI had a scattering artifact due to an uneven coating of cyanoacrylate or to insufficient removal of fascia.

To assess hypercapnia-induced CBF changes, the spatial speckle contrast algorithm was used. For each imaged mouse, four ROIs were selected. The two semi-elliptical ROIs (described above) were used to obtain a more global CBF measurement. Two small ROIs (one left hemisphere, one right hemisphere) were also defined. A representative example of the ROI selection is shown in Fig. 2.3B. For each ROI, a CBF time course was obtained. A 10s sliding median filter was applied to the CBF time courses to remove the pulsatile component. The median-filtered data was downsampled to a sampling frequency of 1Hz. The downsampled data was then normalized to the mean median-filtered CBF calculated over a one-minute interval immediately prior to onset of hypercapnia to create a rCBF time course.

In addition, we determined the smallest vessels that could be resolved in this system by analyzing images from a subset of the mice in ImageJ. First, we applied an automated threshold to detect vessels, created a mask, and smoothed the resulting image with a Guassian blur (sigma set to 0.75). With this procedure, vessels as small as 40 μm could be resolved.

Statistical Analysis

GraphPad Prism 7.02 software was used for statistical analyses. A two-way repeated measures ANOVA followed by a post-hoc Tukey test was used to test the left and right hemispheres, as well as the small and large ROIs for significant differences in rCBF after the start of the hypercapnia challenge from baseline (average of 5 minutes prior to hypercapnia). Differences between groups in the longitudinal imaging dataset were determined using a repeated measures one-way ANOVA, followed by a post-hoc Tukey test. $P < 0.05$ was considered significant.

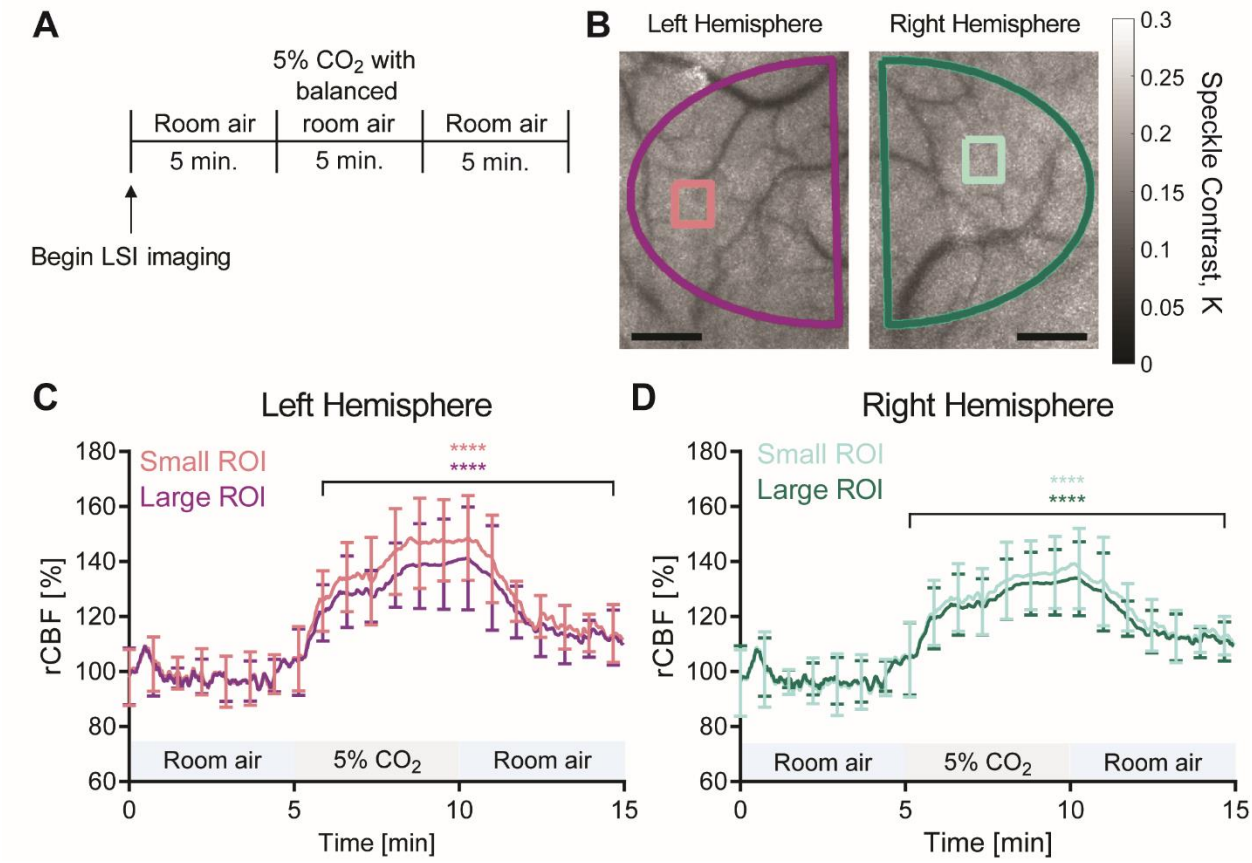

Figure 2.3. Relative cerebral blood flow during hypercapnia challenge. A) Experimental set-up of hypercapnia challenge. B) Speckle contrast image at baseline showing representative large ROIs (half circles) and small ROIs (rectangles) in the right and left hemispheres. Scale bars: 1 mm. C-D) Percent change of rCBF to baseline (prior to challenge). **** $P < 0.0001$; significance was calculated by a repeated measures two-way ANOVA, with a post-hoc Tukey test. Each time point after challenge was compared to baseline. No significant difference was found between the large and small ROIs or left and right hemisphere. Error bars represent SD.

Results & Discussion

We used LSI to measure the CBF of seven mice (four females and three males) for the first two weeks after implementation of the CAS surgical technique (Fig. 2.2E). CBF values from the right and left hemisphere were averaged to account for the blood flow changes across both hemispheres (Fig. 2.2D-E). Overall, we found little difference in CBF among individual mice or between males and females during the first two weeks after surgery.

To assess our ability to detect dynamic CBF changes using LSI after the CAS technique, a hypercapnia challenge induced by CO_2 inhalation was performed (Fig. 2.3A). Hypercapnia is commonly used as a way to assess cerebrovascular reactivity, as it causes a rapid increase in CBF (Ayata et al., 2004a; Dalkara et al., 1995; A Hauge et al., 1980; Wenzel et al., 2020). Consistent with prior studies (Ayata et al., 2004a; Dalkara et al., 1995; Anton Hauge et al., 1980; Wenzel et al., 2020), we detected a significant increase in rCBF in both the left hemisphere (Fig. 2.3C) and the right hemisphere (Fig. 2.3D). These data indicate that acute changes in CBF can be detected by LSI imaging of mice that have undergone the CAS surgical technique. Both large and small ROIs were examined for comparison, and no statistically significant differences between the large and small ROIs, nor the left and right hemispheres were detected. These data indicate that the size of the ROI drawn did not affect the measurement of relative changes in the CBF.

To determine the length of time over which we could maintain optical access for LSI imaging using the CAS technique, we continued to image a subset of mice (two females and two males) for more than 100 dpo. Representative speckle contrast images are shown for 3, 35, 53, and 103 dpo (Fig. 2.4A), and CBF values are shown for all time points (Fig. 2.4B). Over time, there appeared to be a decline in CBF in the mice. To examine this trend, we grouped the

animals into three categories: early (<1 month-post-surgery), middle (1-2 month(s)-post-surgery), and late (2+ months-post-surgery) (Fig. 2.4C). In aggregating the data in this manner, CBF was found to be significantly higher in the early phase post-surgery when compared to the middle and late phases, with no difference between the middle and late phases. Therefore, these data suggest that the surgical procedure may induce a temporary increase in CBF, or that the CBF values decline after the early phase and then stabilize with time after surgery.

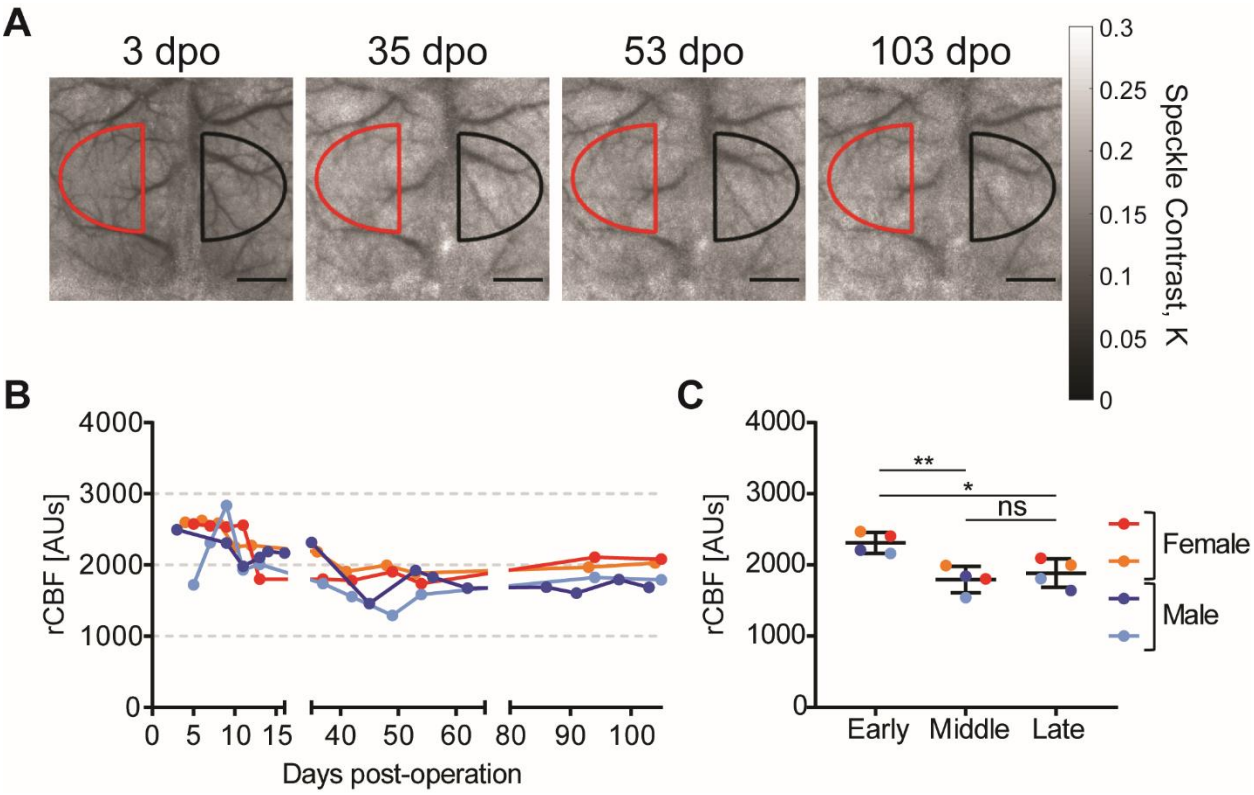

Figure 2.4. Longitudinal cerebral blood flow analysis. A) Speckle contrast imaging at 3, 35, 53, and 103 dpo. Scale bars: 1 mm. B) Longitudinal cerebral blood flow to >100 days post-operation. C) Comparison of the early (< 1 months), middle (1-2 months), and late (2+ months) time periods after surgery. * $P < 0.05$, ** $P < 0.001$, ns: not significant; significance was calculated by a repeated measures ANOVA with a Tukey post-hoc test. Error bars represent SD.

Conclusions

As emerging research reveals that many physiological and pathological conditions affect CBF, reproducible and minimally invasive tools are needed to study changes in CBF in animal models. Though CAS may not have the resolution of techniques that rely on craniotomies for optical access, it has numerous benefits for detecting CBF using LSI. The surgery is relatively fast, easy to master, and less invasive than techniques that involve removing the skull. As we have demonstrated, CAS can be used prior to LSI for detecting acute changes in rCBF (as shown by hypercapnic challenge), as well as for imaging experiments in mice that last over 100 days.

Notably, our data indicate that CBF measurements stabilized after the initial two weeks post-operation. Based on these findings, it may be recommended to begin "baseline" imaging after this point. Another consideration is the use of anesthesia for imaging. In the current study, mice were imaged with isoflurane anesthesia, which has been previously shown to increase CBF (Janssen et al., 2004). In the future, this technique may be refined to allow for imaging of head-constrained awake mice, similar to the method published by Murphy *et al*. (Murphy et al., 2016).

We anticipate that CAS will be a useful surgical preparation for investigating diseases that affect CBF, including processes that take several months to develop (such as models of Alzheimer's disease), as it enables the study of long-term changes in CBF. CAS coupled with LSI imaging may also be useful for analyzing the potential benefits of therapeutics administered to alter CBF. This approach should mitigate any potential effects of an anesthetic agent on CBF measurements. Ultimately, CAS may enhance the understanding and discovery of therapeutics for diseases that result in altered CBF in humans.

Acknowledgments

We thank all members of the Lodoen, Choi, Gandhi, Morrissette, and Andrade labs for their helpful discussions on this project. This work was supported by National Institutes of Health R01 AI120846 (to M.B.L), American Cancer Society 126688-RSG-14-202-01-MPC (to M.B.L.), National Institutes of Health R21 AG066000 (to B.C.), National Institutes of Health R01 1R01EY029490-01A1 (to S.P.G.), National Institutes of Health T32AI060573 (to E.M.H.), National Institutes of Health T32GM008620 (to E.M.H.), National Institutes of Health 5TL1TR001415-06 (to C.C.), American Heart Association Predoctoral Fellowship 19PRE34380476 (to E.M.H.), as well as the Arnold and Mabel Beckman Foundation.

Chapter 3

Toxoplasma gondii infection triggers coagulation at the blood-brain barrier and a reduction in cerebral blood flow

Introduction

Hemostasis is the physiological response to vessel injury, in which the coagulation cascade is activated to form a thrombus or blood clot, consisting of aggregated platelets and cross-linked fibrin. Thrombosis is considered to be a pathological manifestation of hemostasis and occurs when thrombi form within blood vessels, causing vessel occlusion. Infection of individuals with diverse pathogens has been linked to increased risk of blood clots during infection, including in those infected with viruses (e.g., HIV, influenza, SARS-CoV2), blood-borne bacteria (e.g. *E. coli*, *Yersinia enterocolitica*), and eukaryotic parasites (*Plasmodium falciparum*) (Helms et al., 2020; Luo et al., 2013; Massberg et al., 2010; Roberts et al., 1985). In some cases, clotting can be beneficial to the host, helping to sequester the pathogen and limit its dissemination (Engelmann and Massberg, 2012). However, when thrombosis occurs within the brain during infection, it can be associated with negative outcomes, for instance, in pediatric patients with cerebral malaria (Hemmer et al., 1991; Moxon et al., 2015, 2013; Vogetseder et al., 2004), or in COVID-19 adult patients (Soldatelli et al., 2020). Despite the highly vascularized nature of the brain, thrombi in the brain can negatively affect cerebral blood flow (CBF) and BBB function leading to irreversible neuronal loss and neurological sequelae, as seen with stroke patients (Siegel et al., 2015). This ischemia is particularly detrimental to the host since the regulation of CBF is critical to normal brain functioning. Furthermore, patients with sepsis and SARS-CoV2 have been found to have reduced CBF (Helms et al., 2020; Semmler et al., 2008; Soldatelli et al., 2020).

Clotting can be initiated in response to vessel damage due to the subendothelial exposure of tissue factor to coagulation factors in the blood. Clotting is critical in preventing hemorrhage through the formation of a fibrin-platelet clot. Tissue factor is typically found on subendothelial cells (i.e., astrocytes in the brain) (Eddleston et al., 1993); however, it can also be expressed on

myeloid cells during inflammation (Brühl et al., 2012; Massberg et al., 2010; Maugeri et al., 2006; Todoroki et al., 2000). Clotting can also be initiated in response to negatively charged molecules and surfaces (i.e., DNA, RNA, plasma membrane of activated platelets), which activate factor XII in the blood (Grover and Mackman, 2019).

Toxoplasma gondii is a eukaryotic protozoan parasite that is found worldwide (Pappas et al., 2009) and that infects and lyses brain microvascular endothelial cells (Konradt et al., 2016a) prior to parasite entry to the brain. There is also evidence that the cerebral microvasculature is perturbed during *T. gondii* infection (Estato et al., 2018; Marcos et al., 2020). However, little is known about the effect of *T. gondii* infection on the blood-brain barrier and the functional consequences of infection on cerebral blood flow (CBF) during the different stages of infection observed in humans: 1) the acute stage in which *T. gondii* replicates in the peripheral organs and enters the brain from the periphery; 2) the stable chronic stage, in which the parasites are located within cysts in the brain and muscle tissue; and finally, 3) the reactivation stage, which occurs in immunocompromised patients when the latent infection is no longer controlled (Dubey, 1998; Dubey et al., 1997).

Here we use intravital imaging approaches coupled with fixed tissue analysis in mice to demonstrate that brain endothelial cells were activated during acute infection with *T. gondii*, upregulated expression of adhesion molecules ICAM-1 and VCAM-1 and became morphologically more tortuous during infection. Surprisingly, longitudinal two-photon imaging of live mice during infection revealed vascular occlusion in the brain, and formation of platelet-fibrin clots within the cerebral vasculature during acute infection. Longitudinal laser speckle imaging revealed that CBF decreased during acute infection, recovered during stable chronic infection, and decreased again during reactivation of the infection. Finally, we demonstrate that

treatment with a low-molecular-weight heparin, an anticoagulant, partially rescued CBF in *T. gondii*-infected mice. These data suggest that changes in cerebral hemodynamics may be a common feature of systemic inflammation and infection.

Materials and Methods

Animals

All procedures and protocols were approved by the Institutional Animal Care and Use Committee (IACUC) at the University of California, Irvine. Procedures were performed on 2–to-6-month-old male and female mice. Wild-type (WT) C57BL/6J mice were purchased from Jackson Laboratories. Heterozygous Tie-2::eGFP-Claudin-5 transgenic mice were bred in-house to WT C57BL/6J mice and screened by PCR as previously published. (Knowland et al., 2014).

Acute and Chronic Infections and Reactivation

Mice were intraperitoneally (i.p.) injected with 1-5x10^4 *T. gondii* tachyzoites for acute infection experiments and 200 tachyzoites for chronic infection experiments in 200 µL of PBS. GFP- or tdTomato-expressing type II *Prugniaud* parasites were used. Tachyzoites were serially passaged and maintained in human foreskin fibroblasts as described previously (Gov et al., 2013). Mock-infected control mice were injected i.p. with 200 µL of sterile PBS (Corning). Reactivation was induced by i.p. injection of 2 mg of anti-IFN-γ (XMG1.2, Bio X cell) or rat IgG1 isotype control (Bio X cell) per mouse at 28 and 32 dpi. At experimental endpoints, mice were sedated with 2.5% Tribromoethanol (Avertin; Sigma-Aldrich) and perfused transcardially with 30 mL 1× PBS (Corning) to remove non-adherent blood cells, as previously reported (Schneider et al., 2019).

Parasite Quantification

For B1 quantification, the Blood and Tissue kit (Qiagen) was used to extract DNA from 10 mg of homogenized brain tissue following the manufacturer's guidelines. For SAG1 quantification, total RNA was harvested from 10 mg of homogenized brain tissue using the RNeasy Kit (Qiagen) and treated with DNase I (Life Technologies) to remove contaminating genomic DNA. cDNA was synthesized using the Superscript III First-Strand Synthesis kit (Life Technologies), according to the manufacturer's instructions, and subsequently used as a template in quantitative reverse transcription real-time PCR (RT-qPCR). qPCR was performed in triplicate using a Bio-Rad iCycler PCR system and iTaq Universal SYBR Green Supermix (Bio-Rad). All primers were synthesized by Integrated DNA Technologies. Primer pairs for B1: CAGATGTGCTAAAGGCGTCA (sense), GCCCTAGACAGACAGCGAAC (anti-sense). B1 data were used to determine parasite concentration (parasites/mg) by referencing a standard curve of parasites as previously published (Burg et al., 1989). Mouse GAPDH primers were previously published (Morgado et al., 2011). Primers pairs for SAG1: CAGCACTCTTGGTC CTGTCA (sense), TGGCACCATTATCACTCGAA (anti-sense). Primers pairs for human TF: AAGAGTACAGACAGCCCGGTAG (sense), CCACAGCTCCAATGATGTAGAA (anti-sense). Human GAPDH primers were previously published (Gov et al., 2013). qPCR data were analyzed using the threshold cycle method (Livak and Schmittgen, 2001), and gene expression data are shown normalized to that of the housekeeping gene GAPDH. In all RT-qPCR assays, cDNA generated in the absence of reverse transcriptase, as well as water in place of the DNA template, were used as negative controls, and these samples were confirmed to have no amplification.

Immunofluorescence Staining, Imaging, and Analysis

Brains were collected and incubated in 4% PFA for 6-16 hours, cryopreserved with 30% sucrose in 1x PBS until the tissues sunk, and embedded in OCT freezing medium (Thermo Fisher Scientific). After sectioning, tissue was stored in cryoprotection media (30% sucrose, 30% ethylene glycol, 0.1M Phosphate buffer, 1% PVP-40) at -20 °C. Nuclei were stained just prior to the final wash using Hoechst dye (1:20,000; Sigma). For detection of ICAM-1 and VCAM-1, 16-µm-thick sections were blocked and permeabilized in IFA buffer [1X PBS (Corning), 5% normal donkey serum (Southern Biotech, Birmingham, AL), 0.3% Triton-x 100 (Thermo Fisher Scientific)] for 2-4 hr. Antibodies against GLUT1 (1:400; Millipore), ICAM-1 (1:100; Biolegend), or VCAM-1 (1:100; Biolegend) in IFA buffer were incubated with sections for 48 hr. Secondary antibodies (1:500) were incubated with sections for 24 hr. Z-stacks were taken with a 63X objective on a confocal Leica SP8 microscope (Leica Microsystems). Ten random non-adjacent fields of view (FOVs) in the cortex were imaged. For detection of CD41 and fibrin, 100-µm-thick sagittal sections were blocked and permeabilized in IFA buffer for 16 hrs. Antibodies against GLUT1 (1:400; Millipore), fibrin (1:200; Thermo Fisher Scientific), or CD41 (1:100; Biolegend) in IFA buffer were incubated with sections for 72 hr. Secondary antibodies (1:500) were incubated with sections for 48 hr. Immediately prior to imaging, brain tissues were cleared using the ultrafast optical clearing method (Zhu et al., 2019). A widefield (pinhole set to 3 Airy Units) tilescan was imaged with a 20X objective on a Leica SP8 microscope.

The quantification of ICAM-1 and VCAM-1 was done on max z-stack projections. The quantification of CD41 and fibrin was done on ten random 300 x 300 µm FOVs spaced throughout the cortex from widefield (pinhole set to 3 Airy Units) fluorescence tilescans of 100 µm-thick sagittal sections, while blinded to the CD41 or fibrin signal. Images were globally

smoothed using FIJI's smooth function, the channels were split, and a threshold was applied to determine areas that were positive for GLUT1 (to denote vessels), ICAM-1, VCAM-1, CD41, or fibrin. Afterward, the percent positive areas of ICAM-1, VCAM-1, CD41, or fibrin within the GLUT1 positive areas were calculated.

Serum Cytokine Multiplex Assay

Whole blood was collected into coagulation tubes (BD Biosciences) prior to perfusion (Schneider et al., 2019). Coagulated blood was centrifuged per the manufacturer's instructions to isolate sera. Cytokines were measured using the LegendPlex bead-based assay (Biolegend) per kit instructions at a dilution of 1:2. Samples were analyzed on a Novocyte flow cytometer (Agilent).

2-Photon Imaging

Cranial windows were installed in Tie-2::eGFP-Claudin-5 heterozygous mice 1-2 weeks prior to imaging as previously described (Schneider et al., 2019). Imaging was performed using a resonant 2-photon microscope (Neurolabware) equipped with an Olympus 20x (0.8 NA) water-emersion objective. A Ti:Sapphire laser tuned to 900 nm (Mai-Tai HP, SpectraPhysics) was used to stimulate eGFP fluorescence. Emissions were filtered using a 510/84-nm BrightLine bandpass filter (Semrock) and acquired using a using Scanbox acquisition software (Scanbox). We used an electrically tunable lens (Optotune) for volumetric scanning over 1-2 minutes in 5-6 fields. To minimize motion artifacts, mice were anesthetized with Isoflurane (Patterson Veterinary) in O_2 (2% for induction and 1-1.5% for maintenance). Sterile eye ointment (Rugby) was applied to prevent corneal drying and body temperature was maintained at 37˚C with a custom-made closed

loop heating pad. At the end of each imaging session, mice were injected intravenously via the tail vein with 100 µL 0.5% Biocytin-TMR (Invitrogen) in sterile 1x PBS to visualize vascular perfusion. For image processing, focal planes were sum binned and motion corrected using HyperstackReg (DOI 10.5281/zenodo.2252521) in FIJI, a processing package based on ImageJ2 (Schindelin et al., 2012).

Endothelial cell analysis

Day 0 (baseline, prior to infection) and day 6 imaging were performed by 2-photon microscopy of eGFP-claudin-5 mice injected with PBS (control) or infected with *T. gondii*. Endothelial cells were compared in each FOV, and cells within the same FOV at both day 0 and day 6 post-infection were analyzed. Endothelial cell borders delineated by eGFP-claudin-5 were hand-traced in FIJI using a stylus and tablet. Cell area and perimeter were assessed using the measure function, and the shape index was calculated using the standard formula: shape index $= \frac{4\pi * \text{area}}{(\text{perimeter})^2}$, as has previously been published (Ohashi et al., 2007). The fold-change of the shape index was calculated as a ratio of the day 6 to day 0 shape index for each endothelial cell.

Endothelial cell protrusions were counted at day 0 and day 6 along claudin-5 cell borders. The same cell was quantified at each time point. A minimum of 3 vessel sections were quantified for each mouse across at least three fields of view (n = 32-52 cells total per mouse). Protrusions were defined as sections of cell border with a visible open center less than 8 µm in diameter.

Laser speckle imaging

Surgeries and laser speckle imaging (LSI) in mice were performed as previously published (Hoover et al., 2021). In brief, mice were anesthetized with isoflurane (2% for induction and 1.5% for maintenance, Patterson Veterinary). Then the scalp was resected, and cyanoacrylate was applied to the skull. Mice recovered from surgery for at least two weeks prior to infection. Laser speckle imaging to measure cerebral blood flow (CBF) was performed using a long-coherence 785 nm laser. Raw speckle images (10 ms exposure time) were acquired using a 4x Achrovid objective with a 37 mm working distance (Edmund Optics). Cross-polarization optics between the source and detector were used to remove specular reflection.

To measure the changes in cerebral blood flow (CBF) during acute infection, we imaged mice at 0, 4, and 7 dpi. For the chronic infection and reactivation experiments, mice were imaged at 0, 7, 14, 28, 34, and 38 dpi. During LSI, mice were anesthetized with O_2 vaporized isoflurane in the same way as for the 2-photon imaging, and body temperature was maintained at 37˚C with a feedback heating pad (Harvard Apparatus, Holliston, MA). As in Hoover *et al.*, CBF was calculated using a simplified speckle imaging equation $\mathrm{CBF} = \frac{1}{2TK^2}$ (Ramirez-San-Juan et al., 2008). Two semi-elliptical regions of interest (ROIs) were used to obtain longitudinal CBF data from each hemisphere. The median CBF from each ROI was calculated, and the median CBF values for the right and left hemispheres were averaged. Relative CBF (rCBF) was calculated as a percentage of baseline CBF (set to 100%).

Low-molecular-weight heparin treatment

Mice were given subcutaneous injections of 100 units/kg of nadroparin calcium, a low-molecular-weight heparin, in PBS (Sigma-Aldrich) twice daily, roughly twelve hours apart.

Control animals received the same volume of PBS only. Treatment was started at 0 dpi after LSI imaging and continued until 7 dpi when mice were euthanized.

Isolation and infection of primary human neutrophils

Whole blood from healthy donors was provided by the Institute for Clinical and Translational Science (ICTS) at the University of California, Irvine, in accordance with guidelines and approval of the Institutional Review Board. Primary human neutrophils were isolated as previously described (Lima et al., 2018). Briefly, whole blood was mixed with 3% dextran (Sigma-Aldrich) in PBS for 20 min. The top layer was transferred to a fresh conical tube, underlaid with 15 ml of Ficoll-Paque Plus (GE Healthcare), and centrifuged at 300 × *g* for 20 min. The underlying pellet with neutrophils and red blood cells (RBC) was suspended in 1× RBC lysis buffer (eBioscience) and incubated for 10 min. Neutrophils were washed in PBS and suspended in RPMI 1640 (HyClone) supplemented with 10% heat-inactivated fetal bovine serum (FBS) (Omega Scientific), 2 mM L-glutamine (Corning), 100 U ml^{-1} penicillin, and 100 µg ml^{-1} streptomycin (HyClone) (R-10%). Following extraction, 10^7 human neutrophils were immediately infected at a multiplicity of infection (MOI) of 2, given ultrapure lipopolysaccharide (LPS) (List Biological) at 500 ng/ml, or an equivalent volume of sterile media (mock-treated). The cells were maintained at 37°C in 5% CO2 incubators for 1, 4, and 18 hrs before RNA extraction.

Statistics

GraphPad Prism 8.0.1 software was used for statistical analyses. When only two non-longitudinal groups were compared, an unpaired Student's *t*-test was used to test for significance.

A one-way ANOVA with a post-hoc Tukey test was used to test for significance in the sera cytokine analysis and neutrophil TF transcript analysis. For the endothelial cell shape analysis, a paired Student's *t*-test was used to test for significance. For the acute and chronic infection, endothelial cell protrusion analysis, CBF, and weight loss experiments significance was tested with a repeated measures two-way ANOVA, with a post hoc Sidak's multiple comparisons test. For the reactivation and nadroparin-treatment experiments, CBF and weight loss significance was calculated with a mixed-effects analysis with a post-hoc Sidak's multiple comparisons test.

Results

Acute T. gondii infection of the CNS

To track *T. gondii* infection of CNS endothelial cells (ECs) forming the blood-brain barrier (BBB) and the brain parenchyma during acute infection, we utilized transgenic mice that express eGFP fused to the tight junction protein Claudin-5 under the control of the Tie2 promoter (Tie2::eGFP-Claudin-5) to visualize the cerebral blood vessels (Knowland et al., 2014). The mice were infected with tdTomato-expressing type II *T. gondii* (*Prugniaud* strain) or mock-treated with PBS. Brain sections from mock and infected mice were imaged by confocal fluorescence microscopy during acute timepoints post-infection. *T. gondii* was detectable within the CNS blood vessels (Fig. 3.1A) and in the brain (Fig. 3.1B) during these acute timepoints, demonstrating early dissemination of the parasite into the brain during infection. Detection of the *T. gondii*-specific gene B1 by qPCR revealed significantly more parasite DNA in the brains of infected mice than mock-treated mice at 9 dpi (Fig. 3.1C).

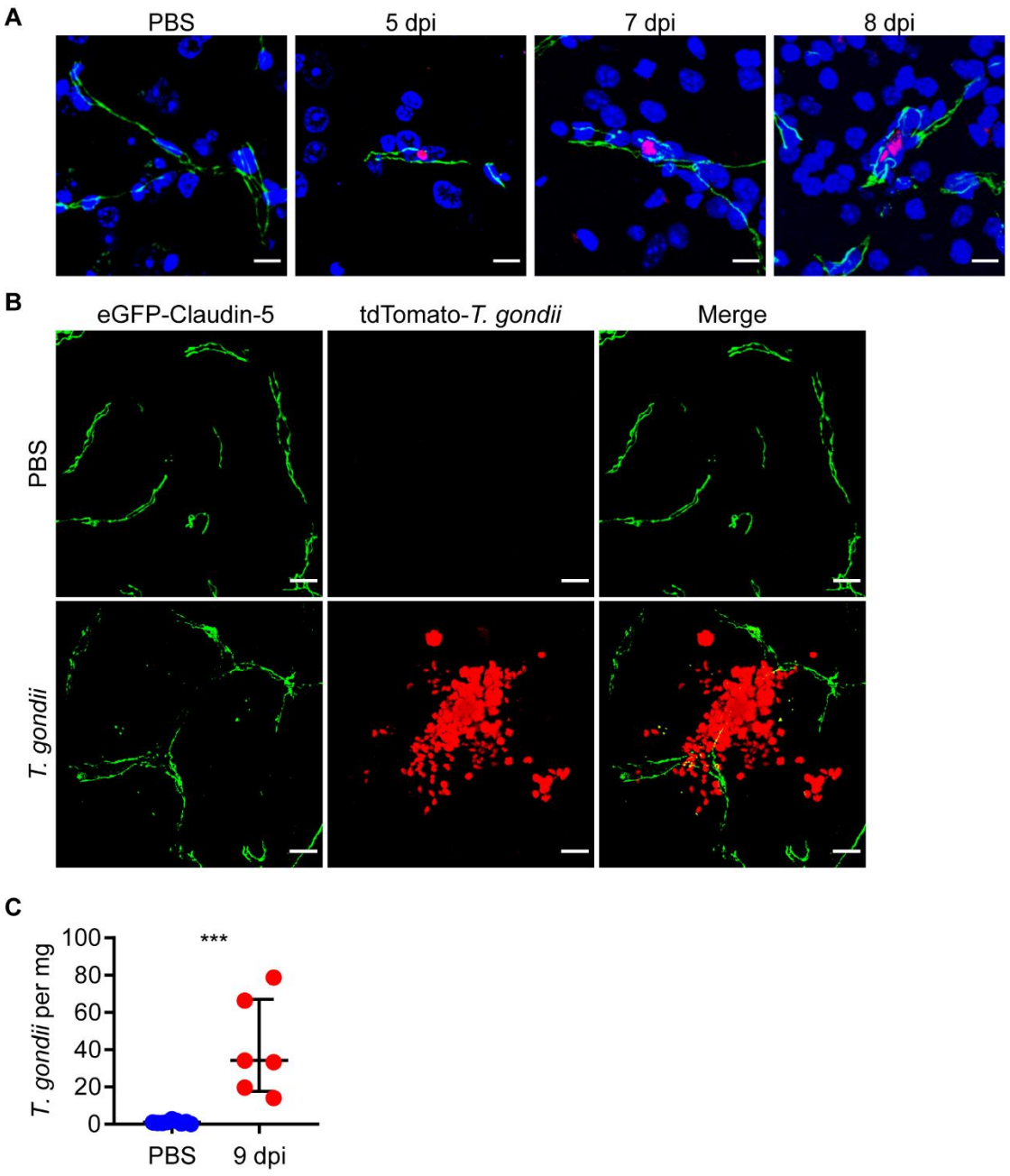

Figure 3.1. *T. gondii* dissemination to the CNS. A) Representative confocal microscopy of brain sections from PBS-injected or tdTomato-expressing *T. gondii*-infected eGFP-claudin-5 mice at 5, 7, and 8 dpi stained with Hoechst (blue) and imaged for eGFP-claudin-5 (green), and tdTomato-T. gondii (red). Scale bars, 10 µm. B) Confocal microscopy from PBS-injected or *T. gondii*-infected mouse at 9 dpi. Scale bars, 15 µm. C) Brain homogenates were examined for the *T. gondii* B1 gene by qPCR to determine *T. gondii* per mg of brain tissue in mice injected with PBS or *T. gondii* (9 dpi). *** $P < 0.001$; Student's t test.

To determine the levels of systemic cytokines circulating at these acute timepoints, we examined serum cytokines, including two key mediators of resistance to *T. gondii* infection, IFN-γ and IL-12, at 2, 4, 6, 8, and 9 dpi. The levels of IFN-γ were significantly elevated by 2 dpi in infected mice compared to mock-treated mice and continued to be detected at high levels throughout the acute infection (Fig. 3.2A). IL-12 was significantly upregulated at 4 dpi and then returned to baseline levels (Fig. 3.2B). TNF-α increased throughout acute infection and was significantly different in infected mice compared to mock by 9 dpi (Fig. 3.2C).

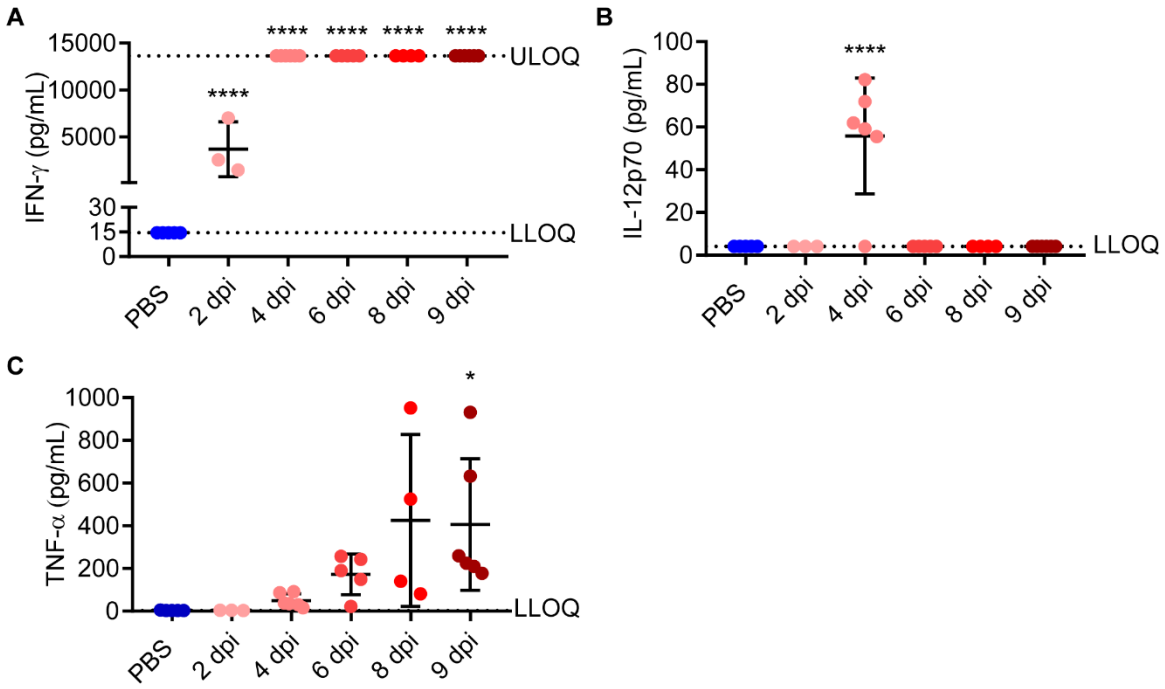

Figure 3.2. Sera cytokine levels during acute *T. gondii* infection. Levels of IFN-γ (A), IL-12p70 (B), and TNF-α (C) in the serum of PBS-injected or T. gondii-infected mice at the indicated timepoints, as measured by multiplex analysis. Each circle represents one mouse. Dotted lines indicated the upper or lower limit of quantification (ULOQ and LLOQ). *n*= 3-10 mice per group. *P < 0.05, ***P < 0.001, ****P < 0.0001 significance was calculated by a one-way ANOVA with a post-hoc Tukey test. All error bars represent SD.

Response of endothelial cells to acute T. gondii infection

Given the presence of inflammatory cytokines in the bloodstream during acute infection, we examined EC activation. Brain sections from mock-treated or acutely infected mice were stained with anti-GLUT1 monoclonal antibodies (mAbs) to delineate blood vessels, as well as mAbs against ICAM-1 or VCAM-1, two cell adhesion molecules that are upregulated in response to inflammation. We observed increased ICAM-1 and VCAM-1 signals in the blood vessels of infected mice compared to mock-treated mice (Fig. 3.3A-B), as previously published (Deckert-Schlüter et al., 1999). Quantifying the percent of ICAM-1 or VCAM-1 signal over GLUT1 signal in cerebral vessels of mock and *T. gondii*-infected mice revealed a significant increase in the vessel coverage of these two adhesion molecules in infected mice (Fig. 3.3C-D), indicating activation of the endothelium. Notably, ICAM-1 and VCAM-1 signal were detected in infected mice in regions both with and without *T. gondii* parasites, indicating a global effect of infection on EC activation.

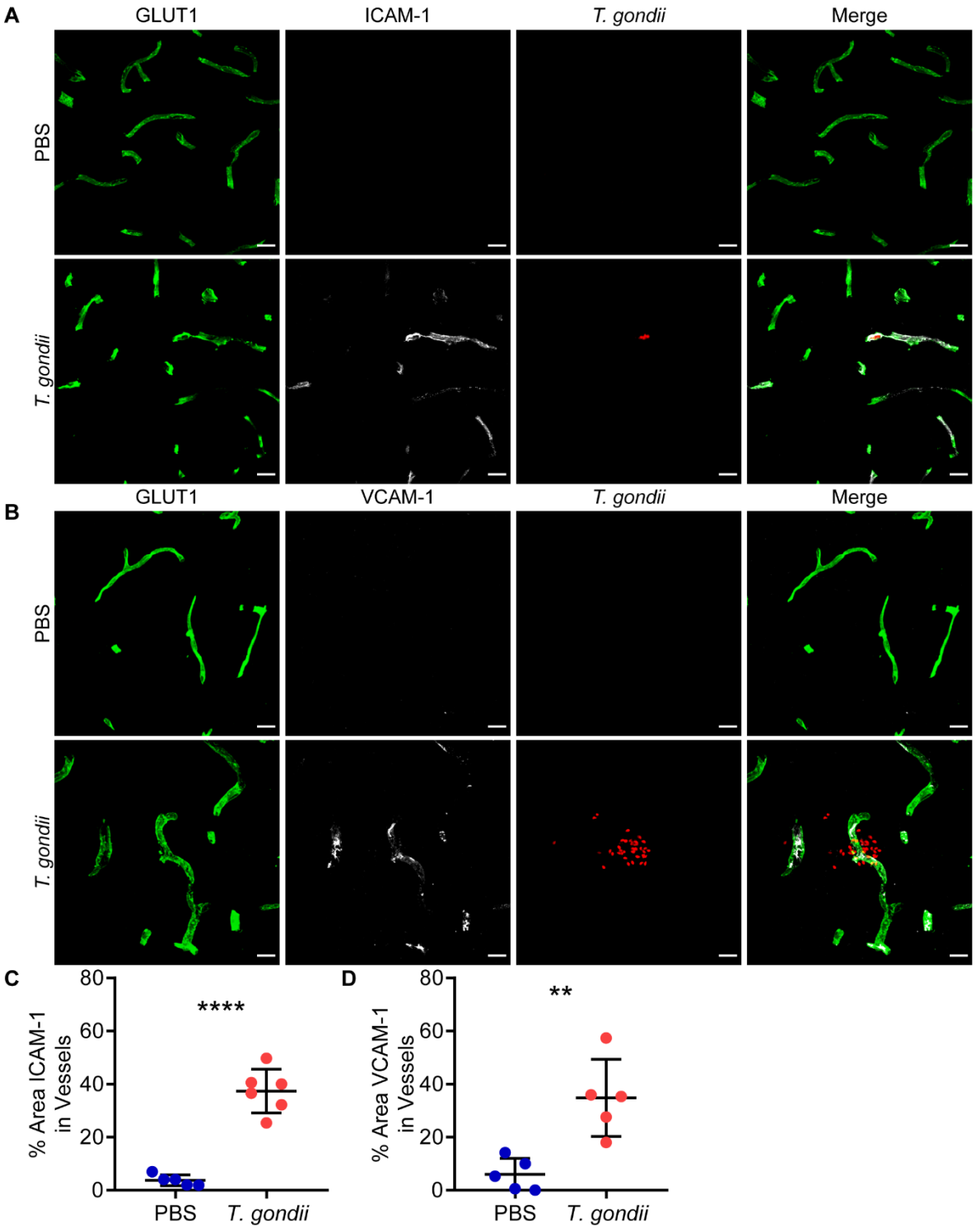

Figure 3.3. Activation of endothelial cells during acute *T. gondii* infection. C57BL/6 mice were injected with PBS or infected with *T. gondii* and brains were harvested at 7 dpi. A-B) Representative confocal images of brain sections stained with antibodies against GLUT1 and (A) ICAM-1 or (B) VCAM-1. Scale bars, 15 µm. C-D) Percent area of ICAM-1 or VCAM-1, respectively, in GLUT1+ vessels. Each circle represents one mouse. *n* = 5-6 mice per group, **P < 0.005, ****P < 0.0001; Student's t test. Error bars represent SD.

To further investigate the effects of *T. gondii* infection on the vascular endothelium in the brain, we conducted 2-photon imaging of the brain in transgenic eGFP-Claudin-5 mice during infection. These mice enable the detection of changes in vascular organization both at the level of the vessel and at the level of individual endothelial cells, since each endothelial cell border is delineated with eGFP-claudin-5 signal. Cranial windows were installed by excising a portion of the skull and attaching a coverslip in its place, as previously described (Knowland et al., 2014; Schneider et al., 2019). After 5-7 days of recovery, time-lapse 2-photon microscopy was used to image mice at day 0 for a baseline reading of cell shape and vessel architecture, and again six days after injection of PBS (mock) or tdTomato-expressing *T. gondii*. This imaging approach enables us to image to 400 μm depth in the brain and return to the same imaging FOVs over time during infection. In conducting this longitudinal imaging, we found that the endothelial cell borders in the infected mice became profoundly distorted, compared to the control PBS-injected mice, which underwent the same surgery and imaging procedures (Fig. 3.4A). We also noted increased numbers of "protrusion" structures in the claudin-5 signal, specifically in *T. gondii*-infected mice (Fig. 3.4A, C). These protrusions have been previously reported and indicate active tight junction remodeling (Knowland et al., 2014).

To quantify the changes in the endothelial cells, we examined the shape index of the cells, which is used to monitor the roundness of endothelial cells (Ohashi et al., 2007). At baseline, both groups of mice had similar shape index values (Fig. 3.4B). However, by 6 dpi, the shape index of cells decreased in the *T. gondii*-infected mice, reflecting the distorted shape of the endothelial cells over time. This change was not observed in the PBS-injected mice (Fig. 3.4B), indicating that this effect resulted from infection and not due to the surgery or imaging procedure. Similar to the endothelial cell activation detected by elevated adhesion molecule

expression, the endothelial shape changes were observed in regions with and without *T. gondii*, further indicating a global effect of infection on the vasculature.

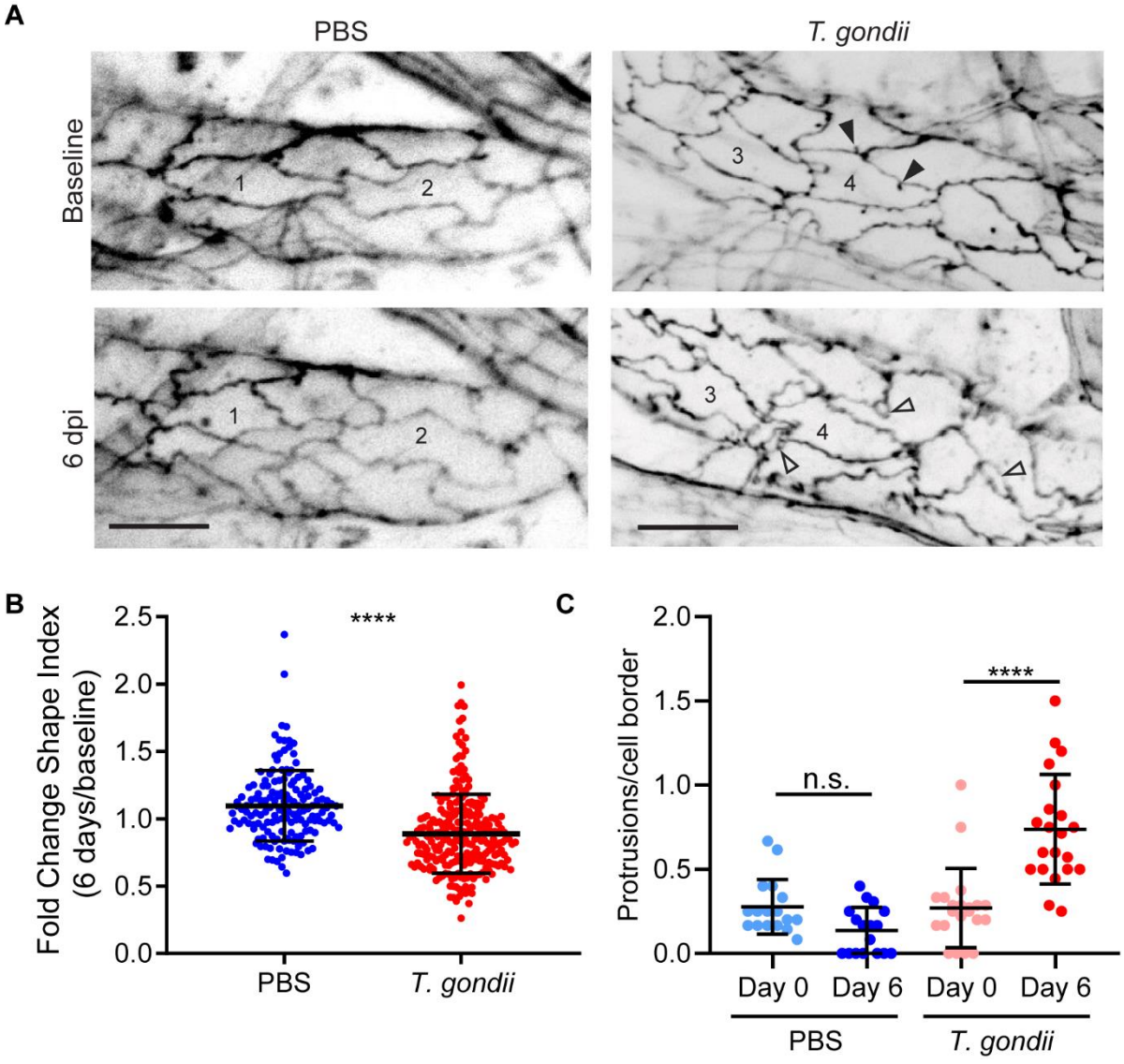

Figure 3.4. Morphology of endothelial cells during acute *T. gondii* infection. Intravital 2-photon imaging was performed through cranial windows on eGFP-claudin-5 mice that were injected with PBS or infected with *T. gondii*. Longitudinal imaging was performed at baseline (0 dpi) and at 6 dpi in both control and infected mice. A) Representative field of view showing blood vessels in the cortex at both timepoints. Numbers indicate the same endothelial cells across days. Open arrowheads represent protrusions that were detected at 6 dpi. Closed arrowheads indicate regions where protrusions disappeared. Scale bars, 20 µm. B) Shape index of brain endothelial cells at 6 dpi compared to baseline. Each dot represents a single endothelial cell. *n* = 150-255 cells per group from 3-4 independent mice per group. C) Endothelial cell protrusions per adjacent cell were counted at day 0 and day 6 along claudin-5 cell borders. The same cell was quantified at each time point. A minimum of 3 vessel sections were quantified for each mouse across at least 3 fields of view (*n* = 32-52 cells total per mouse). ****P < 0.0001; Student's t test (B); one-way ANOVA (C). Error bars represent SD.

To examine the effect of *T. gondii* infection on the BBB more directly, we imaged infected eGFP-Claudin-5 mice for regions with detectable parasites by 2-photon microscopy. Longitudinal imaging of a mouse infected with tdTomato-expressing *T. gondii* revealed a large vacuole of parasites in a cortical capillary (Fig. 3.5B). Notably, this vacuole was not observed 40 min earlier (Fig. 3.5A), suggesting that it arrived at the capillary level within an infected cell circulating in the bloodstream. At 80 min after the start of imaging, the vacuole underwent spontaneous lysis, and individual tachyzoites could be detected (Fig. 3.5C). After 120 min of imaging (Fig. 3.5D), biocytin-TMR, an 860 dalton fluorescent dye, was injected intravenously to determine the effect of this vacuole lysis event on vessel perfusion. Interestingly, we did not detect leakage of this very low-molecular-weight dye near the region of parasites or elsewhere in the FOV suggesting an intact BBB. However, we did detect apparent vessel occlusion near the parasites. Scanning through the z-stacks revealed that the blood vessel region immediately adjacent to the site of parasite lysis was not perfused with dye (Fig. 3.5E, white arrowhead). Surprisingly, we also detected regions not immediately adjacent to parasites, which also appeared to have reduced dye perfusion (Fig. 3.5E, white arrow). These data indicate that *T. gondii* infection leads to changes in the morphology of endothelial cells and reduced perfusion of vascular dyes in cerebral blood vessels, both near parasites and at more distant sites.

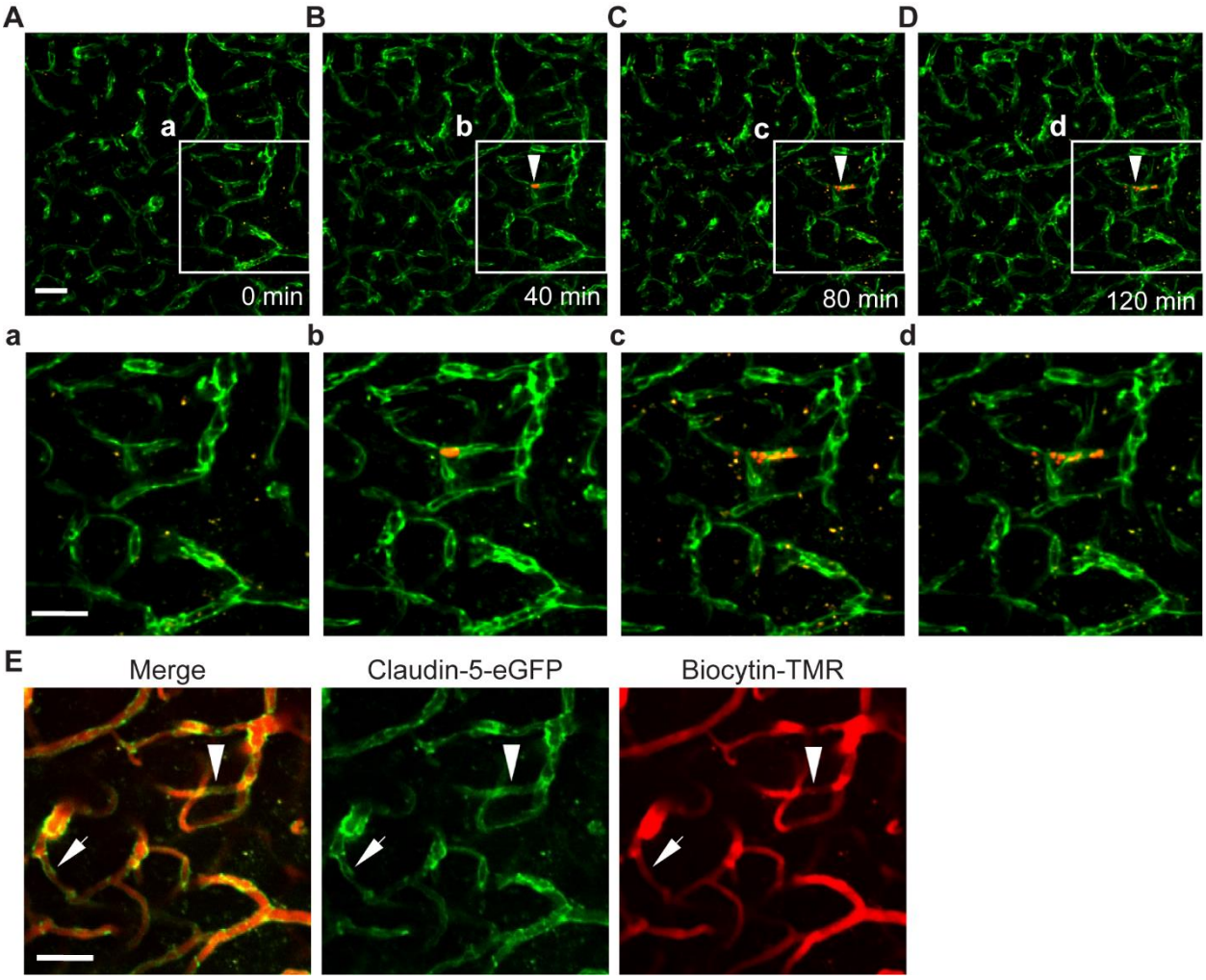

Figure 3.5. Reduced blood vessel perfusion during acute *T. gondii* infection. 2-photon imaging in the cortex of an eGFP-claudin-5 mouse infected with tdTomato-expressing *T. gondii* at 9 dpi. A-D) Imaging in the same FOV at 0, 40, 80, and 120 minutes. Arrowhead shows a vacuole of *T. gondii* parasites. a-d) Insets show a magnified FOV around the T. gondii vacuole. E) Biocytin-TMR (860 Daltons) was injected i.v. during imaging and dye perfusion (red) was imaged in the same FOV as in A-D. Arrow shows location distal to vacuole with reduced perfusion. Scale bars, 50 µm.

T. gondii infection induces clotting in the brain microvasculature

One possible explanation for the reduced dye perfusion in the brains of *T. gondii*-infected mice is the formation of blood clots in the cerebral vessels. To investigate this possibility, we examined the end products of the clotting cascade: platelets (that are $CD41^+$) and fibrin. Indeed, the deposition of platelets and fibrin within $GLUT1^+$ blood vessels were detectable near large sites of parasite infection (Fig. 3.6A). Examining 100 µm-thick sagittal sections that were

optically cleared (Zhu et al., 2019) enabled us to image GLUT1, fibrin, and CD41 throughout the cortex of mock and *T. gondii*-infected mice (Fig. 3.6B-C). GLUT1 signal was not significantly different between the mock and infected mice over several FOV per infected animal (Fig. 3.6D). However, the percent area of CD41 and fibrin in $GLUT1^{+}$ vessels was significantly increased in the brains of infected compared to mock-treated mice. Interestingly, the CD41 and Fibrin deposition most often did not occur near parasitic foci. These data indicate that acute *T. gondii* infection leads to the formation of platelet-fibrin clots in the cerebral vasculature.

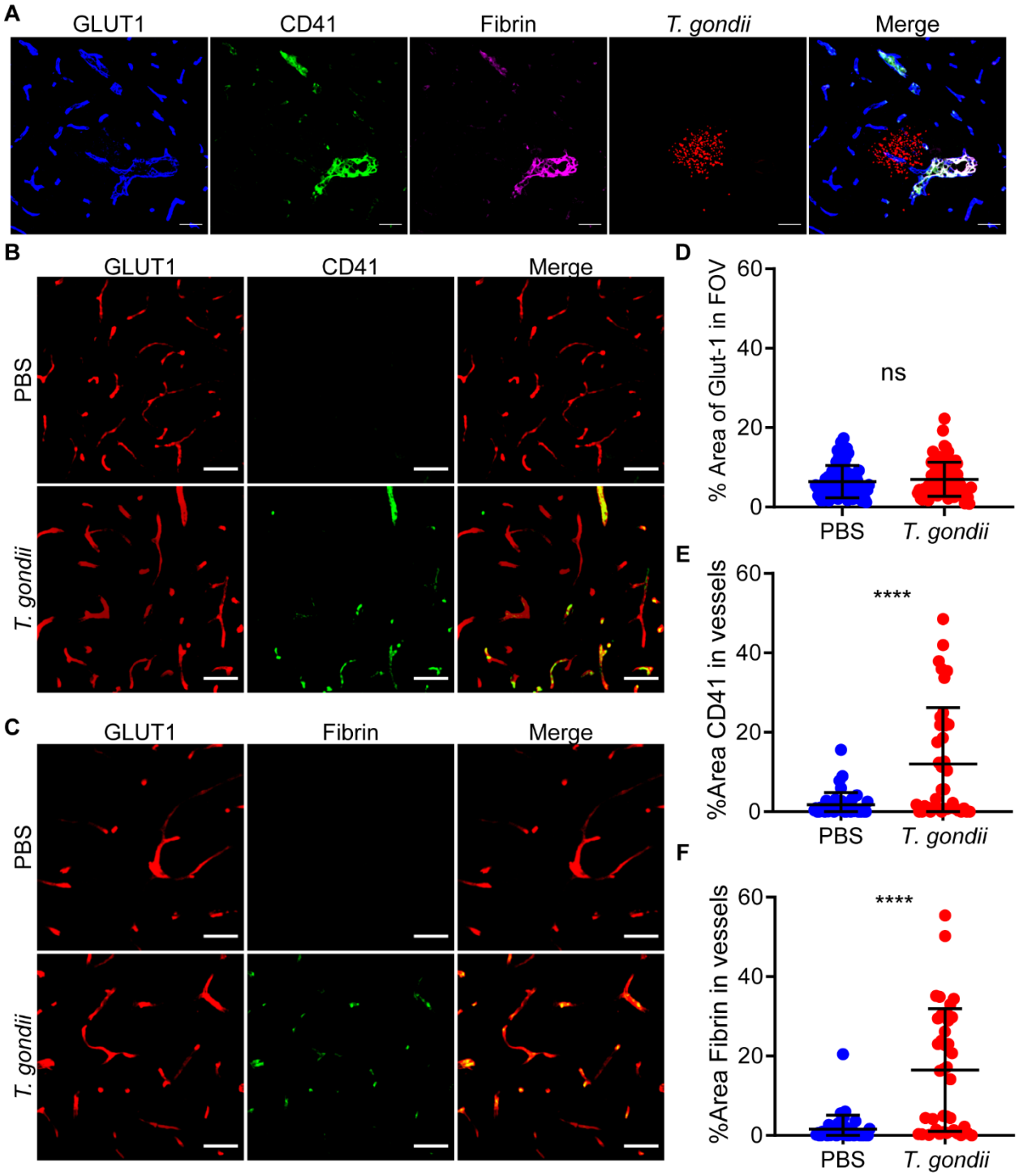

Figure 3.6. Evidence of clot formation in cerebral vessels of *T. gondii*-infected mice. C57BL/6 mice were infected with *T. gondii* or injected with PBS and brains were harvested at 9 dpi. A) Confocal image of brain section stained with antibodies against GLUT1, CD41, and fibrin. Scale bars, 50 µm. B-C) Widefield images of brain sections stained with anti-GLUT1 and anti-CD41 (B) or anti-fibrin (C). Scale bars, 50 µm. D) Percent area of GLUT1 within each FOV. E-F) Percent area of CD41 or fibrin in vessels, respectively. Each circle represents one FOV. *n* = 40-80 FOVs from 4 independent mice per group. *** $P < 0.001$; Student's t test. Error bars represent SD.

Hemodynamic changes during T. gondii infection

Due to the increased tortuosity of endothelial cells at the BBB and the detection of coagulation at the BBB, we next investigated the degree to which acute *T. gondii* infection led to hemodynamic changes. We performed the cyanoacrylate skull (CAS) surgery on C57BL/6J mice prior to laser speckle imaging (LSI) to measure CBF through the intact skull (Hoover et al., 2021). This approach allowed us to image the same mice longitudinally during acute and chronic infection, starting with baseline measurements at 0 dpi, prior to injection with either PBS or *T. gondii* (Fig. 3.7A). We found that relative CBF (rCBF) in PBS-treated mice was stable. However, during acute infection rCBF significantly decreased by 4 dpi, and the decline became more profound by 7 dpi (Fig. 3.7B). Interestingly, the reduction in rCBF preceded weight loss induced by *T. gondii*-infection, as the weight changes of *T. gondii*-infected mice were only significantly different than the mock-treated mice at 6 dpi (Fig. 3.7D).

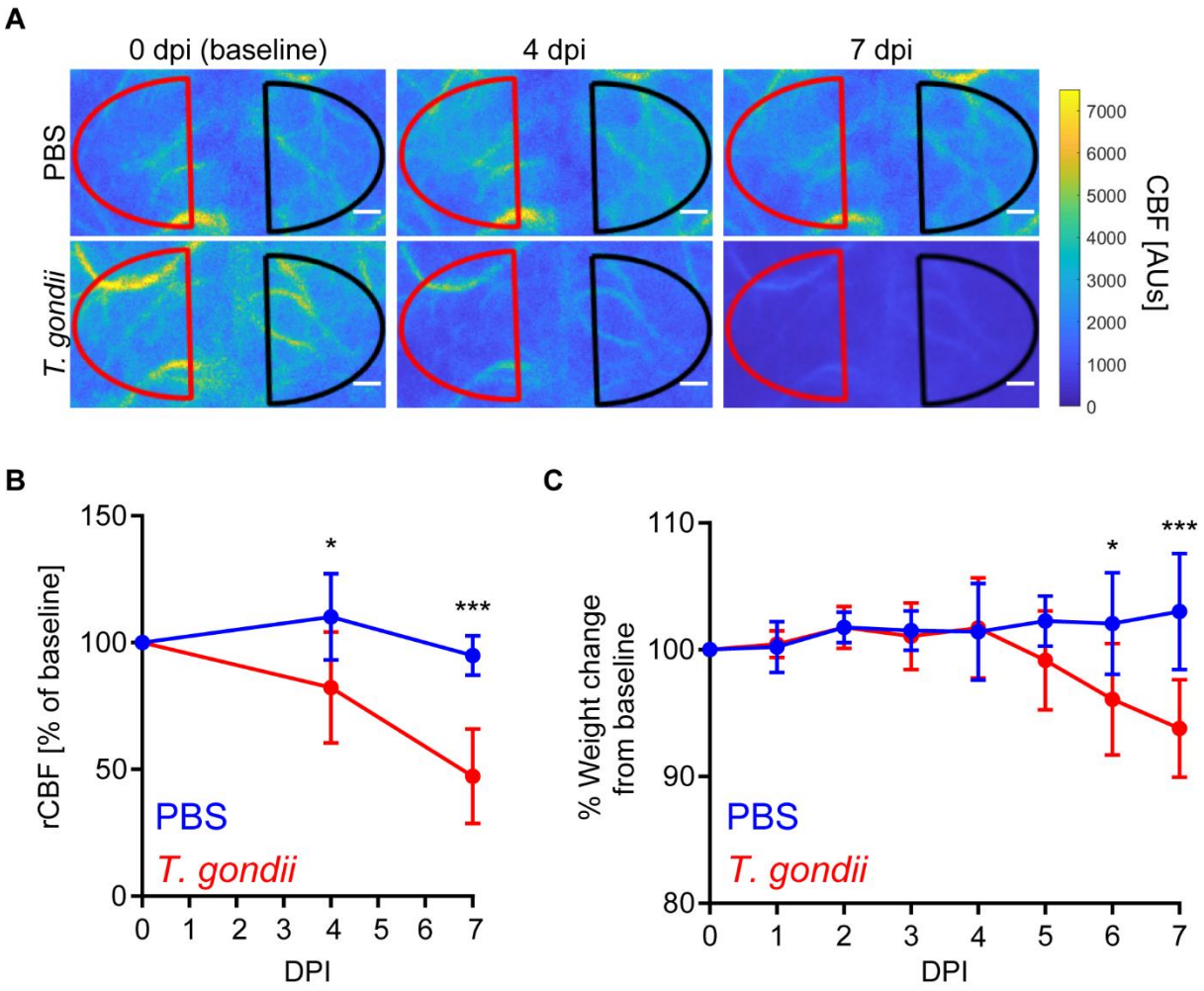

Figure 3.7. CBF changes during acute *T. gondii* infection. C57BL/6 mice were injected with PBS or infected with *T. gondii* and longitudinal laser speckle imaging was performed at 0, 4, and 7 dpi through the intact skull to measure CBF. A) Representative laser speckle images of control and *T. gondii*-infected mice. Scale bars, 400 µm. B) Percent change of rCBF to baseline in control and *T. gondii*-infected mice. C) Percent weight change from baseline in control and *T. gondii*-infected mice. *n* = 4-5 mice per group. *P < 0.05, ***P < 0.001; significance between mock and infected mice at each timepoint was calculated by a repeated measures two-way ANOVA, with a post hoc Sidak's multiple comparisons test. Error bars represent SD.

We next investigated hemodynamic changes over the entire course of infection (acute, chronic, and reactivation stages) by infecting C57BL/6J mice with a lower dose of *T. gondii* and tracking the mice out to 38 dpi (Fig. 3.8A). Since IFN-γ is an essential mediator of host defense against *T. gondii* (Suzuki et al., 1988), the administration of anti-IFN-γ mAb to the mice during the chronic stage of infection effectively neutralizes the cytokine and induces reactivation of chronic infection (Gazzinelli et al., 1992). Anti-IFN-γ was administered at 28 and 32 dpi to induce reactivation, which was confirmed by the elevated levels of SAG1 transcripts detected at 38 dpi in the brains of *T. gondii*-infected mice injected with anti-IFN-γ, but not in infected mice injected with the control Ig (cIg) (Fig. 3.8B).

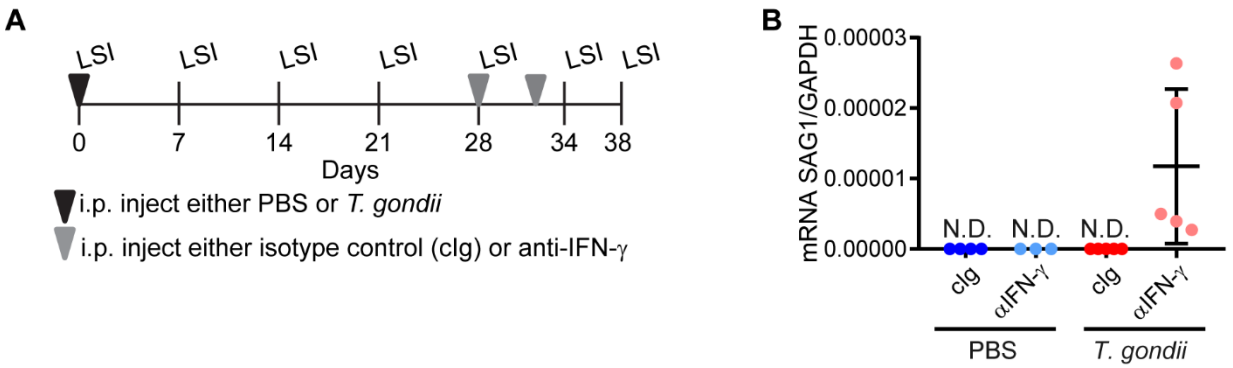

Figure 3.8. Chronic *T. gondii* infection model. A) Experimental set-up for chronic and reactivation laser speckle experiments. B) Relative expression of SAG1 to GAPDH transcripts in brains of control (PBS) and *T. gondii*-infected mice at 38 dpi. Mice were administered control IgG (cIg) or anti-IFN-γ (αIFN-γ) starting at 28 dpi. SAG1 was not detected (ND) in any group except the *T. gondii*-infected mice given anti-IFN-γ.

Longitudinal laser speckle imaging was conducted on these mice, and representative images from the 0, 14, 28, and 38 dpi timepoints are shown (Fig. 3.9A). Consistent with the acute infection data (Fig. 3.7A and B), infected mice had a significant decrease in CBF by 14 dpi compared to PBS-treated mice, but rCBF recovered to the level of the PBS-treated mice by 21 dpi (Fig. 3.9A and B). Notably, the changes in rCBF were distinct from the weight changes in the *T. gondii*-infected mice, which did not regain their pre-infection weight even in chronic infection (Fig. 3.9C). During the reactivation of infection induced by anti-IFN-γ administration, there was again a significant decrease in rCBF, which was not detected in chronically-infected mice injected with the isotype control antibody (Fig. 3.9D). Consistent with the reactivation of infection, this group also experienced significant weight loss (Fig. 3.9E). Collectively, these data demonstrate a reduction in CBF during acute and reactivated *T. gondii* infection, and that the mice recover normal levels of CBF during stable chronic infection.

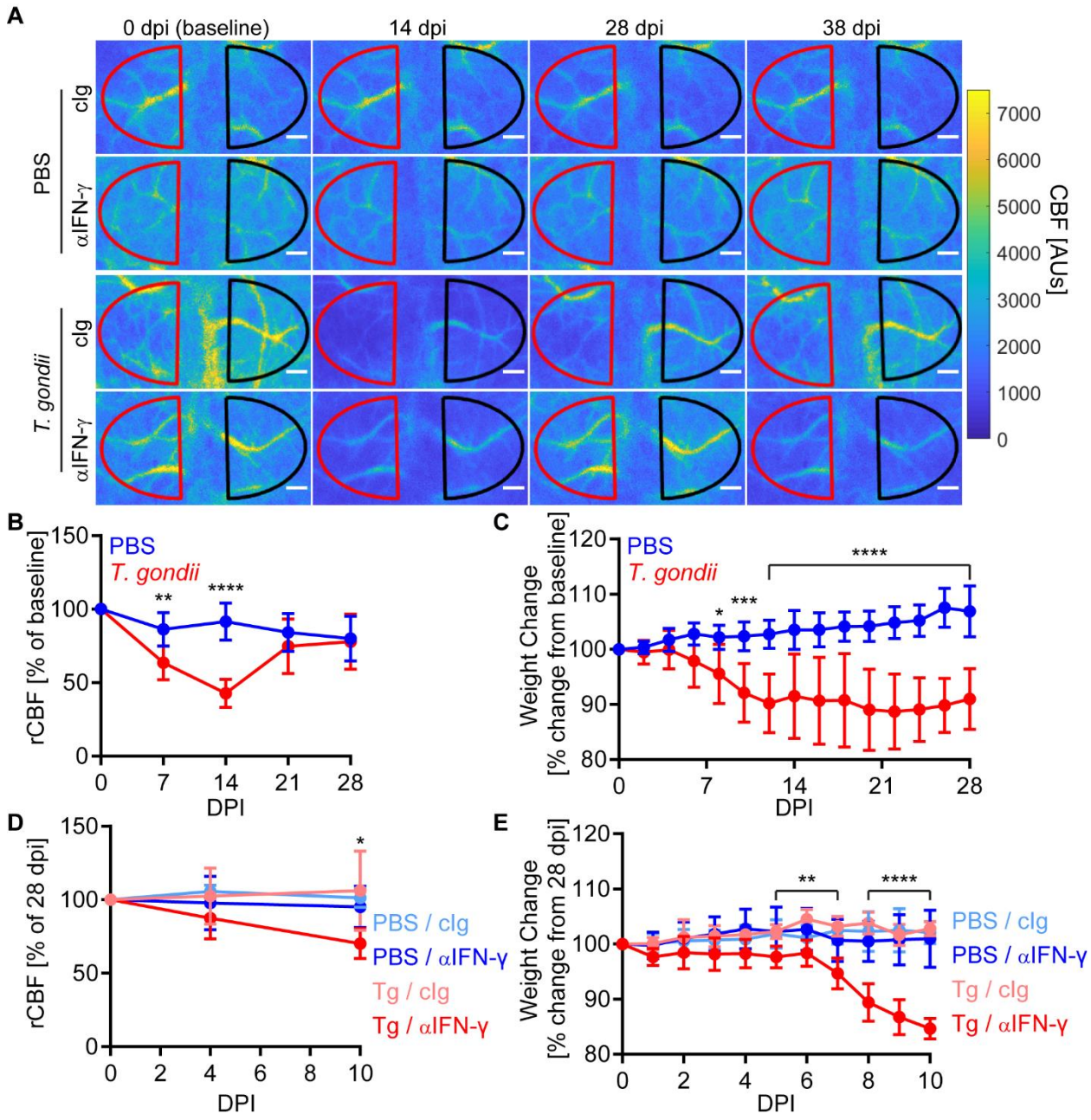

Figure 3.8. CBF changes during chronic *T. gondii* infection. A) Representative laser speckle imaging showing CBF in control (PBS) or *T. gondii*-infected mice at 0, 14, 28, and 38 dpi. Scale bars, 400 µm. B) Percent change of rCBF to baseline in control and *T. gondii*-infected mice over time. C) Percent weight change from baseline in control and *T. gondii*-infected mice. D) Percent change of rCBF in control and *T. gondii*-infected mice (Tg) administered cIg or anti-IFN-γ during reactivation. E) Percent weight change in control and *T. gondii*-infected mice administered cIg or anti-IFN-γ during reactivation. *n* = 8-11 mice (B-C) and 4-7 mice per group (D-E). *P < 0.05, **P < 0.005, ***P < 0.001, ****P < 0.0001; significance between groups at each timepoint was calculated by a two-way ANOVA (A-B) or a mixed-effects analysis (D-E) with a post-hoc Sidak's multiple comparisons test. In D-E significance shown between *T. gondii*-infected mice treated with IgG or anti-IFN-γ. Error bars represent SD.

Next, we assessed the contribution of clotting to CBF changes by treating *T. gondii*-infected mice with a low-molecular-weight heparin, nadroparin calcium, and measuring CBF longitudinally. Low-molecular-weight heparins inhibit clotting by binding to antithrombin and accelerating its inhibition of activated factor X (factor Xa) (Hirsh et al., 2001). Longitudinal laser speckle imaging was performed at 0, 4, and 7 dpi on infected mice treated with nadroparin or the vehicle control. We observed a partial rescue in the rCBF of *T. gondii*-infected mice treated with nadroparin calcium compared to those treated with PBS at 7 dpi (Fig. 3.10A). Interestingly, there was not a significant difference in weight loss between these groups (Fig. 3.10B). Collectively, these data suggest that clotting contributes to decreased CBF during acute *T. gondii* infection.

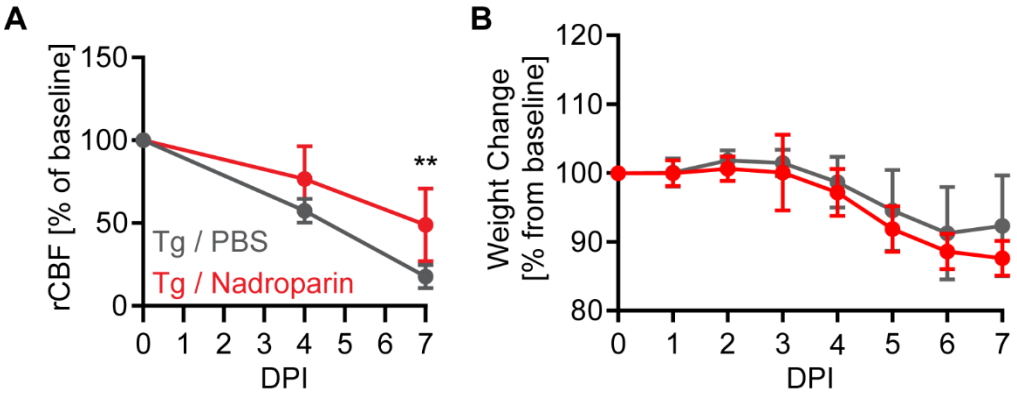

Figure 3.10. Nadroparin calcium treatment of *T. gondii*-infected mice. A) Percent change of rCBF to baseline in *T. gondii*-infected mice treated with PBS or nadroparin calcium at 0, 4, and 7 dpi. B) Percent weight change from baseline in *T. gondii*-infected mice treated with PBS or nadroparin calcium. *n* = 3-6 mice per group. **P < 0.005; significance was calculated by a mixed-effects analysis with a post hoc Sidak's multiple comparisons test. Error bars represent SD.

Finally, we assessed whether *T. gondii* infected human neutrophils expressed TF *in vitro*. To test this, we isolated neutrophils from whole blood donated by healthy human donors. We either infected the cells with *T. gondii*, treated them with LPS, or gave them sterile media, before extracting RNA at 1, 4, and 18 hrs. Notably, we found that *T. gondii*-infected neutrophils expressed similar levels of TF compared to LPS-treated neutrophils, and significantly more than the mock-treated cells at 4 and 18 hrs (Fig. 3.11).

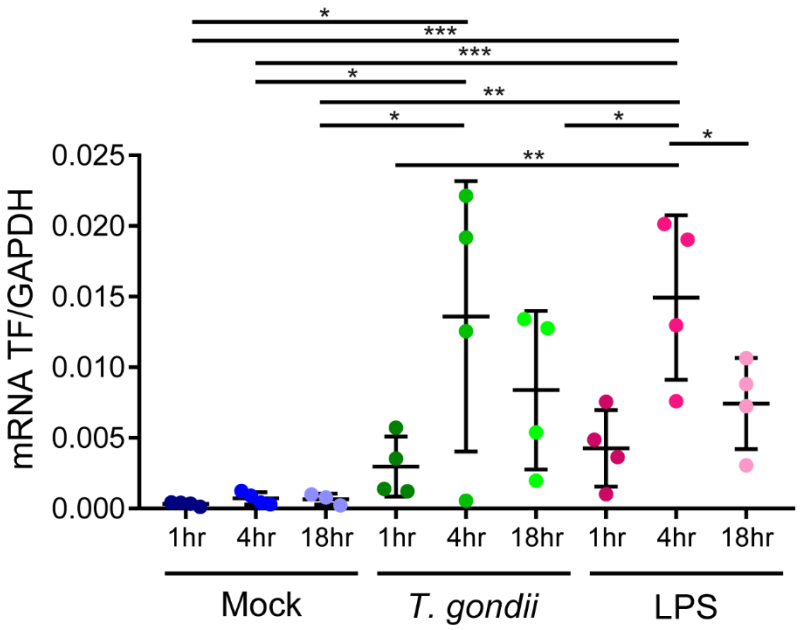

Figure 3.11. TF expression by *T. gondii*-infected neutrophils. Relative expression of tissue factor (TF) calculated using the Pfaffl method corrected for primer efficiency (1.34^(CT(GAPDH))/1.54^(CT(TF)) = Relative Expression) in human neutrophils treated *in vitro* with sterile media (mock), *T. gondii*, or LPS for 1, 4, and 18 hours. *P < 0.05, **P < 0.005, ***P < 0.001, ****P < 0.0001; significance between groups at each timepoint was calculated by a one-way ANOVA.

Discussion

The term ‘immunothrombosis’ was recently coined by Engelmann and Massberg (Engelmann and Massberg, 2012) and refers to an innate immune response induced by the coagulation cascade in blood vessels. In the context of immunothrombosis, coagulation supports the accumulation of myeloid cells, such as neutrophils and monocytes, at sites of infection, as well as the activation of the complement cascade (Engelmann and Massberg, 2012). These processes enhance the ability of the host to limit pathogen dissemination and control the pathogen infection (i.e., *E. coli* and *Yersinia pestis*) (Luo et al., 2013; Massberg et al., 2010).

Although the formation of blood clots may prove beneficial for ensnaring some pathogens in the bloodstream, clotting during infection in the cerebral vasculature has the potential to be detrimental. This may be the case in COVID-19 patients, some of whom have evidence of both cerebral ischemic stroke and reduced CBF (Helms et al., 2020; Soldatelli et al., 2020). Recent research has linked the accumulation of neutrophil extracellular traps (NETs) in the brain microvasculature to this pathology (Middleton et al., 2020). Furthermore, evidence of clotting is associated with negative survival outcomes in pediatric cerebral malaria cases (Hemmer et al., 1991; Moxon et al., 2015, 2013; Vogetseder et al., 2004). The current study demonstrates evidence of coagulation in cerebral vessels during infection with *T. gondii*. Although *Toxoplasma* and *Plasmodium* are both apicomplexan parasites that share many structural and biochemical features, the mechanisms of pathogenesis caused by these two pathogens are distinct. Indeed, in cerebral malaria, thrombosis is associated with regions of infected erythrocytes sequestered in small vessels in the brain due to cytoadhesion of the infected RBCs (Moxon et al., 2013). In particular, the virulence of *P. falciparum* infection is linked to the ability of the parasite-infected RBCs to form “knobs,” which are nanoscale-sized protrusions on

the surface of infected erythrocytes. These knobs are comprised of knob-associated histidine-rich protein (KAHRP) and *P. falciparum* erythrocyte membrane protein 1 (PfEMP1), and they facilitate the binding of infected erythrocytes to the vascular endothelium (Aikawa et al., 1990; Crabb et al., 1997; Roberts et al., 1985).

Unlike in cerebral malaria, clotting during *T. gondii* infection was detected at sites in the vasculature both near and far from clusters of *T. gondii* parasites. Previous research has found an effect of *T. gondii* infection on cerebral blood flow, which was attributed to the pruning of the cerebral microvessels as a consequence of infection (Estato et al., 2018). Interestingly, in this model of infection reported by Estato *et al.*, the reduced CBF was detected during acute infection (10 dpi) and at 40 dpi, only recovering by 180 dpi. Consistent with this work, we also observed decreased CBF during acute infection. However, in our longitudinal study of the same infected mice over time, we found a recovery of CBF, followed by a decline during reactivation induced by IFN-γ depletion. Notably, we observed a partial rescue of CBF with anticoagulation therapy. These findings indicate that other mechanisms also contribute to the reduced CBF during *T. gondii* infection. Our findings and others suggest the reduced CBF may relate to the architecture of the cerebral vasculature. Indeed, Estato *et al.* reported evidence of microvessel pruning, and we detected increased vessel and endothelial cell tortuosity during acute infection. Increased endothelial cell tortuosity has been previously linked to changes in blood pressure, which cause re-arrangement of the cytoskeleton of endothelial cells (Acevedo et al., 1993; Ohashi et al., 2007; Salwen et al., 1998). Vessel tortuosity has been linked to decreased CBF during aging, potentially explaining the decrease in CBF observed during *T. gondii* infection (Li et al., 2018). Future studies will be needed to determine the other factors contributing to decreased cerebral blood flow in *T. gondii* infection.

One outstanding question is the cause of clotting during *T. gondii* infection. One potential explanation for clotting near foci of infection is that an infected endothelial cell has recently been lysed, exposing subendothelial tissue factor (TF), and initiating clotting within the region. Another avenue of research is whether myeloid cells upregulate TF during *T. gondii* infection *in vivo* and trigger coagulation in the sites where they accumulate. Past work has shown that monocytes and neutrophils exposed to LPS can upregulate TF (Brühl et al., 2012; Darbousset et al., 2012; Maugeri et al., 2006; Pawlinski et al., 2010; Todoroki et al., 2000). Furthermore, we found that *in vitro* human neutrophils upregulated TF in response to *T. gondii*-infection. We have previously found that monocytes accumulate in the cerebral vessels of *T. gondii*-infected mice (Schneider et al., 2019), which may explain the coagulation at sites distant from foci of infection. These large numbers of adherent monocytes in the blood vessels could also contribute to the formation of clots by causing more turbulent blood flow, which creates an environment more favorable to clot formation. Coagulation could also be initiated through the intrinsic pathway of coagulation if activated platelets or other negatively charged surfaces are exposed to Factor XII within plasma.

It remains to be determined whether thrombosis during *T. gondii* infection is beneficial to the host or detrimental. Previous research has demonstrated that mice treated with warfarin and fibrinogen-deficient die during acute *T. gondii* infection compared to mock-treated or fibrinogen-sufficient control mice (Johnson et al., 2003a). Future studies will be needed to determine whether clotting helps prevent parasite dissemination or protects against hemorrhage during *T. gondii* infection.

Acknowledgements

We thank all members of the Lodoen, Choi, Gandhi, Morrissette, and Andrade labs for their helpful discussions on this project. This work was supported by National Institutes of Health R01 AI120846 (to M.B.L), American Cancer Society 126688-RSG-14-202-01-MPC (to M.B.L.), National Institutes of Health R21 AG066000 (to B.C.), National Institutes of Health R01 1R01EY029490-01A1 (to S.P.G.), National Institutes of Health T32AI060573 (to E.M.H. and C.A.S), National Institutes of Health T32GM008620 (to E.M.H.), National Institutes of Health 5TL1TR001415-06 (to C.C.), American Heart Association Predoctoral Fellowship 19PRE34380476 (to E.M.H.), as well as the Arnold and Mabel Beckman Foundation. Finally, this study was made possible in part through access to the Optical Biology Core Facility of the Developmental Biology Center, a shared resource supported by the Cancer Center Support Grant (CA-62203) and Center for Complex Biological Systems Support Grant (GM-076516) at the University of California, Irvine.

Chapter 4

Concluding Remarks

Mammals rely on a high-pressure system to oxygenate tissues, which makes us vulnerable to gross hemorrhage in the event of blood vessel damage. To counteract this risk, we have a robust mechanism (i.e., hemostasis) to rapidly seal vessel damage with a fibrin-platelet clot through activation of platelets and the coagulation cascade (Mackman et al., 2007). Occasionally this system is employed within intact vessels due to blood stasis (i.e., deep vein thrombosis) or in response to inflammation (i.e., disseminated intravascular coagulation), resulting in a thrombus (Mackman, 2008). Some systemic pathogens for instance SARS-CoV2, HIV, *E. coli*, and malaria can cause thrombosis in the brain (Helms et al., 2020; Luo et al., 2013; Massberg et al., 2010; Roberts et al., 1985). Thrombosis in the brain can reduce cerebral blood flow, which can be deadly, as demonstrated by ischemic stroke, which causes millions of deaths annually (>3 million in 2013) (Benjamin et al., 2017). Additionally, cerebral malaria patients with evidence of thrombosis have worse outcomes than those without thrombi (Moxon et al., 2015). However, previous research has demonstrated that thrombosis during infection (e.g., with *E. coli* and *Yersinia pestis*) can be a host-defense mechanism, for instance by entrapping pathogens within clots and concentrating immune cells near the invaders (Engelmann and Massberg, 2012), so more research is needed into studying the balance between the host-protective or host-harming effects of thrombosis in the brain during infection.

Recent work has demonstrated that *Toxoplasma gondii* infects and lyses central nervous system (CNS) endothelial cells that form the blood-brain barrier (BBB) (Konradt et al., 2016a). We hypothesized that this vessel damage could lead to clotting, for instance due to the exposure of subendothelial tissue factor on cells such as astrocytes (Eddleston et al., 1993; Mackman et al., 2007). Yet, although previous research had found evidence of clotting in the liver of *T. gondii*-infected mice, it still remained unclear as to whether thrombosis occurred in the brain

microvasculature during infection (Johnson et al., 2003b). Therefore, we investigated whether thrombi were present in the brain during *T. gondii*-infection and whether cerebral blood flow was affected. This parasite offers a good model to study these questions because *T.* gondii can infect BBB endothelial cells, causes high levels of circulating inflammatory cytokines (e.g., IFN-γ and TNF-α), and triggers a robust innate immune response.

Coagulation during T. gondii infection

When we examined brain sections from *T. gondii*-infected mice, we were able to detect fibrin and platelet deposition, which was absent in the control PBS-injected mice. Still to be explored is the cause of thrombosis during *T. gondii*-infection. The related Apicomplexa parasite, *Plasmodium falciparum*, causes clotting near sites in the vasculature where infected erythrocytes are sequestered during cerebral malaria (Moxon et al., 2015). This sequestration is mediated by 'knobs' found on infected erythrocytes (Aikawa et al., 1990; Crabb et al., 1997; Roberts et al., 1985; Zhang et al., 2015). These knobs are nanoscale structures made up of knob-associated histidine rich protein (KAHRP) and *P. falciparum* erythrocyte membrane protein 1 (PfEMP1), and they facilitate cytoadhesion of infected erythrocytes to the endothelium (Aikawa et al., 1990; Crabb et al., 1997; Roberts et al., 1985). However, the mechanism of clotting during *T. gondii* infection is likely to be different, as the clotting does not seem to be limited to regions near *T. gondii* foci. Future studies are needed into the contributions to thrombi formation of endothelial cells, innate immune cells, and the clotting cascade, which are considered below.

Part of what contributes to the thrombotic response is the aggregation of platelets and immune cells on the endothelium (Engelmann and Massberg, 2012). Endothelial adhesion

molecules expressed on activated endothelium are critical for promoting adhesion of platelets and immune cells (Coenen et al., 2017; Diamond et al., 1990; Elices et al., 1990). For instance platelets adhere to intracellular adhesion molecule-1 (ICAM-1) on endothelial cells through the platelet integrin αIIbβ3 (Coenen et al., 2017). ICAM-1 also promotes the adhesion of leukocytes to the endothelium through interactions with LFA-1 and Mac-1 (Diamond et al., 1990). Vascular cell adhesion molecule-1 (VCAM-1) promotes adhesion of leukocytes through interaction with VLA-4 (Elices et al., 1990). During *T. gondii* infection both ICAM-1 and VCAM-1 have been shown to be upregulated during acute and chronic infection in mouse models, and have been shown to be involved in recruiting immune cells into the brain (Deckert-Schlüter et al., 1999; Sa et al., 2014). Our work here confirms these previous data, as we found upregulation of both ICAM-1 and VCAM-1 during acute infection with *T. gondii* in mice. Furthermore, previous research has shown that *T. gondii* can bind to ICAM-1 through the parasite adhesin MIC2 *in vitro* and that this interaction was important for parasite transmigration across an endothelial cell layer, especially under shear stress conditions (Barragan et al., 2005; Harker et al., 2014). Additionally, ICAM-1 may be involved in the dissemination of *T. gondii* to the brain, as previous research showed that ICAM-1 may promote crawling of infected monocytes and the transmigration of infected dendritic cells *in vitro* (Furtado et al., 2012; Ueno et al., 2014). Future studies need to be done to investigate whether blocking ICAM-1 with monoclonal antibodies leads to a reduction in clotting in the brain during *T. gondii* infection due to reduced platelet and/or innate immune cell cytoadhesion in the cerebral blood vessels.

Additionally, the innate immune system can play multiple roles in promoting thrombosis during inflammation. For instance, myeloid cells, such as neutrophils and monocytes, can upregulate tissue factor (TF), when exposed to inflammatory stimulus (Brühl et al., 2012;

Darbousset et al., 2012; Maugeri et al., 2006). Indeed, we found that *T. gondii*-infected human neutrophils upregulated TF transcripts *in vitro*. This could contribute to intravascular thrombi formation. However, the expression of TF by myeloid cells and its role in thrombi formation during *T. gondii* infection *in vivo* still needs to be investigated. This could be done by investigating whether mice deficient in TF on myeloid cells ($TF^{fl/fl}$ LysM-cre) mice have reduced clotting in the brain. Notably, previous work from our lab found instances of monocytes packing microvessels within brains of *T. gondii* infected mice (Schneider et al., 2019). Additionally, neutrophil extracellular traps (NETs) released by neutrophils can contribute to thrombosis (Engelmann and Massberg, 2012). NETs can act as a scaffold for a growing thrombus, activating platelets, and inactivating clotting inhibitors (Fuchs et al., 2010; Massberg et al., 2010). Recent work has found evidence of NET formation after *T. gondii* infection (Abdallah et al., 2012; Lima et al., 2018). However, the formation of NETs in the CNS *in vivo* still needs to be examined, and whether they are a major contributor to thrombosis during *T. gondii* infection remains to be determined.

Finally, both the intrinsic and extrinsic coagulation pathways can be responsible for initiating coagulation. Typically, *in vivo*, the extrinsic pathway, initiated by the exposure of subendothelial tissue factor (TF) to plasma, initiates coagulation, especially in the context of hemostasis (Mackman et al., 2007). Exposure of subendothelial TF during *T. gondii* infection could happen after an infected endothelial cell is lysed (Blader et al., 2015; Konradt et al., 2016b). *In vitro*, the intrinsic pathway was found to be sufficient to trigger coagulation when plasma contacted an artificial surface, such as silica; however, parsing out the contributions of the intrinsic pathway to coagulation *in vivo* has been difficult (Grover and Mackman, 2019). Nevertheless, research into arterial and venous thrombi formation have indicated a role for the

factors of the intrinsic pathway (FXIIa, FXIa, FIXa) in pathological thrombus formation in rodent models (Grover and Mackman, 2019). Interestingly, knocking-out or pharmacologically blocking the intrinsic pathway in these pathological models did not interfere with physiological hemostasis (Grover and Mackman, 2019). Additional research needs to be done to explore the contributions of the extrinsic pathway (and the source of TF) and intrinsic pathway to the initiation and propagation of thrombosis during *T. gondii* infection. This could be addressed by treating mice with antibodies against the intrinsic pathway and employing cell-specific conditional knockout mice (e.g., mice deficient in TF on myeloid cells or astrocytes).

Cerebral blood flow changes during T. gondii infection

Previous work suggested that cerebral blood flow (CBF) was reduced during *T. gondii* infection *in vivo* (Estato et al., 2018). However, the experiments were not performed longitudinally on the same mice, and in our studies, we found that at baseline, there is some variability in the CBF of individual mice. This variability may potentially obscure or magnify differences between mock-treated and *T. gondii*-infected mice due to the baseline difference.

When designing the experiments to longitudinally measure CBF in *T. gondii*-infected mice, we discovered that there were few surgical techniques that would enable chronic optical access over a long period of time without utilizing craniotomies. Because craniotomies themselves can affect the integrity of the blood-brain barrier due to heat from drilling (Shoffstall et al., 2018), we sought to develop a less invasive procedure. Therefore, we developed the cyanoacrylate skull (CAS) surgery, which achieves optical access for >100 days by covering a resected skull with thin coatings of cyanoacrylate (Chapter 2). This allowed us to measure CBF longitudinally in

these mice using laser speckle imaging with a less invasive and quicker surgery than those relying on craniotomies.

We then applied the CAS surgical method with laser speckle imaging to test the changes in CBF throughout the course of infection with *T. gondii*. We found that initially, during acute infection, CBF declines, then it recovers during chronic infection, and decreases again with *T. gondii* reactivation. To specifically investigate whether the decreases in CBF were related to thrombi formation, we treated the mice with a low-molecular weight heparin (nadroparin calcium), which interferes with coagulation by inducing a permanent conformation shift in anti-thrombin. This causes anti-thrombin to become more efficient at deactivating thrombin, thus preventing clotting from occurring (Hirsh et al., 2001). Interestingly, treatment with nadroparin partially restored CBF, indicating that clotting may contribute to some of the CBF changes during *T. gondii*-infection, but not all. Notably, *T. gondii*-infected mice treated with nadroparin calcium did not have significant weight changes or increased mortality during acute infection compared to their PBS-treated controls. This suggests that anti-coagulation therapy did not change the course of infection. Future studies will need to be done to investigate whether thrombosis has resolved by 21 dpi, when we see that CBF has returned to baseline levels in *T. gondii*-infected mice, but this could explain the recovery in CBF. Furthermore, longer term treatment with nadroparin calcium could elucidate whether thrombosis and CBF decreases were harmful to the mice over a longer course of infection.

Other factors that could affect CBF during *T. gondii* infection are changes in the tortuosity of vessels and cerebral autoregulation. In our research, we found that endothelial cells increased in tortuosity during infection with *T. gondii*. Previously, in rodent aging models, vessel tortuosity has been associated with decreased CBF (Li et al., 2018). These changes in the vessel

architecture could also participate in decreasing CBF during *T. gondii* infection. Additionally, previous research has found that sepsis can disrupt cerebral autoregulation, which is the physiological process meant to maintain adequate and stable CBF across changes in systemic blood pressure through changes in vascular tone (either constriction or dilation) (Goodson et al., 2018). Autoregulation is complex and maintained through at least four intersecting mechanisms: 1) myogenic (i.e., smooth muscle contraction or dilation in response to changes in blood pressure), 2) neurogenic (i.e., sympathetic innervation in the blood vessel walls stimulating contraction or dilation), 3) metabolic (i.e., increased CO_2 in the blood results in dilation), 4) endothelial factors (e.g., NO causes vasodilation) (Armstead, 2016). Future research measuring responsiveness of CBF to changes in mean arterial pressure may reveal whether cerebral autoregulation is affected by *T. gondii* infection.

Coagulation and host-defense during T. gondii infection

One major outstanding question of this work is the relationship between coagulation and host-defense. Previous work has shown that coagulation can help the innate immune response to limit dissemination, recruit immune cells, create a scaffold in which immune cells (e.g., monocytes and neutrophils) can accumulate to neutralize an invading pathogen, and activate the complement system (Engelmann and Massberg, 2012). It was previously unclear whether clotting occurred in the CNS during *T. gondii* infection. Although, there have been a several case studies reporting retinal vessel occlusion in human ocular toxoplasmosis (Aggio et al., 2016; Chiang et al., 2012; Miserocchi et al., 2009; Willerson et al., 1977). Additionally, previous work found that *T. gondii*-infected mice deficient in fibrin formation or warfarin-treated mice did not survive acute infection, and had gross hemorrhage in their livers upon necropsy (Johnson et al.,

2003b). The researchers did not report increased parasite burden in the livers of infected mice in the absence of coagulation, but it is still an outstanding question whether clotting limits dissemination into the CNS. Furthermore, since *T. gondii* has a lytic life cycle, coagulation could be responsible for limiting hemorrhage in the host (Blader et al., 2015). Interestingly, in our hands, *T. gondii*-infected mice treated with a low-molecular-weight heparin did not die more quickly and had no significant difference in weight loss during infection compared to PBS-treated controls, unlike in Johnson et al. (Johnson et al., 2003b). This difference in outcomes could be due to the different pharmacokinetics of low-molecular weight heparin vs warfarin. Low-molecular-weight heparins directly act as anti-coagulants through activation of anti-thrombin. However, warfarin initially acts as pro-coagulant, due to the reliance of major anti-coagulative proteins on protein K (i.e. protein C and S) (Ageno et al., 2012). It still needs to be investigated, as to whether hemorrhage occurs in the brains of *T. gondii*-infected mice treated with an anti-clotting drug.

At the same time, coagulation in the brain can reduce CBF, as seen in ischemic stroke (Heiss et al., 1994; Siegel et al., 2015), which can be detrimental to the host, but could conceivably also help to limit dissemination. Alternatively, the reduced flow could bring extracellular parasites and parasitized immune cells in contact with the endothelial cells for longer periods of time, aiding dissemination across the blood-brain barrier. Interestingly, previous research has demonstrated that *T. gondii* is better able to cross endothelial cell barriers *in vitro* under shear stress conditions (Harker et al., 2014). Additional research will be needed to investigate the interplay between CBF changes and *T. gondii* invasion *in vivo*.

Furthermore, a related eukaryotic parasite, *Plasmodium falciparum*, emphasizes that coagulation is not always beneficial, as coagulation during cerebral malaria infection is

correlated with worse clinical outcomes (Aikawa et al., 1990; Moxon et al., 2015). During *Plasmodium* infection, coagulation is often found near areas where infected erythrocytes have adhered to the endothelium (Moxon et al., 2013). Interestingly, in our research, coagulation during *T. gondii*-infection did not seem to be limited to regions near parasites.

In summary, the work described here presents a previously unappreciated view of the hemodynamic response to *T. gondii* and the function consequences to CBF. We affirmed that the endothelium was activated during acute *T. gondii* infection, and that inflammatory cytokines were upregulated. To our knowledge, we are the first to report thrombosis in the brain during *T. gondii* infection. We also developed a relatively non-invasive rapid surgery to achieve chronic optical access and analyze CBF longitudinally in the same animal with laser speckle imaging. We applied this surgical method to *T. gondii*-infected mice, and found that initially CBF declines during acute infection, recovers to baseline during chronic infection, and then decreases again with reactivation. Experiments, using an anti-coagulant therapy showed that at least some of the changes in CBF may be attributed to thrombotic processes. Although further studies must be done, we are hopeful that this new knowledge could further understanding of thrombosis and hemodynamic changes during infection.

References

Abbott, N.J., Rönnbäck, L., Hansson, E., 2006. Astrocyte–endothelial interactions at the blood–brain barrier. Nat. Rev. Neurosci. 7, 41.

Abdallah, D.S.A., Lin, C., Ball, C.J., King, M.R., Duhamel, G.E., Denkers, E.Y., 2012. *Toxoplasma gondii* triggers release of human and mouse neutrophil extracellular traps. Infect. Immun. 80, 768–777. https://doi.org/10.1128/IAI.05730-11

Acevedo, A.D., Bowser, S.S., Gerritsen, M.E., Bizios, R., 1993. Morphological and proliferative responses of endothelial cells to hydrostatic pressure: Role of fibroblast growth factor. J. Cell. Physiol. 157, 603–614. https://doi.org/https://doi.org/10.1002/jcp.1041570321

Adams, L.B., Hibbs, J.B., Taintor, R.R., Krahenbuhl, J.L., 1990. Microbiostatic effect of murine-activated macrophages for *Toxoplasma gondii*. Role for synthesis of inorganic nitrogen oxides from L-arginine. J. Immunol. 144, 2725 LP – 2729.

Ageno, W., Gallus, A.S., Wittkowsky, A., Crowther, M., Hylek, E.M., Palareti, G., 2012. Oral anticoagulant therapy: Antithrombotic Therapy and Prevention of Thrombosis, 9th ed: American College of Chest Physicians Evidence-Based Clinical Practice Guidelines. Chest 141, e44S-e88S. https://doi.org/10.1378/chest.11-2292

Aggio, F.B., Novelli, F.J. de, Rosa, E.L., Nobrega, M.J., 2016. Combined branch retinal vein and artery occlusion in toxoplasmosis. Arq. Bras. Oftalmol. https://doi.org/10.5935/0004-2749.20160054

Aikawa, M., Iseki, M., Barnwell, J.W., Taylor, D., Oo, M.M., Howard, R.J., 1990. The pathology of human cerebral malaria. Am. J. Trop. Med. Hyg. 43, 30–37.

https://doi.org/10.4269/ajtmh.1990.43.30

Armstead, W.M., 2016. Cerebral Blood Flow Autoregulation and Dysautoregulation. Anesthesiol. Clin. 34, 465–477. https://doi.org/10.1016/j.anclin.2016.04.002

Ayata, C., Dunn, A.K., Gursoy-Özdemir, Y., Huang, Z., Boas, D.A., Moskowitz, M.A., 2004a. Laser speckle flowmetry for the study of cerebrovascular physiology in normal and ischemic mouse cortex. J. Cereb. Blood Flow Metab. 24, 744–755. https://doi.org/10.1097/01.WCB.0000122745.72175.D5

Ayata, C., Shin, H.K., Salomone, S., Ozdemir-Gursoy, Y., Boas, D.A., Dunn, A.K., Moskowitz, M.A., 2004b. Pronounced Hypoperfusion during Spreading Depression in Mouse Cortex. J. Cereb. Blood Flow Metab. 24, 1172–1182. https://doi.org/10.1097/01.WCB.0000137057.92786.F3

Barragan, A., Brossier, F., Sibley, L.D., 2005. Transepithelial migration of *Toxoplasma gondii* involves an interaction of intercellular adhesion molecule 1 (ICAM-1) with the parasite adhesin MIC2. Cell. Microbiol. 7, 561–568. https://doi.org/https://doi.org/10.1111/j.1462-5822.2005.00486.x

Beiter, K., Wartha, F., Albiger, B., Normark, S., Zychlinsky, A., Henriques-Normark, B., 2006. An endonuclease allows Streptococcus pneumoniae to escape from neutrophil extracellular traps. Curr. Biol. 16, 401–407. https://doi.org/10.1016/j.cub.2006.01.056

Bekpen, C., Hunn, J.P., Rohde, C., Parvanova, I., Guethlein, L., Dunn, D.M., Glowalla, E., Leptin, M., Howard, J.C., 2005. The interferon-inducible p47 (IRG) GTPases in vertebrates: loss of the cell autonomous resistance mechanism in the human lineage. Genome Biol. 6, R92. https://doi.org/10.1186/gb-2005-6-11-r92

Benjamin, E.J., Blaha, M.J., Chiuve, S.E., Cushman, M., Das, S.R., Deo, R., De Ferranti, S.D., Floyd, J., Fornage, M., Gillespie, C., Isasi, C.R., Jim'nez, M.C., Jordan, L.C., Judd, S.E., Lackland, D., Lichtman, J.H., Lisabeth, L., Liu, S., Longenecker, C.T., MacKey, R.H., Matsushita, K., Mozaffarian, D., Mussolino, M.E., Nasir, K., Neumar, R.W., Palaniappan, L., Pandey, D.K., Thiagarajan, R.R., Reeves, M.J., Ritchey, M., Rodriguez, C.J., Roth, G.A., Rosamond, W.D., Sasson, C., Towfghi, A., Tsao, C.W., Turner, M.B., Virani, S.S., Voeks, J.H., Willey, J.Z., Wilkins, J.T., Wu, J.H.Y., Alger, H.M., Wong, S.S., Muntner, P., 2017. Heart Disease and Stroke Statistics' 2017 Update: A Report from the American Heart Association. Circulation 135, e146–e603. https://doi.org/10.1161/CIR.0000000000000485

Bergmann, S., Hammerschmidt, S., 2007. Fibrinolysis and host response in bacterial infections. Thromb. Haemost. 98, 512–520.

Binquet, C., Lejeune, C., Seror, V., Peyron, F., Bertaux, A.-C., Scemama, O., Quantin, C., Béjean, S., Stillwaggon, E., Wallon, M., 2019. The cost-effectiveness of neonatal versus prenatal screening for congenital toxoplasmosis. PLoS One 14, e0221709.

Biswas, A., Bruder, D., Wolf, S.A., Jeron, A., Mack, M., Heimesaat, M.M., Dunay, I.R., 2015. Ly6C ^{high} Monocytes Control Cerebral Toxoplasmosis. J. Immunol. 194, 3223–3235. https://doi.org/10.4049/jimmunol.1402037

Blader, I.J., Coleman, B.I., Chen, C.-T., Gubbels, M.-J., 2015. Lytic Cycle of *Toxoplasma gondii* : 15 Years Later. Annu. Rev. Microbiol. 69, 463–485. https://doi.org/10.1146/annurev-micro-091014-104100

Blader, I.J., Saeij, J.P., 2009. Communication between *Toxoplasma gondii* and its host: impact on parasite growth, development, immune evasion, and virulence. APMIS 117, 458–476.

https://doi.org/10.1111/j.1600-0463.2009.02453.x

Boas, D.A., Dunn, A.K., 2010. Laser speckle contrast imaging in biomedical optics. J. Biomed. Opt. 15, 11109. https://doi.org/10.1117/1.3285504

Boyle, J.P., Rajasekar, B., Saeij, J.P.J., Ajioka, J.W., Berriman, M., Paulsen, I., Roos, D.S., Sibley, L.D., White, M.W., Boothroyd, J.C., 2006. Just one cross appears capable of dramatically altering the population biology of a eukaryotic pathogen like *Toxoplasma gondii*. Proc. Natl. Acad. Sci. U. S. A. 103, 10514–10519. https://doi.org/10.1073/pnas.0510319103

Brossier, F., Sibley, L.D., 2005. *Toxoplasma gondii*: Microneme protein MIC2. Int. J. Biochem. Cell Biol. 37, 2266–2272. https://doi.org/10.1016/j.biocel.2005.06.006

Brühl, M., Stark, K., Steinhart, A., Chandraratne, S., Konrad, I., Lorenz, M., Khandoga, A., Tirniceriu, A., Coletti, R., Köllnberger, M., Byrne, R.A., Laitinen, I., Walch, A., Brill, A., Pfeiler, S., Manukyan, D., Braun, S., Lange, P., Riegger, J., Ware, J., Eckart, A., Haidari, S., Rudelius, M., Schulz, C., Echtler, K., Brinkmann, V., Schwaiger, M., Preissner, K.T., Wagner, D.D., Mackman, N., Engelmann, B., Massberg, S., 2012. Monocytes, neutrophils, and platelets cooperate to initiate and propagate venous thrombosis in mice in vivo. J. Exp. Med. 209, 819–835. https://doi.org/10.1084/jem.20112322

Burg, J.L., Grover, C.M., Pouletty, P., Boothroyd, J.C., 1989. Direct and sensitive detection of a pathogenic protozoan, *Toxoplasma gondii*, by polymerase chain reaction. J. Clin. Microbiol. 27, 1787–1792. https://doi.org/10.1128/JCM.27.8.1787-1792.1989

Calamante, F., Thomas, D.L., Pell, G.S., Wiersma, J., Turner, R., 1999. Measuring Cerebral Blood Flow Using Magnetic Resonance Imaging Techniques. J. Cereb. Blood Flow Metab.

19, 701–735. https://doi.org/10.1097/00004647-199907000-00001

Cheng, H., Luo, Q., Zeng, S., Chen, S., Cen, J., Gong, H., 2003. Modified laser speckle imaging method with improved spatial resolution. J. Biomed. Opt. 8, 559. https://doi.org/10.1117/1.1578089

Chiang, E., Goldstein, D.A., Shapiro, M.J., Mets, M.B., 2012. Branch retinal artery occlusion caused by toxoplasmosis in an adolescent. Case Rep. Ophthalmol. https://doi.org/10.1159/000343262

Coenen, D.M., Mastenbroek, T.G., Cosemans, J.M.E.M., 2017. Platelet interaction with activated endothelium: mechanistic insights from microfluidics. Blood 130, 2819–2828. https://doi.org/10.1182/blood-2017-04-780825

Coureuil, M., Lécuyer, H., Bourdoulous, S., Nassif, X., 2017. A journey into the brain: insight into how bacterial pathogens cross blood-brain barriers. Nat. Rev. Microbiol. 15, 149–159. https://doi.org/10.1038/nrmicro.2016.178

Courret, N., Darche, S., Sonigo, P., Milon, G., Buzoni-Gatel, D., Tardieux, I., 2006. CD11c- and CD11b-expressing mouse leukocytes transport single *Toxoplasma gondii* tachyzoites to the brain. Blood 107, 309–316. https://doi.org/10.1182/blood-2005-02-0666

Crabb, B.S., Cooke, B.M., Reeder, J.C., Waller, R.F., Caruana, S.R., Davern, K.M., Wickham, M.E., Brown, G. V, Coppel, R.L., Cowman, A.F., 1997. Targeted Gene Disruption Shows That Knobs Enable Malaria-Infected Red Cells to Cytoadhere under Physiological Shear Stress. Cell 89, 287–296. https://doi.org/https://doi.org/10.1016/S0092-8674(00)80207-X

Crouzet, C., Wilson, R.H., Bazrafkan, A., Farahabadi, M.H., Lee, D., Alcocer, J., Tromberg,

B.J., Choi, B., Akbari, Y., 2016. Cerebral blood flow is decoupled from blood pressure and linked to EEG bursting after resuscitation from cardiac arrest. Biomed. Opt. Express 7, 4660–4673. https://doi.org/10.1364/BOE.7.004660

Dalkara, T., Irikura, K., Huang, Z., Panahian, N., Moskowitz, M.A., 1995. Cerebrovascular responses under controlled and monitored physiological conditions in the anesthetized mouse. J. Cereb. blood flow Metab. Off. J. Int. Soc. Cereb. Blood Flow Metab. 15, 631–638. https://doi.org/10.1038/jcbfm.1995.78

Darbousset, R., Thomas, G.M., Mezouar, S., Frère, C., Bonier, R., Mackman, N., Renné, T., Dignat-George, F., Dubois, C., Panicot-Dubois, L., 2012. Tissue factor-positive neutrophils bind to injured endothelial wall and initiate thrombus formation. Blood 120, 2133–2143. https://doi.org/10.1182/blood-2012-06-437772

Dardé, M.L., Villena, I., Pinon, J.M., Beguinot, I., 1998. Severe toxoplasmosis caused by a *Toxoplasma gondii* strain with a new isoenzyme type acquired in French Guyana. J. Clin. Microbiol. 36, 324. https://doi.org/10.1128/JCM.36.1.324-324.1998

Deckert-Schlüter, M., Bluethmann, H., Kaefer, N., Rang, A., Schlüter, D., 1999. Interferon-gamma receptor-mediated but not tumor necrosis factor receptor type 1- or type 2-mediated signaling is crucial for the activation of cerebral blood vessel endothelial cells and microglia in murine Toxoplasma encephalitis. Am. J. Pathol. 154, 1549–1561. https://doi.org/10.1016/s0002-9440(10)65408-9

Demar, M., Ajzenberg, D., Maubon, D., Djossou, F., Panchoe, D., Punwasi, W., Valery, N., Peneau, C., Daigre, J.-L., Aznar, C., Cottrelle, B., Terzan, L., Dardé, M.-L., Carme, B., 2007. Fatal outbreak of human toxoplasmosis along the Maroni River: epidemiological,

clinical, and parasitological aspects. Clin. Infect. Dis. an Off. Publ. Infect. Dis. Soc. Am. 45, e88-95. https://doi.org/10.1086/521246

Diamond, M.S., Staunton, D.E., de Fougerolles, A.R., Stacker, S.A., Garcia-Aguilar, J., Hibbs, M.L., Springer, T.A., 1990. ICAM-1 (CD54): a counter-receptor for Mac-1 (CD11b/CD18). J. Cell Biol. 111, 3129–3139. https://doi.org/10.1083/jcb.111.6.3129

Dorgalaleh, A., Rashidpanah, J., 2016. Blood coagulation factor XIII and factor XIII deficiency. Blood Rev. 30, 461–475. https://doi.org/https://doi.org/10.1016/j.blre.2016.06.002

Drake, T.A., Morrissey, J.H., Edgington, T.S., 1989. Selective cellular expression of tissue factor in human tissues. Implications for disorders of hemostasis and thrombosis. Am. J. Pathol. 134, 1087–1097.

Drew, P.J., Shih, A.Y., Driscoll, J.D., Knutsen, P.M., Blinder, P., Davalos, D., Akassoglou, K., Tsai, P.S., Kleinfeld, D., 2010. Chronic optical access through a polished and reinforced thinned skull. Nat. Methods 7, 981–984. https://doi.org/10.1038/nmeth.1530

Dubey, J.P., 1998. Advances in the life cycle of *Toxoplasma gondii*. Int. J. Parasitol. 28, 1019–1024. https://doi.org/10.1016/S0020-7519(98)00023-X

Dubey, J.P., Frenkel, J.K., 1972. Cyst-induced toxoplasmosis in cats. J. Protozool. 19, 155–177. https://doi.org/10.1111/j.1550-7408.1972.tb03431.x

Dubey, J.P., Speer, C.A., Shen, S.K., Kwok, O.C., Blixt, J.A., 1997. Oocyst-induced murine toxoplasmosis: life cycle, pathogenicity, and stage conversion in mice fed *Toxoplasma gondii* oocysts. J. Parasitol. 83, 870–882. https://doi.org/10.2307/3284282

Dunay, I.R., DaMatta, R.A., Fux, B., Presti, R., Greco, S., Colonna, M., Sibley, L.D., 2008.

Gr1+ Inflammatory Monocytes Are Required for Mucosal Resistance to the Pathogen *Toxoplasma gondii*. Immunity 29, 306–317. https://doi.org/10.1016/j.immuni.2008.05.019

Dunay, I.R., Fuchs, A., David Sibley, L., 2010. Inflammatory monocytes but not neutrophils are necessary to control infection with *Toxoplasma gondii* in mice. Infect. Immun. 78, 1564–1570. https://doi.org/10.1128/IAI.00472-09

Dunn, A.K., Bolay, H., Moskowitz, M.A., Boas, D.A., 2001. Dynamic Imaging of Cerebral Blood Flow Using Laser Speckle. J. Cereb. Blood Flow Metab. 21, 195–201. https://doi.org/10.1097/00004647-200103000-00002

Dunn, D., Wallon, M., Peyron, F., Petersen, E., Peckham, C., Gilbert, R., 1999. Mother-to-child transmission of toxoplasmosis: risk estimates for clinical counselling. Lancet 353, 1829–1833. https://doi.org/https://doi.org/10.1016/S0140-6736(98)08220-8

Dupont, C.D., Christian, D.A., Hunter, C.A., 2012. Immune response and immunopathology during toxoplasmosis. Semin. Immunopathol. 34, 793–813. https://doi.org/10.1007/s00281-012-0339-3

Eddleston, M., de la Torre, J.C., Oldstone, M.B., Loskutoff, D.J., Edgington, T.S., Mackman, N., 1993. Astrocytes are the primary source of tissue factor in the murine central nervous system. A role for astrocytes in cerebral hemostasis. J. Clin. Invest. 92, 349–358. https://doi.org/10.1172/JCI116573

Elices, M.J., Osborn, L., Takada, Y., Crouse, C., Luhowskyj, S., Hemler, M.E., Lobb, R.R., 1990. VCAM-1 on activated endothelium interacts with the leukocyte integrin VLA-4 at a site distinct from the VLA-4/fibronectin binding site. Cell 60, 577–584. https://doi.org/10.1016/0092-8674(90)90661-w

Engelmann, B., Massberg, S., 2012. Thrombosis as an intravascular effector of innate immunity. Nat. Rev. Immunol. 13, 34–45. https://doi.org/10.1038/nri3345

Estato, V., Stipursky, J., Gomes, F., Mergener, T.C., Frazão-Teixeira, E., Allodi, S., Tibiriçá, E., Barbosa, H.S., Adesse, D., 2018. The Neurotropic Parasite *Toxoplasma gondii* Induces Sustained Neuroinflammation with Microvascular Dysfunction in Infected Mice. Am. J. Pathol. 188, 2674–2687. https://doi.org/10.1016/j.ajpath.2018.07.007

Fang, F.C., 2004. Antimicrobial reactive oxygen and nitrogen species: concepts and controversies. Nat. Rev. Microbiol. 2, 820–832. https://doi.org/10.1038/nrmicro1004

Fercher, A.F., Briers, J.D., 1981. Flow visualization by means of single-exposure speckle photography. Opt. Commun. 37, 326–330. https://doi.org/https://doi.org/10.1016/0030-4018(81)90428-4

Fleck, R.A., Rao, L. V, Rapaport, S.I., Varki, N., 1990. Localization of human tissue factor antigen by immunostaining with monospecific, polyclonal anti-human tissue factor antibody. Thromb. Res. 59, 421–437. https://doi.org/10.1016/0049-3848(90)90148-6

Fox, B.A., Gigley, J.P., Bzik, D.J., 2004. *Toxoplasma gondii* lacks the enzymes required for de novo arginine biosynthesis and arginine starvation triggers cyst formation. Int. J. Parasitol. 34, 323–331. https://doi.org/10.1016/j.ijpara.2003.12.001

Frenkel, J.K., Dubey, J.P., Miller, N.L., 1970. *Toxoplasma gondii* in Cats: Fecal Stages Identified as Coccidian Oocysts. Science (80-.). 167, 893 LP – 896. https://doi.org/10.1126/science.167.3919.893

Fuchs, T.A., Brill, A., Duerschmied, D., Schatzberg, D., Monestier, M., Myers, D.D., Wrobleski,

S.K., Wakefield, T.W., Hartwig, J.H., Wagner, D.D., 2010. Extracellular DNA traps promote thrombosis. Proc. Natl. Acad. Sci. 107, 15880 LP – 15885. https://doi.org/10.1073/pnas.1005743107

Furtado, J.M., Bharadwaj, A.S., Ashander, L.M., Olivas, A., Smith, J.R., 2012. Migration of *Toxoplasma gondii*-infected dendritic cells across human retinal vascular endothelium. Invest. Ophthalmol. Vis. Sci. 53, 6856–6862. https://doi.org/10.1167/iovs.12-10384

Gazzinelli, R., Xu, Y., Hieny, S., Cheever, A., Sher, A., 1992. Simultaneous depletion of CD4+ and CD8+ T lymphocytes is required to reactivate chronic infection with *Toxoplasma gondii*. J. Immunol. 149, 175 LP – 180.

Glaser, C.B., Morser, J., Clarke, J.H., Blasko, E., McLean, K., Kuhn, I., Chang, R.J., Lin, J.H., Vilander, L., Andrews, W.H., Light, D.R., 1992. Oxidation of a specific methionine in thrombomodulin by activated neutrophil products blocks cofactor activity. A potential rapid mechanism for modulation of coagulation. J. Clin. Invest. 90, 2565–2573. https://doi.org/10.1172/jci116151

Goldey, G.J., Roumis, D.K., Glickfeld, L.L., Kerlin, A.M., Reid, R.C., Bonin, V., Schafer, D.P., Andermann, M.L., 2014. Removable cranial windows for long-term imaging in awake mice. Nat. Protoc. 9, 2515–2538. https://doi.org/10.1038/nprot.2014.165

Goodson, C.M., Rosenblatt, K., Rivera-Lara, L., Nyquist, P., Hogue, C.W., 2018. Cerebral blood flow autoregulation in sepsis for the intensivist: Why its monitoring may be the future of individualized care. J. Intensive Care Med. 33, 63–73. https://doi.org/10.1177/0885066616673973

Gov, L., Karimzadeh, A., Ueno, N., Lodoen, M.B., 2013. Human innate immunity to

Toxoplasma gondii is mediated by host caspase-1 and ASC and parasite GRA15. MBio 4, e00255–13. https://doi.org/10.1128/mBio.00255-13

Grigg, M.E., Ganatra, J., Boothroyd, J.C., Margolis, T.P., 2001. Unusual abundance of atypical strains associated with human ocular toxoplasmosis. J. Infect. Dis. 184, 633–639. https://doi.org/10.1086/322800

Grover, S.P., Mackman, N., 2019. Intrinsic pathway of coagulation and thrombosis: Insights from animal models. Arterioscler. Thromb. Vasc. Biol. 39, 331–338. https://doi.org/10.1161/ATVBAHA.118.312130

Harker, K.S., Jivan, E., McWhorter, F.Y., Liu, W.F., Lodoen, M.B., 2014. Shear forces enhance *Toxoplasma gondii* tachyzoite motility on vascular endothelium. MBio 5, e01111-13. https://doi.org/10.1128/mBio.01111-13

Hauge, A, Thoresen, M., Walløe, L., 1980. Changes in cerebral blood flow during hyperventilation and CO2-breathing measured transcutaneously in humans by a bidirectional, pulsed, ultrasound Doppler blood velocitymeter. Acta Physiol. Scand. 110, 167–173. https://doi.org/10.1111/j.1748-1716.1980.tb06647.x

Hauge, Anton, Thoresen, M., Walløe, L., 1980. Changes in cerebral blood flow during hyperventilation and CO2-breathing measured transcutaneously in humans by a bidirectional, pulsed, ultrasound doppler blood velocitymeter. Acta Physiol. Scand. 110, 167–173. https://doi.org/10.1111/j.1748-1716.1980.tb06647.x

Heiss, W.-D., Graf, R., Wienhard, K., Löttgen, J., Saito, R., Fujita, T., Rosner, G., Wagner, R., 1994. Dynamic Penumbra Demonstrated by Sequential Multitracer PET after Middle Cerebral Artery Occlusion in Cats. J. Cereb. Blood Flow Metab. 14, 892–902.

https://doi.org/10.1038/jcbfm.1994.120

Helms, J., Kremer, S., Merdji, H., Clere-Jehl, R., Schenck, M., Kummerlen, C., Collange, O., Boulay, C., Fafi-Kremer, S., Ohana, M., Anheim, M., Meziani, F., 2020. Neurologic Features in Severe SARS-CoV-2 Infection. N. Engl. J. Med. 382, 2268–2270. https://doi.org/10.1056/NEJMc2008597

Hemmer, C.J., Kern, P., Holst, F.G.E., Radtke, K.P., Egbring, R., Bierhaus, A., Nawroth, P.P., Dietrich, M., 1991. Activation of the host response in human plasmodium falciparum malaria: Relation of parasitemia to tumor necrosis factor/cachectin, thrombin-antithrombin III, and protein C levels. Am. J. Med. 91, 37–44. https://doi.org/https://doi.org/10.1016/0002-9343(91)90071-5

Hill, D., Dubey, J.P., 2002. *Toxoplasma gondii*: Transmission, diagnosis, and prevention. Clin. Microbiol. Infect. 8, 634–640. https://doi.org/10.1046/j.1469-0691.2002.00485.x

Hirsh, J., Warkentin, T.E., Shaughnessy, S.G., Anand, S.S., Halperin, J.L., Raschke, R., Granger, C., Ohman, E.M., Dalen, J.E., 2001. Heparin and Low-Molecular-Weight Heparin Mechanisms of Action, Pharmacokinetics, Dosing, Monitoring, Efficacy, and Safety. Chest 119, 64S-94S. https://doi.org/https://doi.org/10.1378/chest.119.1_suppl.64S

Holbrook, A.M., Pereira, J.A., Labiris, R., McDonald, H., Douketis, J.D., Crowther, M., Wells, P.S., 2005. Systematic overview of warfarin and its drug and food interactions. Arch. Intern. Med. 165, 1095–1106. https://doi.org/10.1001/archinte.165.10.1095

Hoover, E.M., Crouzet, C., Bordas, J.M., Figueroa Velez, D.X., Gandhi, S.P., Choi, B., Lodoen, M.B., 2021. Transcranial chronic optical access to longitudinally measure cerebral blood flow. J. Neurosci. Methods 350, 109044.

https://doi.org/https://doi.org/10.1016/j.jneumeth.2020.109044

Horowitz Brown, S., Zarnowski, R., Sharpee, W.C., Keller, N.P., 2008. Morphological transitions governed by density dependence and lipoxygenase activity in *Aspergillus flavus*. Appl. Environ. Microbiol. 74, 5674–5685. https://doi.org/10.1128/AEM.00565-08

Hunter, C.A., Abrams, J.S., Beaman, M.H., Remington, J.S., 1993. Cytokine mRNA in the central nervous system of SCID mice infected with *Toxoplasma gondii*: importance of T-cell-independent regulation of resistance to *T. gondii*. Infect. Immun. 61, 4038–4044. https://doi.org/10.1128/IAI.61.10.4038-4044.1993

Huynh, M.-H., Carruthers, V.B., 2006. *Toxoplasma* MIC2 Is a Major Determinant of Invasion and Virulence. PLOS Pathog. 2, e84.

Janssen, B.J.A., De Celle, T., Debets, J.J.M., Brouns, A.E., Callahan, M.F., Smith, T.L., 2004. Effects of anesthetics on systemic hemodynamics in mice. Am. J. Physiol. Circ. Physiol. 287, H1618–H1624. https://doi.org/10.1152/ajpheart.01192.2003

Johnson, L.L., 1992. SCID mouse models of acute and relapsing chronic *Toxoplasma gondii* infections. Infect. Immun. 60, 3719–3724. https://doi.org/10.1128/IAI.60.9.3719-3724.1992

Johnson, L.L., Berggren, K.N., Szaba, F.M., Chen, W., Smiley, S.T., 2003a. Fibrin-mediated protection against infection-stimulated immunopathology. J. Exp. Med. 197, 801–6. https://doi.org/10.1084/jem.20021493

Johnson, L.L., Berggren, K.N., Szaba, F.M., Chen, W., Smiley, S.T., 2003b. Fibrin-mediated Protection Against Infection-stimulated Immunopathology. J. Exp. Med. 197, 801 LP – 806.

Khan, A., Dubey, J.P., Su, C., Ajioka, J.W., Rosenthal, B.M., Sibley, L.D., 2011. Genetic

analyses of atypical *Toxoplasma gondii* strains reveal a fourth clonal lineage in North America. Int. J. Parasitol. 41, 645–655. https://doi.org/10.1016/j.ijpara.2011.01.005

Khan, A., Fux, B., Su, C., Dubey, J.P., Darde, M.L., Ajioka, J.W., Rosenthal, B.M., Sibley, L.D., 2007. Recent transcontinental sweep of *Toxoplasma gondii* driven by a single monomorphic chromosome. Proc. Natl. Acad. Sci. U. S. A. 104, 14872–14877. https://doi.org/10.1073/pnas.0702356104

Kleinfeld, D., Mitra, P.P., Helmchen, F., Denk, W., 1998. Fluctuations and stimulus-induced changes in blood flow observed in individual capillaries in layers 2 through 4 of rat neocortex. Proc. Natl. Acad. Sci. 95, 15741 LP – 15746. https://doi.org/10.1073/pnas.95.26.15741

Knowland, D., Arac, A., Sekiguchi, K.J., Hsu, M., Lutz, S.E., Perrino, J., Steinberg, G.K., Barres, B.A., Nimmerjahn, A., Agalliu, D., 2014. Stepwise Recruitment of Transcellular and Paracellular Pathways Underlies Blood-Brain Barrier Breakdown in Stroke. Neuron 82, 603–617. https://doi.org/https://doi.org/10.1016/j.neuron.2014.03.003

Kogure, D., Matsuda, H., Ohnishi, T., Asada, T., Uno, M., Kunihiro, T., Nakano, S., Takasaki, M., 2000. Longitudinal evaluation of early Alzheimer's disease using brain perfusion SPECT. J. Nucl. Med. 41, 1155–1162.

Konradt, C., Ueno, N., Christian, D.A., Delong, J.H., Pritchard, G.H., Herz, J., Bzik, D.J., Koshy, A.A., McGavern, D.B., Lodoen, M.B., Hunter, C.A., 2016a. Endothelial cells are a replicative niche for entry of *Toxoplasma gondii* to the central nervous system. Nat. Microbiol. 1, 16001. https://doi.org/10.1038/nmicrobiol.2016.1

Konradt, C., Ueno, N., Christian, D.A., Delong, J.H., Pritchard, G.H., Herz, J., Bzik, D.J.,

Koshy, A.A., McGavern, D.B., Lodoen, M.B., Hunter, C.A., 2016b. Endothelial cells are a replicative niche for entry of *Toxoplasma gondii* to the central nervous system. Nat. Microbiol. 1, 16001.

Krem, M.M., Cera, E. Di, 2002. Evolution of enzyme cascades from embryonic development to blood coagulation. Trends Biochem. Sci. 27, 67–74. https://doi.org/https://doi.org/10.1016/S0968-0004(01)02007-2

Kumar, H., Tolia, N.H., 2019. Getting in: The structural biology of malaria invasion. PLoS Pathog. 15, e1007943–e1007943. https://doi.org/10.1371/journal.ppat.1007943

Lachenmaier, S.M., Deli, M.A., Meissner, M., Liesenfeld, O., 2011. Intracellular transport of *Toxoplasma gondii* through the blood-brain barrier. J. Neuroimmunol. 232, 119–130. https://doi.org/10.1016/j.jneuroim.2010.10.029

Lekutis, C., Ferguson, D.J.P., Grigg, M.E., Camps, M., Boothroyd, J.C., 2001. Surface antigens of *Toxoplasma gondii*: variations on a theme. Int. J. Parasitol. 31, 1285–1292. https://doi.org/https://doi.org/10.1016/S0020-7519(01)00261-2

Lertsakdadet, B., Yang, B.Y., Dunn, C.E., Ponticorvo, A., Crouzet, C., Bernal, N., Durkin, A.J., Choi, B., 2018. Correcting for motion artifact in handheld laser speckle images. J. Biomed. Opt. 23, 1–7. https://doi.org/10.1117/1.JBO.23.3.036006

Li, P., Ni, S., Zhang, L., Zeng, S., Luo, Q., 2006. Imaging cerebral blood flow through the intact rat skull with temporal laser speckle imaging. Opt. Lett. 31, 1824–1826. https://doi.org/10.1364/OL.31.001824

Li, Y., Choi, W.J., Wei, W., Song, S., Zhang, Q., Liu, J., Wang, R.K., 2018. Aging-associated

changes in cerebral vasculature and blood flow as determined by quantitative optical coherence tomography angiography. Neurobiol. Aging 70, 148–159. https://doi.org/https://doi.org/10.1016/j.neurobiolaging.2018.06.017

Lima, T.S., Gov, L., Lodoen, M.B., 2018. Evasion of Human Neutrophil-Mediated Host Defense during *Toxoplasma gondii* Infection. MBio 9, e02027-17. https://doi.org/10.1128/mBio.02027-17

Ling, Y.M., Shaw, M.H., Ayala, C., Coppens, I., Taylor, G.A., Ferguson, D.J.P., Yap, G.S., 2006. Vacuolar and plasma membrane stripping and autophagic elimination of *Toxoplasma gondii* in primed effector macrophages. J. Exp. Med. 203, 2063–2071. https://doi.org/10.1084/jem.20061318

Livak, K.J., Schmittgen, T.D., 2001. Analysis of relative gene expression data using real-time quantitative PCR and the 2(-Delta Delta C(T)) Method. Methods 25, 402–408. https://doi.org/10.1006/meth.2001.1262

Loof, Torsten G, Mörgelin, M., Johansson, L., Oehmcke, S., Olin, A.I., Dickneite, G., Norrby-Teglund, A., Theopold, U., Herwald, H., 2011. Coagulation, an ancestral serine protease cascade, exerts a novel function in early immune defense. Blood 118, 2589–2598. https://doi.org/https://doi.org/10.1182/blood-2011-02-337568

Loof, T G, Schmidt, O., Herwald, H., Theopold, U., 2011. Coagulation Systems of Invertebrates and Vertebrates and Their Roles in Innate Immunity: The Same Side of Two Coins? J. Innate Immun. 3, 34–40. https://doi.org/10.1159/000321641

Luan, L., Wei, X., Zhao, Z., Siegel, J.J., Potnis, O., Tuppen, C.A., Lin, S., Kazmi, S., Fowler, R.A., Holloway, S., Dunn, A.K., Chitwood, R.A., Xie, C., 2017. Ultraflexible

nanoelectronic probes form reliable, glial scar–free neural integration. Sci. Adv. 3, e1601966. https://doi.org/10.1126/sciadv.1601966

Lubiana, P., Bouws, P., Roth, L.K., Dörpinghaus, M., Rehn, T., Brehmer, J., Wichers, J.S., Bachmann, A., Höhn, K., Roeder, T., Thye, T., Gutsmann, T., Burmester, T., Bruchhaus, I., Metwally, N.G., 2020. Adhesion between *P. falciparum* infected erythrocytes and human endothelial receptors follows alternative binding dynamics under flow and febrile conditions. Sci. Rep. 10, 4548. https://doi.org/10.1038/s41598-020-61388-2

Luft, B.J., Remington, J.S., 1992. Toxoplasmic Encephalitis in AIDS. Clin. Infect. Dis. 15, 211–222. https://doi.org/10.1093/clinids/15.2.211

Luo, D., Lin, J.-S., Parent, M.A., Mullarky-Kanevsky, I., Szaba, F.M., Kummer, L.W., Duso, D.K., Tighe, M., Hill, J., Gruber, A., Mackman, N., Gailani, D., Smiley, S.T., 2013. Fibrin Facilitates Both Innate and T Cell Mediated Defense against *Yersinia pestis*. J. Immunol. 190, 4149–4161. https://doi.org/10.4049/jimmunol.1203253

Mackman, N., 2008. Triggers, targets and treatments for thrombosis. Nature 451, 914–918. https://doi.org/10.1038/nature06797

Mackman, N., 2005. Tissue-specific hemostasis in mice. Arterioscler. Thromb. Vasc. Biol. https://doi.org/10.1161/01.ATV.0000183884.06371.52

Mackman, N., Sawdey, M.S., Keeton, M.R., Loskutoff, D.J., 1993. Murine tissue factor gene expression *in vivo*. Tissue and cell specificity and regulation by lipopolysaccharide. Am. J. Pathol. 143, 76–84.

Mackman, N., Tilley, R.E., Key, N.S., 2007. Role of the extrinsic pathway of blood coagulation

in hemostasis and thrombosis. Arterioscler. Thromb. Vasc. Biol. 27, 1687–1693. https://doi.org/10.1161/ATVBAHA.107.141911

Maldonado, Y.A., Read, J.S., Byington, C.L., Barnett, E.D., Davies, H.D., Edwards, K.M., Lynfield, R., Munoz, F.M., Nolt, D., Nyquist, A.C., Rathore, M.H., Sawyer, M.H., Steinbach, W.J., Tan, T.Q., Zaoutis, T.E., 2017. Diagnosis, treatment, and prevention of congenital toxoplasmosis in the United States. Pediatrics 139, e20163860. https://doi.org/10.1542/peds.2016-3860

Marcos, A.C., Siqueira, M., Alvarez-Rosa, L., Cascabulho, C.M., Waghabi, M.C., Barbosa, H.S., Adesse, D., Stipursky, J., 2020. *Toxoplasma gondii* infection impairs radial glia differentiation and its potential to modulate brain microvascular endothelial cell function in the cerebral cortex. Microvasc. Res. 131, 104024. https://doi.org/10.1016/j.mvr.2020.104024

Marra, C.M., 2018. Chapter 9 - Central nervous system infection with *Toxoplasma gondii*, in: Brew, B.J.B.T.-H. of C.N. (Ed.), The Neurology of HIV Infection. Elsevier, pp. 117–122. https://doi.org/https://doi.org/10.1016/B978-0-444-63849-6.00009-8

Martens, S., Parvanova, I., Zerrahn, J., Griffiths, G., Schell, G., Reichmann, G., Howard, J.C., 2005. Disruption of *Toxoplasma gondii* Parasitophorous Vacuoles by the Mouse p47-Resistance GTPases. PLOS Pathog. 1, e24.

Martin, A.J., Friston, K.J., Colebatch, J.G., Frackowiak, R.S.J., 1991. Decreases in Regional Cerebral Blood Flow with Normal Aging. J. Cereb. Blood Flow Metab. 11, 684–689. https://doi.org/10.1038/jcbfm.1991.121

Martorelli Di Genova, B., Wilson, S.K., Dubey, J.P., Knoll, L.J., 2019. Intestinal delta-6-

desaturase activity determines host range for *Toxoplasma* sexual reproduction. PLOS Biol. 17, e3000364.

Massberg, S., Grahl, L., Von Bruehl, M.L., Manukyan, D., Pfeiler, S., Goosmann, C., Brinkmann, V., Lorenz, M., Bidzhekov, K., Khandagale, A.B., Konrad, I., Kennerknecht, E., Reges, K., Holdenrieder, S., Braun, S., Reinhardt, C., Spannagl, M., Preissner, K.T., Engelmann, B., 2010. Reciprocal coupling of coagulation and innate immunity via neutrophil serine proteases. Nat. Med. 16, 887–896. https://doi.org/10.1038/nm.2184

Maugeri, N., Brambilla, M., Camera, M., Carbone, A., Tremoli, E., Donati, M.B., De Gaetano, G., Cerletti, C., 2006. Human polymorphonuclear leukocytes produce and express functional tissue factor upon stimulation. J. Thromb. Haemost. 4, 1323–1330. https://doi.org/10.1111/j.1538-7836.2006.01968.x

Middleton, E.A., He, X.-Y., Denorme, F., Campbell, R.A., Ng, D., Salvatore, S.P., Mostyka, M., Baxter-Stoltzfus, A., Borczuk, A.C., Loda, M., Cody, M.J., Manne, B.K., Portier, I., Harris, E.S., Petrey, A.C., Beswick, E.J., Caulin, A.F., Iovino, A., Abegglen, L.M., Weyrich, A.S., Rondina, M.T., Egeblad, M., Schiffman, J.D., Yost, C.C., 2020. Neutrophil extracellular traps contribute to immunothrombosis in COVID-19 acute respiratory distress syndrome. Blood 136, 1169–1179. https://doi.org/10.1182/blood.2020007008

Miserocchi, E., Modorati, G., Rama, P., 2009. Atypical toxoplasmosis masquerading late occurrence of typical findings. Eur. J. Ophthalmol. 19, 1091–1093.

Montoya, J.G., Liesenfeld, O., 2004. Toxoplasmosis. Lancet 363, 1965–1976. https://doi.org/10.1016/S0140-6736(04)16412-X

Mordue, D.G., Håkansson, S., Niesman, I., Sibley, L.D., 1999. *Toxoplasma gondii* resides in a

vacuole that avoids fusion with host cell endocytic and exocytic vesicular trafficking pathways. Exp. Parasitol. 92, 87–99. https://doi.org/10.1006/expr.1999.4412

Morgado, P., Ong, Y.-C., Boothroyd, J.C., Lodoen, M.B., 2011. *Toxoplasma gondii* induces B7-2 expression through activation of JNK signal transduction. Infect. Immun. 79, 4401–4412. https://doi.org/10.1128/IAI.05562-11

Moxon, C.A., Chisala, N. V, Mzikamanda, R., MacCormick, I., Harding, S., Downey, C., Molyneux, M., Seydel, K.B., Taylor, T.E., Heyderman, R.S., Toh, C.-H., 2015. Laboratory evidence of disseminated intravascular coagulation is associated with a fatal outcome in children with cerebral malaria despite an absence of clinically evident thrombosis or bleeding. J. Thromb. Haemost. 13, 1653–1664. https://doi.org/https://doi.org/10.1111/jth.13060

Moxon, C.A., Wassmer, S.C., Milner, D.A.J., Chisala, N. V, Taylor, T.E., Seydel, K.B., Molyneux, M.E., Faragher, B., Esmon, C.T., Downey, C., Toh, C.-H., Craig, A.G., Heyderman, R.S., 2013. Loss of endothelial protein C receptors links coagulation and inflammation to parasite sequestration in cerebral malaria in African children. Blood 122, 842–851. https://doi.org/10.1182/blood-2013-03-490219

Mullarky, I.K., Szaba, F.M., Winchel, C.G., Parent, M.A., Kummer, L.W., Mackman, N., Johnson, L.L., Smiley, S.T., 2006. In situ assays demonstrate that interferon-gamma suppresses infection-stimulated hepatic fibrin deposition by promoting fibrinolysis. J. Thromb. Haemost. 4, 1580–1587. https://doi.org/10.1111/j.1538-7836.2006.02010.x

Murphy, T.H., Boyd, J.D., Bolaños, F., Vanni, M.P., Silasi, G., Haupt, D., Ledue, J.M., 2016. High-throughput automated home-cage mesoscopic functional imaging of mouse cortex.

Nat. Commun. 7, 11611. https://doi.org/10.1038/ncomms11611

Niessen, F., Schaffner, F., Furlan-Freguia, C., Pawlinski, R., Bhattacharjee, G., Chun, J., Derian, C.K., Andrade-Gordon, P., Rosen, H., Ruf, W., 2008. Dendritic cell PAR1–S1P3 signalling couples coagulation and inflammation. Nature 452, 654–658. https://doi.org/10.1038/nature06663

Ohashi, T., Sugaya, Y., Sakamoto, N., Sato, M., 2007. Hydrostatic pressure influences morphology and expression of VE-cadherin of vascular endothelial cells. J. Biomech. 40, 2399–2405. https://doi.org/https://doi.org/10.1016/j.jbiomech.2006.11.023

Pappas, G., Roussos, N., Falagas, M.E., 2009. Toxoplasmosis snapshots: Global status of *Toxoplasma gondii* seroprevalence and implications for pregnancy and congenital toxoplasmosis. Int. J. Parasitol. 39, 1385–1394. https://doi.org/10.1016/j.ijpara.2009.04.003

Pawlinski, R., Wang, J.-G., Owens, A.P. 3rd, Williams, J., Antoniak, S., Tencati, M., Luther, T., Rowley, J.W., Low, E.N., Weyrich, A.S., Mackman, N., 2010. Hematopoietic and nonhematopoietic cell tissue factor activates the coagulation cascade in endotoxemic mice. Blood 116, 806–814. https://doi.org/10.1182/blood-2009-12-259267

Pfefferkorn, E.R., 1984. Interferon γ blocks the growth of *Toxoplasma gondii* in human fibroblasts by inducing the host cells to degrade tryptophan. Proc. Natl. Acad. Sci. U. S. A. 81, 908–912. https://doi.org/10.1073/pnas.81.3.908

Pfefferkorn, E.R., Rebhun, S., Eckel, M., 1986. Characterization of an Indoleamine 2,3-Dioxygenase Induced by Gamma-Interferon in Cultured Human Fibroblasts. J. Interferon Res. 6, 267–279. https://doi.org/10.1089/jir.1986.6.267

Ramirez-San-Juan, J.C., Ramos-Garcia, R., Guizar-Iturbide, I., Martinez-Niconoff, G., Choi, B., 2008. Impact of velocity distribution assumption on simplified laser speckle imaging equation. Opt. Express 16, 3197–3203. https://doi.org/10.1364/OE.16.003197

Ramirez-San-Juan, J.C., Regan, C., Coyotl-Ocelotl, B., Choi, B., 2014. Spatial versus temporal laser speckle contrast analyses in the presence of static optical scatterers. J. Biomed. Opt. 19, 106009. https://doi.org/10.1117/1.JBO.19.10.106009

Robben, P.M., LaRegina, M., Kuziel, W.A., Sibley, L.D., 2005. Recruitment of Gr-1+ monocytes is essential for control of acute toxoplasmosis. J. Exp. Med. 201, 1761–1769. https://doi.org/10.1084/jem.20050054

Roberts, D.D., Sherwood, J.A., Spitalnik, S.L., Panton, L.J., Howard, R.J., Dixit, V.M., Frazier, W.A., Miller, L.H., Ginsburg, V., 1985. Thrombospondin binds falciparum malaria parasitized erythrocytes and may mediate cytoadherence. Nature 318, 64–66. https://doi.org/10.1038/318064a0

Roth, A., Roth, B., Höffken, G., Steuber, S., Khalifa, K.I., Janitschke, K., 1992. Application of the polymerase chain reaction in the diagnosis of pulmonary toxoplasmosis in immunocompromised patients. Eur. J. Clin. Microbiol. Infect. Dis. 11, 1177–1181. https://doi.org/10.1007/BF01961141

Rowe, J.A., Claessens, A., Corrigan, R.A., Arman, M., 2009. Adhesion of *Plasmodium falciparum*-infected erythrocytes to human cells: molecular mechanisms and therapeutic implications. Expert Rev. Mol. Med. 11, e16. https://doi.org/10.1017/S1462399409001082

Ruitenberg, A., den Heijer, T., Bakker, S.L.M., van Swieten, J.C., Koudstaal, P.J., Hofman, A., Breteler, M.M.B., 2005. Cerebral hypoperfusion and clinical onset of dementia: The

Rotterdam study. Ann. Neurol. 57, 789–794. https://doi.org/10.1002/ana.20493

Sa, Q., Ochiai, E., Sengoku, T., Wilson, M.E., Brogli, M., Crutcher, S., Michie, S.A., Xu, B., Payne, L., Wang, X., Suzuki, Y., 2014. VCAM-1/α4β1 integrin interaction is crucial for prompt recruitment of immune T cells into the brain during the early stage of reactivation of chronic infection with *Toxoplasma gondii* to prevent toxoplasmic encephalitis. Infect. Immun. 82, 2826–2839. https://doi.org/10.1128/IAI.01494-13

Salwen, S.A., Szarowski, D.H., Turner, J.N., Bizios, R., 1998. Three-dimensional changes of the cytoskeleton of vascular endothelial cells exposed to sustained hydrostatic pressure. Med. Biol. Eng. Comput. 36, 520–527. https://doi.org/10.1007/BF02523225

Schaffer, C.B., Friedman, B., Nishimura, N., Schroeder, L.F., Tsai, P.S., Ebner, F.F., Lyden, P.D., Kleinfeld, D., 2006. Two-photon imaging of cortical surface microvessels reveals a robust redistribution in blood flow after vascular occlusion. PLoS Biol. 4, 258–270. https://doi.org/10.1371/journal.pbio.0040022

Scharton-Kersten, T., Nakajima, H., Yap, G., Sher, A., Leonard, W.J., 1998. Infection of mice lacking the common cytokine receptor gamma-chain (gamma(c)) reveals an unexpected role for CD4+ T lymphocytes in early IFN-gamma-dependent resistance to *Toxoplasma gondii*. J. Immunol. 160, 2565–2569.

Schindelin, J., Arganda-Carreras, I., Frise, E., Kaynig, V., Longair, M., Pietzsch, T., Preibisch, S., Rueden, C., Saalfeld, S., Schmid, B., Tinevez, J.-Y., White, D.J., Hartenstein, V., Eliceiri, K., Tomancak, P., Cardona, A., 2012. Fiji: an open-source platform for biological-image analysis. Nat. Methods 9, 676–682. https://doi.org/10.1038/nmeth.2019

Schlüter, D., Barragan, A., 2019. Advances and Challenges in Understanding Cerebral

Toxoplasmosis. Front. Immunol. 10, 242. https://doi.org/10.3389/fimmu.2019.00242

Schneider, C.A., Figueroa Velez, D.X., Azevedo, R., Hoover, E.M., Tran, C.J., Lo, C., Vadpey, O., Gandhi, S.P., Lodoen, M.B., 2019. Imaging the dynamic recruitment of monocytes to the blood–brain barrier and specific brain regions during *Toxoplasma gondii* infection. Proc. Natl. Acad. Sci. U. S. A. 116, 24796–24807. https://doi.org/10.1073/pnas.1915778116

Schrandt, C.J., Kazmi, S.M.S., Jones, T.A., Dunn, A.K., 2015. Chronic Monitoring of Vascular Progression after Ischemic Stroke Using Multiexposure Speckle Imaging and Two-Photon Fluorescence Microscopy. J. Cereb. Blood Flow Metab. 35, 933–942. https://doi.org/10.1038/jcbfm.2015.26

Semeraro, F., Ammollo, C.T., Morrissey, J.H., Dale, G.L., Friese, P., Esmon, N.L., Esmon, C.T., 2011. Extracellular histones promote thrombin generation through platelet-dependent mechanisms: involvement of platelet TLR2 and TLR4. Blood 118, 1952–1961. https://doi.org/10.1182/blood-2011-03-343061

Semmler, A., Hermann, S., Mormann, F., Weberpals, M., Paxian, S.A., Okulla, T., Schäfers, M., Kummer, M.P., Klockgether, T., Heneka, M.T., 2008. Sepsis causes neuroinflammation and concomitant decrease of cerebral metabolism. J. Neuroinflammation 5, 1–10. https://doi.org/10.1186/1742-2094-5-38

Semple, J.W., Italiano, J.E.J., Freedman, J., 2011. Platelets and the immune continuum. Nat. Rev. Immunol. 11, 264–274. https://doi.org/10.1038/nri2956

Shamseddin, J., Akhlaghi, L., Razmjou, E., Shojaee, S., Monavari, S.H.R., Tajik, N., Ebrahimi, S.A., Meamar, A.R., 2015. Conjugated Linoleic Acid Stimulates Apoptosis in RH and Tehran Strains of *Toxoplasma gondii*, in Vitro. Iran. J. Parasitol. 10, 238–244.

Shih, A.Y., Driscoll, J.D., Drew, P.J., Nishimura, N., Schaffer, C.B., Kleinfeld, D., 2012. Two-Photon Microscopy as a Tool to Study Blood Flow and Neurovascular Coupling in the Rodent Brain. J. Cereb. Blood Flow Metab. 32, 1277–1309. https://doi.org/10.1038/jcbfm.2011.196

Shih, A.Y., Rühlmann, C., Blinder, P., Devor, A., Drew, P.J., Friedman, B., Knutsen, P.M., Lyden, P.D., Matéo, C., Mellander, L., Nishimura, N., Schaffer, C.B., Tsai, P.S., Kleinfeld, D., 2015. Robust and fragile aspects of cortical blood flow in relation to the underlying angioarchitecture. Microcirculation 22, 204–218. https://doi.org/10.1111/micc.12195

Shoffstall, A.J., Paiz, J.E., Miller, D.M., Rial, G.M., Willis, M.T., Menendez, D.M., Hostler, S.R., Capadona, J.R., 2018. Potential for thermal damage to the blood–brain barrier during craniotomy: implications for intracortical recording microelectrodes. J. Neural Eng. 15, 34001. https://doi.org/10.1088/1741-2552/aa9f32

Siegel, J.S., Snyder, A.Z., Ramsey, L., Shulman, G.L., Corbetta, M., 2015. The effects of hemodynamic lag on functional connectivity and behavior after stroke. J. Cereb. Blood Flow Metab. 36, 2162–2176. https://doi.org/10.1177/0271678X15614846

Sinclair, A.J., McLean, J.G., Monger, E.A., 1979. Metabolism of linoleic acid in the cat. Lipids 14, 932–936. https://doi.org/10.1007/BF02533508

Soldatelli, M.D., Amaral, L.F. do, Veiga, V.C., Rojas, S.S.O., Omar, S., Marussi, V.H.R., 2020. Neurovascular and perfusion imaging findings in coronavirus disease 2019: Case report and literature review. Neuroradiol. J. 33, 368–373. https://doi.org/10.1177/1971400920941652

Sterkers, Y., Pratlong, F., Albaba, S., Loubersac, J., Picot, M.-C., Pretet, V., Issert, E., Boulot, P., Bastien, P., 2012. Novel Interpretation of Molecular Diagnosis of Congenital

Toxoplasmosis According to Gestational Age at the Time of Maternal Infection. J. Clin. Microbiol. 50, 3944 LP – 3951. https://doi.org/10.1128/JCM.00918-12

Sturge, C.R., Benson, A., Raetz, M., Wilhelm, C.L., Mirpuri, J., Vitetta, E.S., Yarovinsky, F., 2013. TLR-independent neutrophil-derived IFN-γ is important for host resistance to intracellular pathogens. Proc. Natl. Acad. Sci. 110, 10711 LP – 10716. https://doi.org/10.1073/pnas.1307868110

Su, C., Khan, A., Zhou, P., Majumdar, D., Ajzenberg, D., Dardé, M.L., Zhu, X.Q., Ajioka, J.W., Rosenthal, B.M., Dubey, J.P., Sibley, L.D., 2012. Globally diverse *Toxoplasma gondii* isolates comprise six major clades originating from a small number of distinct ancestral lineages. Proc. Natl. Acad. Sci. U. S. A. 109, 5844–5849. https://doi.org/10.1073/pnas.1203190109

Su, C., Zhang, X., Dubey, J.P., 2006. Genotyping of *Toxoplasma gondii* by multilocus PCR-RFLP markers: A high resolution and simple method for identification of parasites. Int. J. Parasitol. 36, 841–848. https://doi.org/https://doi.org/10.1016/j.ijpara.2006.03.003

Sun, H., Ringdahl, U., Homeister, J.W., Fay, W.P., Engleberg, N.C., Yang, A.Y., Rozek, L.S., Wang, X., Sjöbring, U., Ginsburg, D., 2004. Plasminogen Is a Critical Host Pathogenicity Factor for Group A Streptococcal Infection. Science (80-.). 305, 1283 LP – 1286. https://doi.org/10.1126/science.1101245

Sunil, S., Erdener, S.E., Lee, B.S., Postnov, D., Tang, J., Kura, S., Cheng, X., Chen, I.A., Boas, D.A., Kılıç, K., 2020. Awake chronic mouse model of targeted pial vessel occlusion via photothrombosis. Neurophotonics 7, 1. https://doi.org/10.1117/1.nph.7.1.015005

Suzuki, Y., Orellana, M.A., Schreiber, R.D., Remington, J.S., 1988. Interferon-gamma: the

major mediator of resistance against *Toxoplasma gondii*. Science 240, 516–518. https://doi.org/10.1126/science.3128869

Tenter, A.M., Heckeroth, A.R., Weiss, L.M., 2000. *Toxoplasma gondii*: from animals to humans. Int. J. Parasitol. 30, 1217–1258. https://doi.org/10.1016/s0020-7519(00)00124-7

Todoroki, H., Nakamura, S., Higure, A., Okamoto, K., Takeda, S., Nagata, N., Itoh, H., Ohsato, K., 2000. Neutrophils express tissue factor in a monkey model of sepsis. Surgery 127, 209–216. https://doi.org/10.1067/msy.2000.103027

Turner, L., Lavstsen, T., Berger, S.S., Wang, C.W., Petersen, J.E. V, Avril, M., Brazier, A.J., Freeth, J., Jespersen, J.S., Nielsen, M.A., Magistrado, P., Lusingu, J., Smith, J.D., Higgins, M.K., Theander, T.G., 2013. Severe malaria is associated with parasite binding to endothelial protein C receptor. Nature 498, 502–505. https://doi.org/10.1038/nature12216

Ueno, N., Harker, K.S., Clarke, E. V, McWhorter, F.Y., Liu, W.F., Tenner, A.J., Lodoen, M.B., 2014. Real-time imaging of Toxoplasma-infected human monocytes under fluidic shear stress reveals rapid translocation of intracellular parasites across endothelial barriers. Cell. Microbiol. 16, 580–595. https://doi.org/10.1111/cmi.12239

Vogetseder, A., Ospelt, C., Reindl, M., Schober, M., Schmutzhard, E., 2004. Time course of coagulation parameters, cytokines and adhesion molecules in *Plasmodium falciparum* malaria. Trop. Med. Int. Heal. 9, 767–773. https://doi.org/https://doi.org/10.1111/j.1365-3156.2004.01265.x

Wenzel, J., Hansen, C.E., Bettoni, C., Vogt, M.A., Lembrich, B., Natsagdorj, R., Huber, G., Brands, J., Schmidt, K., Assmann, J.C., Stölting, I., Saar, K., Sedlacik, J., Fiehler, J., Ludewig, P., Wegmann, M., Feller, N., Richter, M., Müller-Fielitz, H., Walther, T., König,

G.M., Kostenis, E., Raasch, W., Hübner, N., Gass, P., Offermanns, S., De Wit, C., Wagner, C.A., Schwaninger, M., 2020. Impaired endothelium-mediated cerebrovascular reactivity promotes anxiety and respiration disorders in mice. Proc. Natl. Acad. Sci. U. S. A. 117, 1753–1761. https://doi.org/10.1073/pnas.1907467117

Willerson, D., Aaberg, T.M., Reeser, F., Meredith, T.A., 1977. Unusual ocular presentation of acute toxoplasmosis. Br. J. Ophthalmol. 61, 693 LP – 698. https://doi.org/10.1136/bjo.61.11.693

Xu, H.-T., Pan, F., Yang, G., Gan, W.-B., 2007. Choice of cranial window type for in vivo imaging affects dendritic spine turnover in the cortex. Nat. Neurosci. 10, 549–551. https://doi.org/10.1038/nn1883

Xu, J., Zhang, X., Monestier, M., Esmon, N.L., Esmon, C.T., 2011. Extracellular histones are mediators of death through TLR2 and TLR4 in mouse fatal liver injury. J. Immunol. 187, 2626–2631. https://doi.org/10.4049/jimmunol.1003930

Yap, G.S., Sher, A., 1999. Cell-mediated immunity to *Toxoplasma gondii*: initiation, regulation and effector function. Immunobiology 201, 240–247. https://doi.org/10.1016/S0171-2985(99)80064-3

Yarovinsky, F., 2014. Innate immunity to *Toxoplasma gondii* infection. Nat. Rev. Immunol. 14, 109–121. https://doi.org/10.1038/nri3598

Yeaman, M.R., 2010. Platelets in defense against bacterial pathogens. Cell. Mol. Life Sci. 67, 525–544. https://doi.org/10.1007/s00018-009-0210-4

Zhang, S., Murphy, T.H., 2007. Imaging the impact of cortical microcirculation on synaptic

structure and sensory-evoked hemodynamic responses in vivo. PLoS Biol. 5, 1152–1167. https://doi.org/10.1371/journal.pbio.0050119

Zhang, Y., Huang, C., Kim, S., Golkaram, M., Dixon, M.W.A., Tilley, L., Li, J., Zhang, S., Suresh, S., 2015. Multiple stiffening effects of nanoscale knobs on human red blood cells infected with *Plasmodium falciparum* malaria parasite. Proc. Natl. Acad. Sci. U. S. A. 112, 6068–6073. https://doi.org/10.1073/pnas.1505584112

Zhu, X., Huang, L., Zheng, Y., Song, Y., Xu, Q., Wang, J., Si, K., Duan, S., Gong, W., 2019. Ultrafast optical clearing method for three-dimensional imaging with cellular resolution. Proc. Natl. Acad. Sci. U. S. A. 166, 11480–11489. https://doi.org/10.1073/pnas.1819583116